NORTHWESTERN UNIVERSITY

Changes in Motor Unit Firing Patterns as a Function of Age, Muscle, and Following a Unilateral Brain Injury: Ionotropic and Metabotropic Effects

A DISSERTATION

SUBMITTED TO THE GRADUATE SCHOOL IN PARTIAL FULFILLMENT OF THE REQUIREMENTS

For the degree

DOCTOR OF PHILOSOPHY

Field of Biomedical Engineering

By

Altamash Shamsul Hassan

EVANSTON, ILLINOIS

September 2021

Abstract

Changes in Motor Unit Firing Patterns as a Function of Age, Muscle, and Following a Unilateral Brain Injury: Ionotropic and Metabotropic Effects

Altamash S. Hassan

Coordinated movement relies on the precise and controlled activation of populations of motor units, which convert the commands of the nervous system into muscle forces. Motor unit firing patterns are often nonlinear and generated through the response to a combination of ionotropic excitatory and inhibitory commands, as well as metabotropic neuromodulatory inputs. Analysis of these motor unit firing patterns provides insight into the motor commands utilized for movement in both healthy and pathological states. Through a series of experiments, we sought to analyze motor unit firing patterns to understand the changes in both ionotropic and metabotropic motor commands that occur in various cohorts. This was accomplished through a comprehensive characterization of modern motor unit analyses methods in young, healthy adults, followed by an investigation into the changes in motor unit patterns associated with healthy aging, and finally the comparison of the motor unit firing patterns of neurologically-intact individuals and those who had suffered a unilateral brain injury, within the same age group.

Novel techniques allow for the recording of populations of motor units concurrently. We investigated the distribution of motor units decomposed using these new methods and population recordings to conduct a sensitivity analysis of a common motor unit measure of persistent inward currents, which are modulated by metabotropic inputs. Together these studies enable us to take full advantage of the novel motor unit recording method and facilitate the comparison of the results

presented in this dissertation with previous work using different computational or recording methods.

In our third study we investigated the changes in motor unit firing patterns that occur with aging in the absence of disease. We found significant reductions in motor unit firing rates and estimates of persistent inward current amplitude in older adults. These findings were seen at both elbow flexor and extensor muscles. Further, this study also provided greater context to the changes in motor unit firing patterns observed following hemiparetic stroke, as most stroke survivors are aged individuals.

To understand the effects of a unilateral brain injury on motor unit firing patterns, we quantified the firing patterns of elbow flexor and extensor motor units in both upper extremities of individuals with chronic hemiparetic stroke. Estimates of persistent inward currents were increased in both paretic and non-paretic limbs of stroke participants, while motor unit firing rates and rate modulation were primarily reduced in the paretic limb. Together these results suggest that changes in metabotropic drive to motoneurons following a stroke is systemic, while alterations in ionotropic neural drive are more selective.

Finally, we further probed the changes in neural drive following unilateral brain injury through the comparison of motor unit firing patterns during voluntary and synergy-driven contractions of the biceps brachii. Rate modulation impairments were more pronounced during synergy-driven contractions of the biceps, than during voluntary activation. We postulate that the rate modulation impairments seen following stroke are due to increased use of the corticobulbar pathways, which play a larger role during the synergy-driven contractions.

Acknowledgments

To my advisor and mentor, Dr. Jules Dewald, I would like to express my gratitude for all of your guidance and advice throughout the last 6 years. You brought insight and enthusiasm in every answer you provided me, no matter if I was asking about a research project, future career decisions, or even just looking for a good restaurant. Your passion for interdisciplinary research and creative problem solving drove me to develop new connections through collaboration and expand my skillset by learning new techniques. The environment that you have created in your lab, which effortlessly united students and researchers from varied backgrounds in an energetic and vibrant pursuit of advancing scientific research in the field of neurorehabilitation, gave me the opportunity best utilize my strengths, as well as improve on my weaknesses and broaden my horizons. It is undeniable that you have shaped me as a scientist, and I hope to emulate your passion, optimism, and collaborative spirit in all of my future endeavors.

I would also like to take this opportunity to thank my co-advisor, Dr. Laura McPherson, for all her guidance on data collection, analysis, and bringing me into the world of motoneurons! I cannot overstate how much I benefitted from running my first experiments with you there to guide me. Additionally, your recent experience with the BME program was an invaluable resource as I developed my committee and handled official deadlines. Importantly, your input and advice on my first papers and presentations helped craft my scientific voice, and provided me with a strong foundation to build on with future work.

I would like to thank the members of my doctoral committee, Drs. CJ Heckman, Matt Tresch, and Francesco Negro, for all of the constructive feedback you have provided on my research efforts and academic development. I always emerged from our committee meetings

energized and full of direction. I would also like to thank Dr. Jun Yao for her time on my committee, which helped me take my initial steps towards developing my first research project.

I would also like to acknowledge the generous funding support that I have received throughout my pursuit of my PhD. I have been supported by the National Institutes of Health (T32 HD07418, R01HD039343, and R01NS098509), Northwestern University Department of Physical Therapy and Human Movement Sciences, and Northwestern University Department of Biomedical Engineering. Thank you for investing in my research and providing me the opportunity to grow professionally.

Of course, none of this work could have been completed without the efforts of my research participants. Your willingness to take time out of your busy lives to participate in our research studies, and to always bring patience and energy to each experiment made all of this possible.

Further, I would like to thank my colleagues, friends, and family for all the support they have provided to aid me in my PhD pursuit:

To the members of the Dewald lab and the PTHMS family:

I appreciate the eagerness to collaborate, provide feedback, and advise on experimental design or data analysis that you all provided. I was lucky to have such a large, yet surprisingly close knit, support structure in the department, and I thoroughly enjoyed socializing with you at work, after work, and while at conferences.

I'd like to give a special shout out to Carolina Carmona, and Di Zhang for all their help with experimental setups and recruiting participants. Carolina, you made experiments go smoothly and I always enjoyed chatting while we ran them. Di, your ability to manufacture new devices and integrate them in a seamless manner in such short time frames was astounding! You allowed me to keep my research going while projects shifted and parts broke.

To Mark Cummings and Sabeen Admani:

You both provided so much help in keeping my research going smoothly. Sabeen, your total revamp of the isometric set-up was crucial to all of my research projects. Mark, I have no idea how long my PhD would have taken without you there to help me run experiments and analyze all the data we collected. I hope you can find someone to help you during your PhD, as much as you helped me during mine. However, more than all the help with the research, I am most grateful for how fun you both made working at PTHMS. Working together with you both made even the most frustrating tasks (load cell recalibration…) into a hilarious and enjoyable experience.

To my friends from home and college:

It's amazing how much love and support you all provided, despite being scattered across the country. Garrett, Kevin, and Juan, thank you for providing me with ample music recommendations, intense NBA takes, hours of videogame play, and regular visits that make sure I am experiencing Chicago to the fullest. Paul, Stan, Luke, and Vikash, you all never cease to invigorate my day with passionate debates about the most trivial topics and advice on any decision big or small. Anthony and Will, you both bring me oft-needed doses of optimism and levity that can make me forget about a bad day. Visiting all of you gave me ample opportunities to explore new places with close friends and avoid some of the harsh Chicago winters.

To the Taco Tuesday crew:

Amy and Anne, you were my first friends when I moved here and knew absolutely no one, and now it's been six years and you have become some of my closest friends. Katherine, your strong opinions brought plenty of humor to the group, and you are one of my favorite people to talk to because of your empathy and emotional investment in all our lives. You three are such a large part of why Chicago feels like home to me, and while I am full of excitement for your next

adventures, the city just won't feel the same without you. Hussain, I can't believe you have put up with being my roommate for 4 years now, you've always been both a considerate roommate and I enjoy our daily chats while we wait to make coffee. Here's to another year at *The Briar*!

To Glenn and Appi:

You both have been so supportive of me from the moment when each of you entered my life. Having the unconditional love and support from two extra parents has made so many things in my life easier, and I am unbelievably lucky to have the two of you in my life.

To my sisters Michelle, Anayah, and Zaynah:

Anayah and Zaynah, you have both grown up so much since I started my PhD and I am proud of how inquisitive and intelligent you both have become. Spending time with you two has been one of the best ways to procrastinate! Michelle, I have always looked up to you, and I can't count all of the choices I have made over the years to follow in your footsteps. You're truly one of my best friends and having you in Chicago more often the last few years has been fantastic. Thank you for pushing me to try new places, new foods, and to go on new adventures.

To my parents:

I can't begin to list all of the things you both have done to get me to this point in my life. You have provided the most loving and supportive homes anyone could ever ask for, and you made sure I knew how to set lofty aspirations and work hard enough to make them a reality. From a very young age you have instilled in me the importance of education and nurtured my early interests in math and science. Throughout all of my education, you were always there to alleviate stress, and keep me calm and collected as everything seemed chaotic. You have been the bedrock of my support system and I could not have achieved this without both of you being there for me every step of the way.

List of Abbreviations

ADL: anterior deltoid

BIC: biceps brachii

EE: elbow extension

EF: elbow flexion

EMG: electromyography

FMA: Fugl-Meyer Assessment

FR: firing rate

HD-sEMG: high-density surface electromyography

IDL: intermediate (lateral) deltoid

M1: primary motor cortex

MN: motoneuron

MRI: magnetic resonance imaging

MU: motor unit

MVC: maximum voluntary contraction

MVT: maximum voluntary torque

N: Newton

Nm: Newton-meter

PIC: Persistent Inward Current

PM: premotor

PMRF: pontomedullary reticular formation

SABD: shoulder abduction

SADD: shoulder adduction

SD: standard deviation

SE: standard error

SM: supplementary motor

TRI: triceps brachii

Table of Contents

List of Figures

List of Tables

1. Introduction

1.1 Problem Statement

Motor unit recordings enable the non-invasive investigation of human motor control patterns. As the primary output of the central nervous system, the motor unit firing patterns are influenced by the combination of all three components of motor commands (excitation, inhibition, and neuromodulation), and can therefore be used to fully understand how these inputs work in concert to generate muscle activity in both healthy and pathologic states. Additionally, novel techniques utilizing HD-sEMG and automatic decomposition algorithms enable larger motor unit yields from single recordings. While the properties of the units decomposed from surface EMG should be investigated, the large number of motor units allows for thorough sensitivity analyses of commonly used motor unit analysis techniques.

Stroke survivors often exhibit long-term motor deficits, which may be further understood through analyses of motor unit firing patterns. Previous work has implicated that a disruption of corticospinal drive results in a shift towards the reliance of corticobulbospinal pathways. However, the mechanisms by which this reorganization of motor control pathways leads to the observed motor deficits is not fully understood. Further, how the interactions between the hypothesized changes in excitatory input, monoaminergic drive, and inhibitory input affect motor control following stroke has not been thoroughly investigated.

As the incidence of stroke increases with age, a proper characterization of stroke deficits requires knowledge of the motor control changes associated with healthy aging. While age-related weakness has been primarily attributed to alterations in the muscle, the role of neural changes must

be considered. Previous work has found inconsistent results across muscles, and further investigation is necessary.

1.2 Research Goal

The primary research goal of this dissertation was to examine firing patterns of populations of motor units to understand the changes in both ionotropic and metabotropic motor commands across muscle, age, and post-stroke. Specifically, we sought to investigate differences in motor unit firing patterns between: (1) young healthy controls and older neurologically intact individuals, (2) individuals following stroke and neurologically intact individuals in a similar age range, and (3) voluntary and involuntary flexion synergy-induced contractions in individuals with chronic hemiparetic stroke.

In order to examine populations of motor units, a combination of HD-sEMG and automatic motor unit decomposition algorithms were used. The relative novelty of these methods and the large distributions of motor units provided by these methods, led to the secondary goals of investigating the distribution of motor units provided by HD-sEMG decomposition and conducting a thorough sensitivity analysis of the parameters often used to assess motor unit excitability. These efforts provided further context for the findings from our primary research goals, and allowed for easier comparisons between the results in the coming chapters and previous work conducted with differing methods.

1.3 Aims

The research goals above were investigated through the completion of the following research aims:

Aim 1: To investigate the distribution of motor units decomposed using high-density surface EMG recordings and automatic decomposition algorithms.

Aim 2: To systematically determine the impact of commonly used computational parameters on ΔF estimates of motoneuron excitability, and provide recommendations for standardized parameters for the ΔF technique.

Aim 3: To investigate the changes in motor unit firing patterns of the upper limb associated with aging.

Aim 4: To estimate whether persistent inward currents are increased bilaterally post stroke and to determine motor unit firing patterns in elbow flexor and extensor muscles.

Aim 5: To compare the motor unit firing patterns of the biceps brachii during voluntary and synergy-driven elbow flexion contractions.

1.4 Dissertation Outline

The following chapter provides background information on motoneuron firing patterns and their behavior in response to different motor command inputs, as well as information pertaining to descending motor pathways, and the etiology and pathophysiology of stroke. An overview of age related changes in motor control is included in the introduction section of Chapter 5.

Chapters 3-7 directly address the five research aims above, and include individual introduction, methods, results, and discussion sections. Chapters 3 and 4 present experimental results to address Aims 1 and 2. Chapters 3 and 4 have been published and the information for these publications is below:

Hassan AS, Kim EH, Khurram OU, Cummings M, Thompson CK, Miller McPherson L, Heckman CJ, Dewald JPA, Negro F., 2019. "Properties of Motor Units of Elbow and Ankle Muscles Decomposed Using High-Density Surface EMG." *Conf Proc IEEE Eng Med Biol Soc.* 3874-3878. doi: 10.1109/EMBC.2019.8857475.

Hassan, A., Thompson, C.K., Negro, F., Cummings, M., Powers, R.K., Heckman, C.J., Dewald, J.P. and McPherson, L.M., 2020. "Impact of parameter selection on estimates of motoneuron excitability using paired motor unit analysis." *J Neural Eng,* 17(1), p.016063. doi: 10.1088/1741-2552/ab5eda.

Chapters 5, 6, and 7 present experimental studies and results directly addressing aims 3, 4, and 5, respectively.

2. Background

2.1 Motor units and their responses to motor commands

Motor units serve as the primary output of the combined motor commands from the central nervous system onto the muscles. Motor units consist of a motoneuron, with a nucleus in the spinal cord or brainstem, and a group of muscle fibers innervated by the axon of the motoneuron (Heckman & Enoka, 2012). Motor units are heterogeneous with vast differences in the size and electrical properties of the motoneurons as well as the number and mechanical properties of the muscle fibers that are innervated by the motoneuron (Mendell & Henneman, 1971; Heckman & Enoka, 2012). The distributions of motor unit size, electrical properties, and mechanical properties are all continuous, however, motor units are often categorized into 3 groups: slow (S), fast fatigue resistant (FR), and fast fatigable (FF). S motoneurons are smaller and therefore require a lower amount of synaptic current to reach the firing threshold. Additionally, S muscle fibers contract slowly, but have the highest resistance to fatigue. FF motoneurons are the largest, requiring a large amount of synaptic current to reach the firing threshold, while the FF muscle fibers contract rapidly but fatigue easily. FR motor units behave with properties between those of S and FF units. During normal movement, motor units are recruited in an orderly fashion according to motoneuron size, with small S units recruited first, followed by FR units, and lastly FF units. This recruitment order is referred to as Henneman's size principle (Henneman *et al.*, 1965). There are three major components to the motor command given to motor units: ionotropic excitatory drive, ionotropic inhibitory drive, and metabotropic neuromodulatory drive. The sections below will provide more detail on these inputs and how they impact motor unit firing patterns.

2.1.1 Excitatory inputs

The excitatory motor command comes from both descending drive from the corticospinal and bulbospinal pathways and afferent input from sensory fibers. The ionotropic excitatory inputs from these sources serve to directly depolarize the motoneuron and are often related to specific motor commands. It has been hypothesized that the temporal pattern of a movement is set thorough ionotropic excitation (Johnson *et al.*, 2017). The distribution of the excitatory command varies across the motoneuron pool. Descending excitatory input, particularly from corticospinal and rubrospinal sources, favors the activation of type F units (Powers *et al.*, 1993; Binder *et al.*, 1998), while excitatory input from Ia afferents favors the activation of type S units (Heckman & Binder, 1988).

2.1.2 Inhibitory inputs

Inhibitory motor commands are often relayed through inhibitory spinal interneurons, which are modulated through both descending drive and afferent sensory input (Heckman & Enoka, 2012). Ionotropic inhibition serves to directly hyperpolarize the motoneuron. Animal models show evidence of tonic inhibitory drive to motoneurons in the awake and active primate (Prut & Perlmutter, 2003b, a) and the decerebrate cat (Johnson *et al.*, 2012). The temporal pattern of tonic background inhibition, and its relationship to the pattern of excitation can play a major role on motor unit firing patterns. Some hypothesized and previously simulated patterns of inhibition include (Powers *et al.*, 2012; Johnson *et al.*, 2017): inhibition held constant while excitation varies (constant), inhibition decreasing while excitation increases (push-pull), and inhibition increasing in proportion to excitation (balanced). Figure 2.1 below shows the simulated motor unit firing patterns for motor units receiving constant inhibition (blue), push-pull inhibition (red), or balanced

inhibition (green). Inhibition may also play a major role in focusing the effects of the diffuse neuromodulatory drive (Heckman & Enoka, 2012). The descending neuromodulatory pathways project to multiple motor pools across joints and therefore has broad effects on motoneuron excitability. However, the persistent inward currents facilitated by this neuromodulatory input are highly sensitive to inhibition (Hultborn *et al.*, 2003; Kuo *et al.*, 2003). Thus, inhibition may be used to enable selective modulation of motoneuron excitability from the broadly synapsing neuromodulatory inputs. Neuromodulatory drive and persistent inward currents are discussed further in the following section.

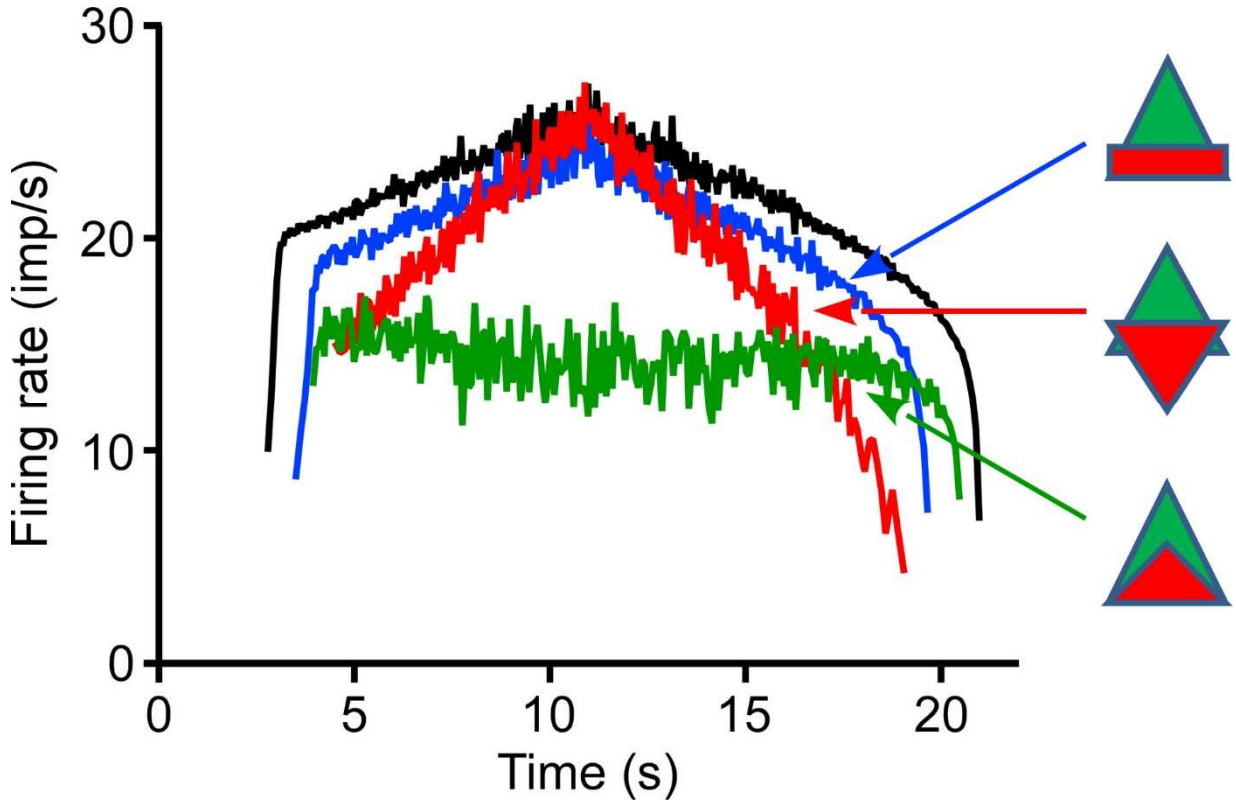

Figure 2.1: Inhibition and motor unit firing patterns (adapted from Johnson et al. 2017)
Computer simulations showing the motor unit firing rates in response to 3 different patterns of inhibition. Blue shows a constant background inhibition, Red shows inhibition varying inversely with excitation (push-pull), and Green shows inhibition varying in phase with excitation (balanced). The black trace shows motor unit firing in the absence of any inhibition.

2.1.3 Neuromodulatory inputs and persistent inward currents (PICs)

Neuromodulatory inputs control the excitability of the motoneuron by modulating the motoneuron's responses to excitatory and inhibitory ionotropic input. Instead of directly acting to depolarize or hyperpolarize the motoneuron, neuromodulatory inputs act through binding to G-protein coupled receptors to activate intracellular signaling pathways inside the motoneuron. The neuromodulatory inputs with the most potent effects on motoneurons are serotonin (5-HT) and norepinephrine (NE), which descend onto the spinal cord from the raphe nucleus and locus ceruleus, respectively, in the brainstem (Binder & Powers, 2001; Heckman & Enoka, 2012). Serotonergic activity is hypothesized to increase with proportion to motor output (Jacobs *et al.*, 2002), while noradrenergic input varies with arousal (Aston-Jones *et al.*, 2000). These inputs have substantial effects on the excitability of motoneurons including: reducing recruitment thresholds, reducing the spike afterhyperpolarization (AHP), and facilitating persistent inward currents (PICs).

PICs were first studied in motoneurons by Schwindt and Crill (Schwindt & Crill, 1980) who identified that these currents could generate the observed "bistable" behavior of motoneuron firing. PICs are generated by voltage sensitive Na and Ca currents (Hounsgaard & Kiehn, 1989) which provide a sustained depolarization of the motoneuron and can dramatically affect the firing rate patterns of motor units. Both the CaPIC and the NaPIC are strongly facilitated by 5-HT and NE (Heckman & Enoka, 2012), and the level of monoaminergic drive can adjust the PICs amplification of synaptic input (Lee & Heckman, 2000). PICs serve to prolong and amplify the response of the motoneuron to ionotropic excitatory input, as shown in panels A-C of figure 2.2 below. The prolongation and amplification of the synaptic input leads to nonlinearities in the firing patterns of motoneurons showing a strong PIC, including: an initial rapid acceleration of the firing rate immediately following recruitment of the motor unit, a second phase displaying low rate

modulation and a reduced sensitivity to descending input once the PIC is fully active, and derecruitment hysteresis with derecruitment occurring at a substantially lower level of input than was required to recruit the unit. An example of the firing patterns of a motor unit with strong PICs present is shown in figure 2.2 D.

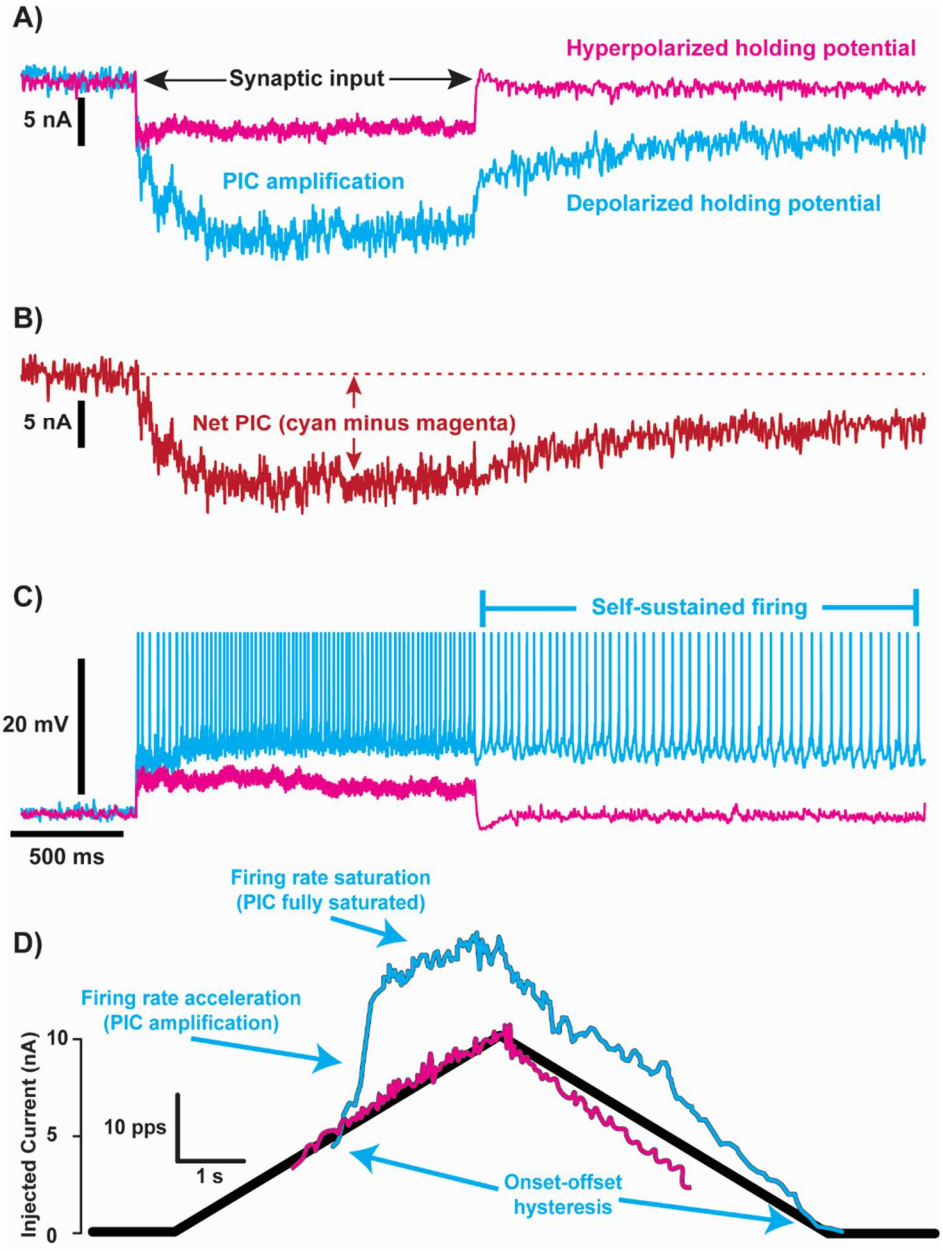

Figure 2.2: PIC effects on motoneuron firing

(adapted from Khurram, Pearcey et al. (in review) and Johnson et al. 2017)

A, B show the activity of a low threshold cat motoneuron which is voltage clamped to either -90mV (magenta) to deactivate the PIC effects, or 55mv (cyan) to display the PIC effects. In panel A, the prolongation and amplification effect of the PIC can be clearly seen in the depolarized motoneuron (cyan) as compared to the hyperpolarized motoneuron (magenta), in response to the same input. B: the net PIC in red, generated by subtracting the magenta trace from the cyan trace seen in A. C: the firing pattern of the motoneuron when it is unclamped. The cyan trace shows repetitive motor unit firing that is sustained, even following the cessation of the input, while the magenta trace does not achieve repetitive firing. D: An intracellular recording of a spinal neuron in response to a triangular current ramp. The magenta trace shows the linear motoneuron firing in the absence of PICs, the cyan trace shows the nonlinear firing patterns when PICs are present. These include: 1) a rapid acceleration phase, 2) a period of rate saturation, 3) recruitment-derecruitment hysteresis.

2.2 Motor unit recordings in humans

The conceptualization of the motor unit by Liddell and Sherrington (Liddell & Sherrington, 1925) was closely followed by the development of the technology to allow for the recording of single motor units from humans (Adrian & Bronk, 1929). There is a tight coupling between the motoneuron and the muscle fibers it innervates, with a motoneuron action potential almost always eliciting a single action potential in the muscle fibers. This affords a unique ability to directly record the motor output of the central nervous system, as the larger action potentials of the muscle fibers serve to amplify the activity of the motoneuron enabling easier recording. Recordings of motor unit discharge during voluntary activity provides fundamental insight into human motor control. From the original concentric needle electrodes to modern fine wire and high-density surface EMG arrays, the methods of collecting motor unit recordings has evolved greatly in the last 90 years. The sections below provide a brief summary of modern motor unit recording techniques, as well as some of the motor unit analyses which were utilized to accomplish the research aims of this dissertation.

2.2.1 Intramuscular fine-wire EMG

Intramuscular EMG using fine wire electrodes provided a major improvement over the original concentric needle electrode for the recording of motor unit activity. The wire electrodes are inserted into the muscle using a hypodermic needle, which is then removed. These flexible wire electrodes reduced discomfort, and allowed multiple motor units to be differentiated based on the size and the shape of the action potentials seen by the electrode. However, there are several limitations in utilizing intramuscular recordings to understanding motor commands. Importantly, fine wire electrodes are restricted by their high spatial selectivity, allowing only a small sample of

motor units to be identified from a contraction. Identification of motor units from higher intensity contractions is also difficult, due to the superposition of multiple motor unit action potentials. Additionally, accurate discrimination of motor unit firings from intramuscular recordings often requires a trained operator.

2.2.2 HD-sEMG and motor unit decomposition

In recent years, the development of multi-channel EMG grids paired with automatic decomposition algorithms has enabled the simultaneous recording of larger numbers of motor units. These high-density surface EMG (HD-sEMG) grids aim to discriminate motor unit activity through the differences in the spatial representation of the motor unit action potentials seen across the EMG grid. This technique allows recordings from larger populations of motor units, and across a wider range of contraction intensities than intramuscular EMG (Holobar *et al.*, 2014; Negro *et al.*, 2016). Further, the accuracy of these techniques is comparable to that of intramuscular EMG (Farina *et al.*, 2008; Holobar *et al.*, 2010; Holobar *et al.*, 2014; Farina & Negro, 2015; Martinez-Valdes *et al.*, 2017), while being non-invasive. However, there are some limitations to this technique as well. Similar to fine wire recordings, HD-sEMG decomposition is primarily constrained to recordings during isometric muscle contractions, though new work in dynamic tasks is being conducted (Glaser & Holobar, 2019), and the ability to decompose motor units is hampered at higher contraction levels. Additionally, recording from the surface of the skin may play a role in the population of motor units which can be sampled using this technique; the role surface recordings may play in the distribution of motor units recorded is investigated and further discussed in Chapter 3.

Several algorithms have been developed for the decomposition of these HD-sEMG signals into motor unit spike trains. The convolutive blind source separation algorithm developed by Negro, Farina, and colleagues (Negro *et al.*, 2016), was the primary motor unit decomposition technique utilized for the research studies discussed in the later chapters of this dissertation. This decomposition algorithm is comprised of two main iterations: 1) a separation of separate sparse components from the HD-sEMG signal using an independent component analysis, and (2) a source estimation refinement based on the convolution kernel compensation approach. This is only a brief overview of the steps involved in motor unit decomposition, however, an in-depth discussion of the theory and steps of this decomposition algorithm is beyond the scope of this dissertation.

2.2.3 Common motor unit analyses

The firing patterns of motor units obtained from muscle recordings are used to provide insight into the motor commands used to generate movement. As such, these motor unit recordings are usually obtained during controlled movements, often isometric contractions while maintaining a desired contraction level or slowly increasing and decreasing to a target contraction intensity. Contraction intensity is usually estimated using joint torque, either absolute or as a percentage of maximum, or occasionally using EMG amplitude. In this dissertation all motor unit recordings were conducted during isometric torque tasks, with contraction intensity estimated using joint torques normalized to maximum voluntary levels.

During voluntary contractions, motor unit firing rates are commonly quantified, including analyses of peak values, ranges, and variability. Further, the firing patterns of motor units can also be used to investigate the frequency content of the drive to the motor unit pool through coherence analyses (Conway *et al.*, 1995; Farmer *et al.*, 1997). Analyses of the amplitude and spatial

distribution of the action potentials of decomposed motor units can be used to understanding the organization of the muscle fibers that are innervated by the motoneuron pool. Contractions with slowly varying contraction intensity provide the ability to investigate the response of the motor unit pool to changes in excitatory input. This includes investigations of recruitment and derecruitment patterns as well as sensitivity of motor unit firing rates to increasing input. Additionally, ramp contractions allow for estimation of PICs through a measure of relative hysteresis of motor units (Bennett *et al.*, 2001a; Gorassini *et al.*, 2002; Afsharipour *et al.*, 2020). The details of estimation method are further discussed in Chapter 4 of this dissertation.

2.3 Motor control pathways

The motor cortex controls the activity of motoneurons and spinal circuitry through both direct cortical projections and indirect projections to brainstem structures which then project on to the spinal cord. In neurologically intact individuals, direct cortical projections provide fine motor control for fractionated movements and are primarily responsible for control of the wrist and fingers (Lawrence & Kuypers, 1968; Lemon, 2008). In contrast, the indirect brainstem projections largely provide postural control of the trunk and shoulder and pelvic girdles (Lawrence & Kuypers, 1968; Lemon, 2008). In short, going from the trunk to the wrist and fingers progressively increases the dependence on direct cortical projections. In the following sections will briefly review the anatomy and function of motor pathways pertinent to the research aims of this dissertation. This is not an exhaustive review of these pathways, but should provide enough detail to aid in the interpretation of the studies presented in the coming chapters.

2.3.1 Corticospinal tract

The corticospinal tract consists of the axons of pyramidal cells from the primary motor cortex, the premotor cortices, and the supplementary and cingulate motor areas. The axons of the corticospinal tract descend through the internal capsule and split into two groups. The lateral corticospinal tract, roughly 85% of the corticospinal fibers, decussate to the dorsolateral columns of the spinal cord and are primarily responsible for the motor control of the contralateral extremities. The anterior corticospinal tract is composed of the ~15% of fibers that did not decussate and are primarily responsible for the motor control of the ipsilateral trunk.

The corticospinal motor pathway is unique to mammals (Lemon & Griffiths, 2005), and the level of dexterity in the forelimb of a given mammalian species is correlated to the extent of corticospinal innervation (Lemon, 2008). In non-human primates and humans, the corticospinal tract includes monosynaptic connections from the motor cortex to the motoneurons which provide the necessary dexterity and fine motor control of the extremities.

2.3.2 Reticulospinal tract

The motor cortices relay information through indirect brainstem motor pathways via the corticobulbar tract, which travels in parallel to the corticospinal tract and terminates at the brainstem. The reticulospinal tract is one indirect motor pathway of interest, which originates from the reticular formation, a cluster of several connected nuclei throughout the brainstem, and terminates primarily on motoneurons and interneurons in the medial portion of the spinal cord.

As suggested by the medial nature of its termination, the reticulospinal tract is primarily involved in the control of postural muscles and locomotion. Further, reticulospinal projects branch across multiple spinal segments to enable the activation of multiple muscles across joints for

postural tasks (Matsuyama *et al.*, 1997). However, studies in non-human primates have shown reticulospinal projections to the motoneurons of the forearm (Riddle *et al.*, 2009) and the hand (Baker *et al.*, 2015). The reticulospinal motor pathways project bilaterally. In the upper limb the ipsilateral reticulospinal tract facilitates ipsilateral flexors while suppressing ipsilateral extensors. In addition to its ionotropic motor connections, the reticular formation also includes monoaminergic nuclei. The serotonergic raphe nucleus and the noradrenergic locus ceruleus provide neuromodulatory input to motoneurons and which play a role in setting the excitability of the motoneuron to descending input.

2.3.3 Rubrospinal Tract

The rubrospinal tract is another indirect motor pathway; it originates in the red nucleus, decussates in the midbrain and descends contralaterally to the cervical level of the spinal cord where it terminates in the lateral portion of the ventral horn (Lemon, 2008). Following corticospinal lesions, the rubrospinal tract shows a bias towards flexors in the upper limb and has been shown to play a role in motor recovery of the hand in non-human primates (Lawrence & Kuypers, 1968; Baker *et al.*, 2015). However, in humans the rubrospinal system is less developed, or even absent (Nathan & Smith, 1982; Onodera & Hicks, 2010).

2.3.4 Vestibulospinal tract

The vestibulospinal tract originates from the vestibular nuclei and descends to the spinal cord without decussating (Lemon, 2008; Li & Francisco, 2015). The vestibulospinal tract includes a medial and a lateral tract. The lateral vestibulospinal tract originates from the lateral vestibular nucleus and the fibers descend through the full spinal cord. The medial vestibulospinal tract originates from the medial vestibular nucleus, and its fibers only project to the cervical segments

of the spinal cord. The medial vestibulospinal tract primarily projects to motoneurons innervating axial muscles to promote stabilization of the head and coordination of head and eye movements, while the lateral vestibulospinal tract projects to the motoneuron pools of trunk and proximal limb muscles to provide postural control and drive to anti-gravity muscles.

2.3.5 Propriospinal tract

The propriospinal tracts are a collection of nerve fibers running between segments of the spinal cord in the cervical and lumbar enlargements (Alstermark *et al.*, 1984; Alstermark *et al.*, 1990). There is mounting evidence that a portion of the descending motor command is passed through propriospinal neurons en route to the motoneurons in humans. The propriospinal system is thought to integrate descending motor commands with afferent feedback from the limbs to enable accurate movement.

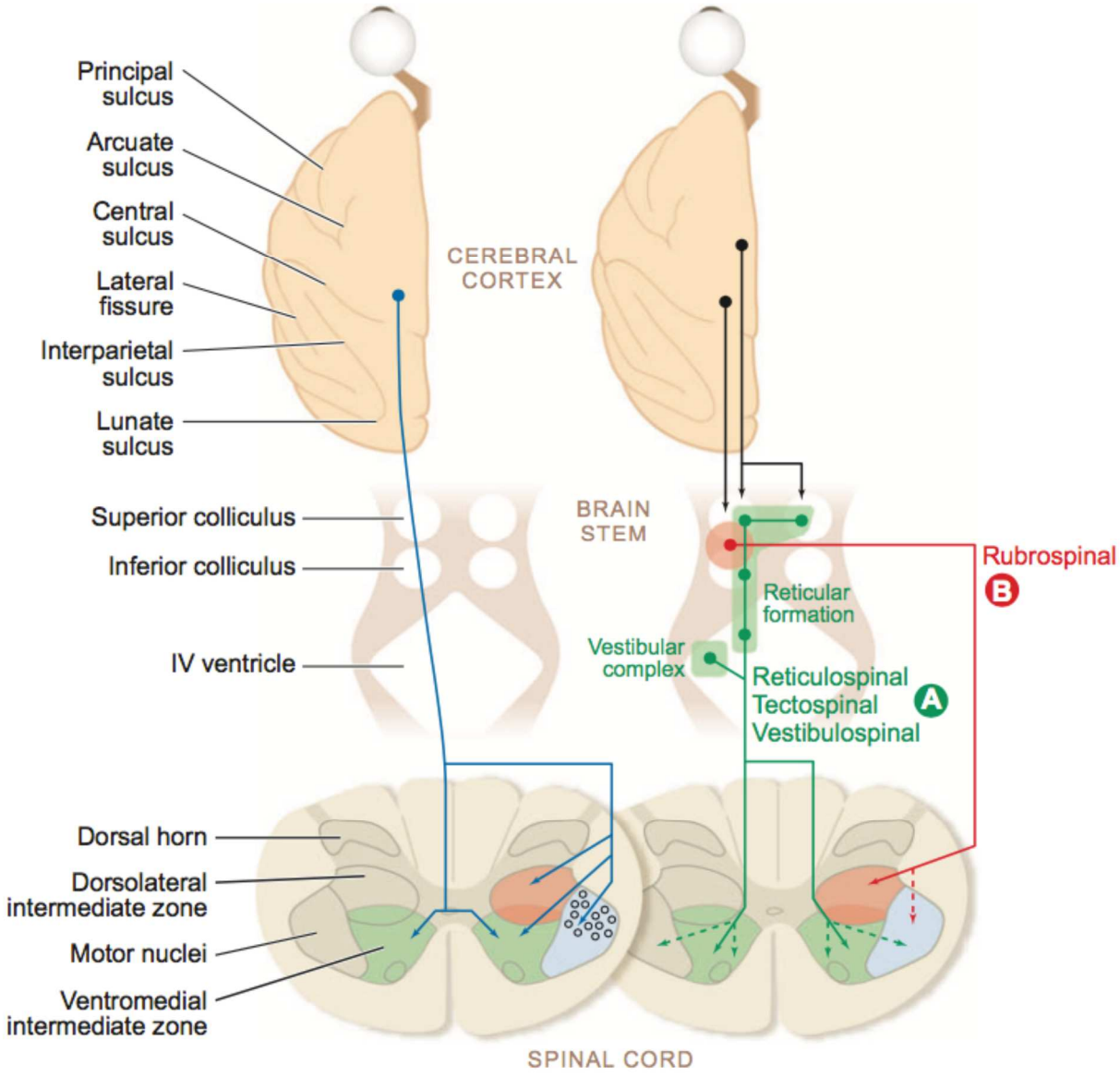

Figure 2.3: Descending Pathways (adapted from Lemon 2008)
Left: *blue lines show projections from the corticospinal tract to the dorsolateral and ventromedial intermediate zones (red and green areas, respectively), and the direct projections onto motoneurons (black circles within the blue zone).* ***Right:*** *black lines show corticobulbar projections to the brainstem motor nuclei. Group A, in green, shows projections from the brainstem motor pathways which terminate bilaterally. Group A includes the Reticulospinal and Vestibulospinal pathways. Group B, in red, shows the rubrospinal projections from the red nucleus to the contralateral dorsolateral intermediate zone.*

2.4 Etiology of stroke

A stroke occurs when blood flow to the brain is interrupted due to either blockage or a rupture of blood vessels in the brain. Strokes are classified by the cause of the disruption of blood

flow. Ischemic strokes are caused by an obstruction of a vessel providing blood to the brain, due to thromboses or emboli**.** Hemorrhagic strokes occur due to a rupture of blood vessels in the brain. Ischemic strokes are more common, accounting for 80-90% of all strokes, while, hemorrhagic strokes are less common, accounting for about 13% of all strokes. However, hemorrhagic strokes are typically more severe.

These disruptions in blood flow lead to damage to tissues in the brain. Following an ischemic stroke, the interruption in blood flow leads to initial tissue damage due to hypoxia. This is followed by a cascade of pathophysiological events including excitotoxicity and oxidative stress that lead to further neuronal cell death (Brouns & De Deyn, 2009). Following a hemorrhagic stroke tissue damage occurs due to anoxia and compression of brain tissue due to bleeding.

While a stroke can occur in any part of the brain, the most common location for a stroke to occur is in the middle cerebral artery (MCA); more than 50% of ischemic strokes occur in the MCA. The MCA provides blood to the lateral portions of the frontal, temporal, and parietal lobes of the brain. Additionally, the basal ganglia and internal capsule also receive blood from the MCA. Following a stroke in the MCA common deficits include contralateral weakness, sensory impairments, aphasia, and impaired spatial perception. Of particular interest to the research presented in this dissertation are the contralateral weakness, or hemiparesis, and the interruptions in white matter that occur following damage to the internal capsule. The internal capsule carries descending motor commands through corticospinal and corticobulbar fibers.

2.5 Motor deficits in the upper limb following stroke

Stroke is the leading cause of long-term disability and impairments following stroke can vary widely due to size and location of the lesion. Of most interest to the work in this dissertation,

are the deficits seen in the upper limb in individuals with chronic stroke. Most stroke survivors never recover the motor function of their upper limb. Common motor impairments seen in the upper limb include paresis, spasticity, and loss of independent joint control.

2.5.1 Weakness

Post stroke weakness is attributed to damage to the corticospinal tract, leading to an inability to efficiently and fully activate muscles. This weakness manifests itself in impairments in initiating, grading, and timing muscle contractions appropriately. Additionally, upper limb paresis is thought to be greater in the distal muscles, due to the increased role of corticospinal drive in control of the wrist and hand.

2.5.2 Spasticity and hypertonia

Individuals with chronic hemiparetic stroke often exhibit hypertonia and hyperactive stretch reflexes. These impairments are often investigated through measurements of spasticity, which is defined as a velocity-dependent increase in stretch reflexes. Hypertonicity and the associated spasticity are associated with increased excitability of motoneurons, likely due to an increase in monoaminergic drive following stroke. While spasticity has been extensively investigated as a major deficit following stroke, weakness and loss of independent joint control have been found to have the greatest impact on motor function (Sukal *et al.*, 2007; Ellis *et al.*, 2009).

2.5.3 Limb synergies

A loss of independent joint control (limb synergies) are often seen in the upper limb following stroke, with 40-60% of the stroke population exhibiting synergies. Twitchell (Twitchell, 1951) first systematically described a coupling of movements across joints in individuals post

stroke, and Brunnstrom (Brunnstrom, 1970) further categorized the coupled movements in the upper limb as part of either the flexion or extension synergy. The flexion synergy couples shoulder abduction with external rotation at the shoulder, elbow flexion, and supination of the forearm, while the extension synergy couples shoulder adduction with internal shoulder rotation, elbow extension, and pronation of the forearm. This abnormal muscle coactivation pattern is thought to be due to an increased reliance on the reticulospinal tract and its diffuse connections following stroke-induced interruption of corticospinal drive.

2.6 The hypothesized role of brainstem pathways in motor control following stroke

Following a stroke there is often a disruption of the corticospinal and corticobulbar pathways in one hemisphere (Werring *et al.*, 2000). This interruption leads to an increased reliance on corticobulbar projections from the non-lesioned hemisphere and the indirect brainstem pathways (Karbasforoushan *et al.*, 2019).

Damage to corticospinal pathways can lead to extensive losses in dexterous movements of the arm and hand (Kuypers, 1964). Previous work has shown that the level of motor impairment following stroke is correlated with damage to the corticospinal tract (Maraka *et al.*, 2014), and that motor recovery is both related to the integrity (Stinear *et al.*, 2007) and the utilization of remaining corticospinal resources (Favre *et al.*, 2014). Additionally, paresis may be caused by the reduction in corticospinal input reducing the voluntary activation of the muscles following stroke (Garmirian *et al.*, 2019).

The inefficient motor commands elicited from the compensatory brainstem pathways has been a hypothesized cause of the impaired motor activation following stroke. An increased reliance on reticulospinal resources also aligns with the observed motor deficits following stroke. The loss

of independent joint control and the prevalence of the flexion synergy may be caused by the diffuse connections of the reticulospinal tract, and the preferential facilitation of flexors (Ellis *et al.*, 2012; McPherson & Dewald, 2019). Most supraspinal strokes would not impact the reticulospinal fibers, and contralesional corticobulbar fibers can relay motor commands to the bilaterally projecting reticular formation. Additionally, the hypertonicity and spasticity seen in the upper limb may be due to increased neuromodulatory drive from the monoaminergic nuclei in the reticular formation (McPherson *et al.*, 2008; McPherson *et al.*, 2018c).

In addition to the reticulospinal system, other brainstem and spinal pathways may play a role in relaying the motor commands following a stroke. There is some evidence that spasticity and increased motoneuron excitability observed post-stroke may be influenced by alterations in vestibulospinal drive (Miller *et al.*, 2014a; Li & Francisco, 2015) and drive from the vestibulospinal system has been hypothesized to play a role in the extension synergy of the upper limb (McPherson & Dewald, 2019). The propriospinal tract may also play an increased role following stroke, likely from distributing motor commands from the reticulospinal tract. Additionally, the diffuse multi-joint connections of the propriospinal neurons (Alstermark *et al.*, 1990), may play a role in the limb synergies observed post-stroke.

3. Properties of Motor Units of Elbow and Ankle Muscles Decomposed Using High-Density Surface EMG

3.1 Abstract

Analyses of motor unit activity provide a window to the neural control of motor output. In recent years, considerable advancements in surface EMG decomposition methods have allowed for the discrimination of dozens of individual motor units across a range of muscle forces. While these non-invasive methods show great potential as an emerging technology, they have difficulty discriminating a representative sample of the motor pool. In the present study, we investigate the distribution of recruitment thresholds and motor unit action potential waveforms obtained from high density EMG across four muscles: soleus, tibialis anterior, biceps brachii, and triceps brachii. Ten young and healthy control subjects generated isometric torque ramps between 10-50% maximum voluntary torque during elbow or ankle flexion and extension. Hundreds of motor unit spike trains were decomposed for each muscle across all trials. For lower contraction levels and speeds, surface EMG decomposition discriminated a large number of low-threshold units. However, during contractions of greater speed and torque level the proportion of low threshold motor units decomposed was reduced, resulting in a relatively uniform distribution of recruitment thresholds. The number of motor units decomposed decreased as the contraction level and speed increased. The decomposed units showed a wide range of recruitment thresholds and motor unit action potential amplitudes. In conclusion, although surface EMG decomposition is a useful tool to study large populations of motor units, results of such methods should be interpreted in the context of limitations in sampling of the motor pool.

3.2 Introduction

Investigation of motor unit activity in humans affords a more comprehensive view of the neural drive underlying motor output. Traditionally, motor unit recordings were carried out with intramuscular concentric needle or fine wire electrodes. Though these invasive approaches are used in both clinical and research settings, they are usually only effective during low levels of muscle contraction due to the increased superimposition of motor unit action potentials (MUAPs) at higher forces. Further, these methods show high selectivity, can usually only detect a handful of motor units, and often require a trained operator to discriminate individual MUAPs. All of these factors have been a major hurdle in clarifying fundamental questions about the neural control of motor output (Duchateau & Enoka, 2011). In recent years, decomposition algorithms utilizing high-density surface EMG arrays have allowed for non-invasive recordings from a larger population of motor units, across a wider range of contraction levels, and with greater efficiency (Holobar *et al.*, 2014; Negro *et al.*, 2016). These advancements have made it possible to detect dozens of motor units during the same contraction.

Despite these obvious advantages, investigators using these methods must remain aware that surface EMG decomposition may not provide a representative sample of motor units from all muscles. When recording from the skin, the ability to decompose a motor unit is based on the statistical characteristics (spatial and temporal) (Martinez-Valdes *et al.*, 2017; Thompson *et al.*, 2018) and the surface energy of its action potentials (Holobar *et al.*, 2009). This may impede identification of lower-amplitude smaller MUAPs, including those originating deeper within the muscle. Additionally, the number of active motor units comprising the EMG signals may reduce the capacity of the decomposition approaches to separate the contribution of individual units, though to a lesser degree than conventional intramuscular single motor unit analysis techniques.

The goal of the present study was to investigate the distribution of motor unit recruitment threshold and MUAP amplitude in a large sample of recordings from the soleus (SOL), the tibialis anterior (TA), the biceps brachii (BIC), and the triceps brachii (TRI), using an automatic high-density surface EMG decomposition approach (Negro *et al.*, 2016; Martinez-Valdes *et al.*, 2017). According to Hennemans size principle, smaller motor units are recruited before their larger counterparts due to the intrinsic electrophysiological properties of motor units (Somjen *et al.*, 1965). Fine wire analysis has shown that the number of motor units recruited decreases exponentially as force increases, including muscles reported in this paper (Milner-Brown *et al.*, 1972; Kukulka & Clamann, 1981; Feiereisen *et al.*, 1997). Similarly, Oya and colleagues discovered that in the SOL, the number of recruited units decreases as the torque level increases until about 50% MVT and increases afterward (Oya *et al.*, 2009). This is consistent with the notion of a relatively large number of slow motor units with fewer large motor units (Enoka & Fuglevand, 2001). Our current results are contrary to this expectation. However, a moderate level of correlation between MUAP amplitude and force recruitment threshold has been shown previously (Del Vecchio *et al.*, 2018; Martinez-Valdes *et al.*, 2018) and, as stated above, the decomposition algorithm may be biased by amplitude. For the higher contraction levels, the distribution of motor units recruitment threshold was relatively uniform. The number of motor units identified was muscle dependent and decreased considerably at higher torque levels. These factors should be considered in the interpretation of results discriminated from surface EMG decomposition methods.

3.3 Methods

3.3.1 Participants

The data shown in this paper is from two separate experiments, one in the upper limb and one in the lower limb. Ten healthy adults (aged 26.4 ± 3.6, 40% female, 729 units from females, 2196 units from males) participated in these two experiments, with five participants in each. All participants reported having no known neurological or motor impairments. All participants provided informed consent prior to participation in these experiments, which were approved by the Institutional Review Board of Northwestern University (IRB Number: STU00202964 (lower limb); STU00084502 (upper limb)).

Table 3.1: Participants

Subject	Limb	Age	Gender	Units Decomposed
1	Lower	23	F	SOL: 161 TA: 81
2	Lower	26	M	SOL: 108 TA: 195
3	Lower	31	F	SOL: 130 TA: 57
4	Lower	23	M	SOL: 155 TA: 314
5	Lower	25	M	SOL: 176 TA: 313
6	Upper	33	F	BIC: 42 TRI: 69
7	Upper	27	M	BIC: 120 TRI: 131
8	Upper	25	M	TRI: 252
9	Upper	29	M	BIC: 179 TRI: 253
10	Upper	22	F	BIC: 84 TRI: 105

3.3.2 Experimental Apparatuses

Upper limb. Participants were seated in a Biodex experimental chair (Biodex Medical Systems, Shirley, NY) and secured with shoulder and waist straps to minimize trunk movement. In order to measure isometric shoulder and elbow torques, the participant's dominant forearm was placed in a fiberglass cast and rigidly fixed to a six degrees-of-freedom load cell (JR3, Inc, Woodland, CA). The arm was positioned at a shoulder abduction (SABD) angle of 75° and an elbow flexion (EF) angle of 90°. The fingers were placed on a custom hand piece at 0° wrist and finger (metacarpophalangeal) flexion/extension.

Lower limb. Participants were seated in a Biodex experimental chair and secured with shoulder and thigh straps to minimize change in position. Each participant's dominant foot was

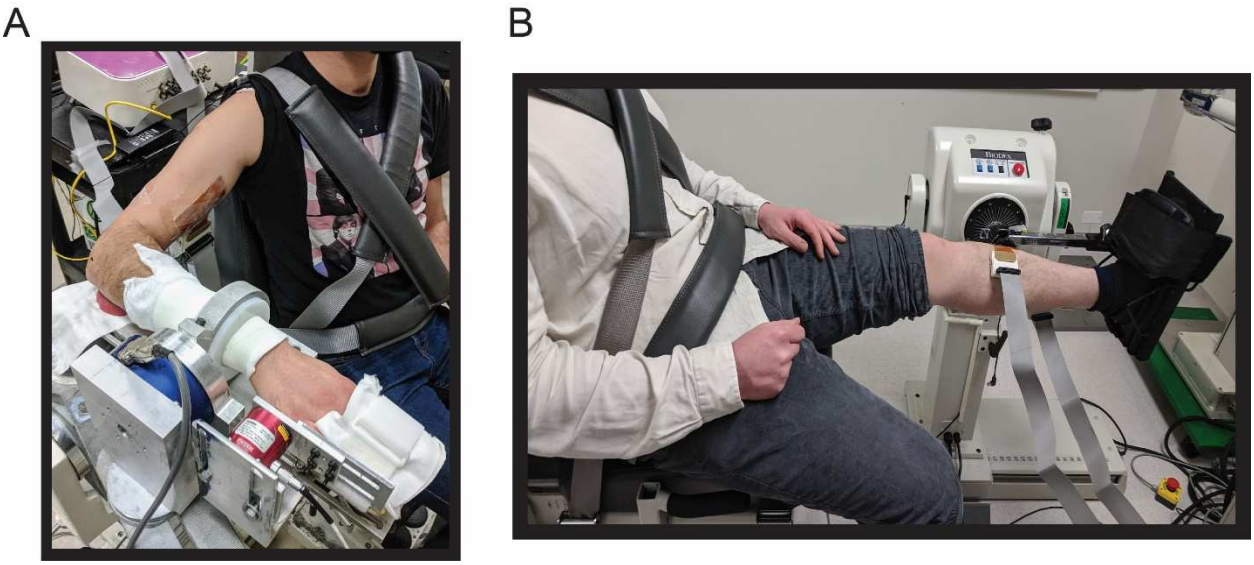

Figure 3.1: Experimental Set-ups
(A) Isometric joint torque recording device with high-density surface EMG grids on the biceps brachii and triceps brachii. (B) Lower limb isometric joint torque recording device with high-density surface EMG grids on the soleus and tibialis anterior.

strapped to an ankle attachment, which was attached to Systems 2 Dynanometer (Biodex Medical Systems, Shirley, NY) to measure the torque. Unless participant expressed discomfort, the ankle was positioned at an angle of 100° and the knee were positioned at an angle of 160°. Bipolar surface EMG recordings were collected from the biceps brachii (BIC), the triceps brachii (TRI), the soleus (SOL), and the tibialis anterior (TA) using grids of 64 electrodes, with 8mm inter-electrode distance. The signals were amplified (x150), band-pass filtered (10-500Hz) and sampled at 2048 Hz (EMG-USB2 for 2 lower limb subjects and Quattrocento for rest, OT Bioelettronica, Turin, IT).

3.3.3 Protocol

Participants were asked to generate maximum voluntary torques (MVTs) during elbow flexion (EF) and elbow extension (EE), in the upper limb, and ankle dorsiflexion (DF) and

plantarflexion (PF), in the lower limb. Trials within a direction were repeated until three trials with peaks within 10% of the maximum torque were collected. Participants were provided with enthusiastic vocal encouragement, as well as real time visual feedback during MVT trials.

Upper limb. Experimental trials entailed the generation of triangular isometric torque ramps. Participants were instructed to gradually increase their EF/EE torque to 20% MVT over 10 seconds, followed by gradually relaxing back to baseline over 10 seconds. Trials consisted of either two or three ramps with ten seconds between ramps and five seconds of baseline at the beginning and end of each trial.

Lower limb. In this experiment, data were collected at varying contraction speed and level; participants were instructed to gradually increase their DF/PF to 10%, 30%, or 50% MVT over 10 seconds, followed by gradual relaxation over 10 seconds. Trials consisted of two ramps with ten seconds between ramps and five seconds of baseline at the beginning and end of each trial.

3.3.4 Data Analysis

All surface EMG channels were visually inspected and those with substantial artifacts or noise were removed. The remaining surface EMG channels were analyzed based on convolutive blind source separation to provide motor unit spike trains (Negro *et al.*, 2016). The silhouette threshold for decomposition was 0.85 for upper limb trials and 0.87 for lower limb trials. All motor units were manually inspected by experienced investigators and only reliable discharge patterns with physiological variability were considered for the analysis. Throughout the decomposition process duplicate motor units were detected and removed if it's cross correlation with an existing unit was greater than 0.3.

MUAPs were reconstructed based on spike-triggered averaging of each of the surface EMG channels in the high-density surface array grid. The root mean square (RMS) amplitude of the MUAP was calculated over a 25 ms window within each channel. In order to reduce inter-subject variance, the RMS amplitudes of the reconstructed MUAPs were all normalized to the maximum RMS MUAP amplitude seen during the highest contraction level trials, within each subject.

3.3.5 Statistical Analysis

Values are presented as means ± standard deviation (SD). For all distributions shown, normality was assessed using the Kolmogorov-Smirnov. Kurtosis and skewness were used to quantify the tailedness and asymmetry, respectively, of the distributions. Wilcoxon rank-sum was performed to compare MUAP RMS values between contraction levels within the SOL and the TA, because data were non-normal. A confidence level of $p < 0.05$ was considered statistically significant.

3.4 Results

3.4.1 Number of decomposed motor units

Figure 3.2 shows firing patterns of motor units during a typical trial. Shown here are 14 units from the TRI with wide range of recruitment thresholds that were collected and decomposed. The black line represents the torque generated by the subject under 20% MVT condition. A total of 730 and 960 motor unit spike trains were decomposed and analyzed for the

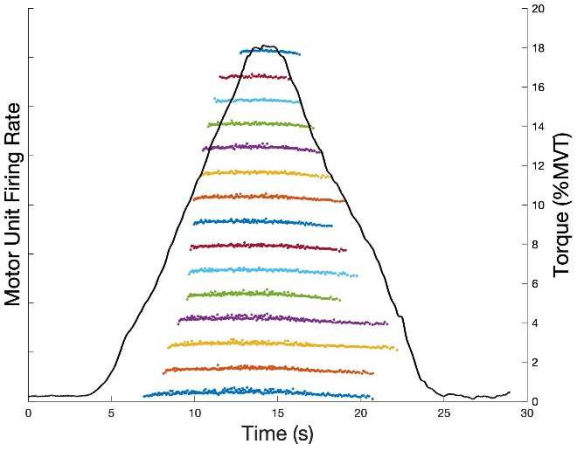

Figure 3.2: Decomposed motor units
The firing patterns of 14 motor units decomposed from the triceps of one subject during a single elbow extension trial, along with the torque trace (black)

SOL and TA, respectively. For 10% MVT, 286 and 338 motor unit spike trains were analyzed; for 30% MVT, 253 and 355 motor unit spike trains were analyzed; and for 50% MVT, 191 and 267 motor unit spike trains were analyzed, for the SOL and TA respectively. A total of 445 motor unit spike trains were analyzed for the BIC and 930 for the TRI.

3.4.2 Recruitment threshold

Figure 3.3 shows the distributions of %MVT at motor unit recruitment from all four muscles during different %MVT ramps. The average recruitment threshold for 10% MVT per subject is 4.4 ± 3%

Table 3.2: Recruitment Threshold Distributions

Muscle	%MVT	Skewness	Kurtosis
Biceps	20	-0.50	3.3
Triceps	20	-0.02	2.3
Soleus	10	0.41	2.1
	30	-0.21	1.9
	50	-0.26	2.1
TA	10	1.1	3.4
	30	0.44	1.7
	50	0.31	1.6

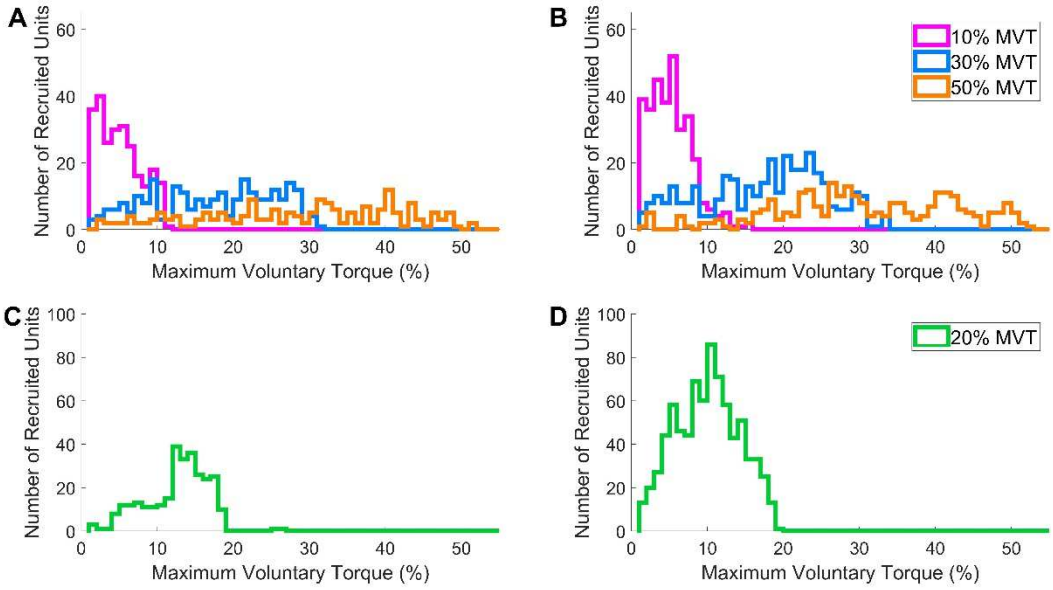

Figure 3.3: Motor unit recruitment thresholds
During 10%, 30%, and 50% MVC for soleus (A) and TA (B). Motor unit recruitment thresholds for biceps (C) and triceps (D) during 20% MVC.

MVT for the SOL and 2.7 ± 3.3% MVT for the TA. The average recruitment threshold for 30% MVT per subject is 16.9 ± 8.3% MVT for the SOL and 10.2 ± 10.6% MVT for the TA. Finally, the average recruitment threshold for 50% MVT per subject is 28.5 ± 12.8% MVT for the SOL and 17.9 ± 17.6% MVT for the TA. In the upper limb, the average recruitment threshold for the BIC and TRI is 12.6 ± 4.1% MVT and 10.0 ± 4.2% MVT respectively, measured at 20% MVT. The skewness and kurtosis for these distributions is showed in Table 3.2.

3.4.3 MUAP amplitude

Figure 3.4 shows the normalized root-mean-squared amplitudes of MUAPs from all four muscles. There is no unit because all the values are normalized. The average MUAP RMS amplitude at 10% MVT for the SOL and TA are 0.35 ± 0.25 and 0.21 ± 0.16, respectively. The same measurement for 30% MVT is 0.36 ± 0.21 in the SOL and 0.29 ± 0.19 in the TA. For 50%

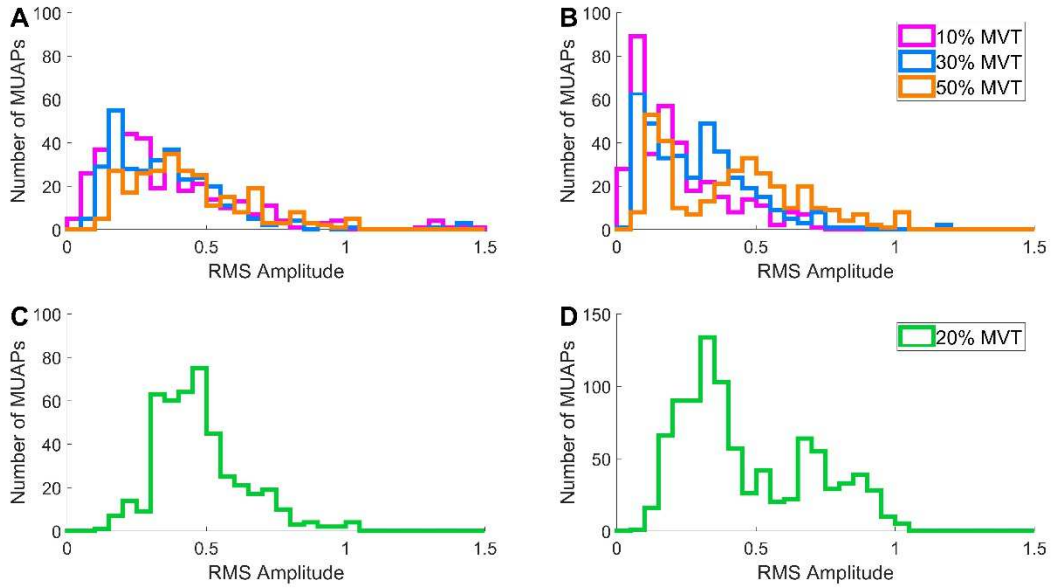

Figure 3.4: Distribution of MUAP RMS amplitude:
for the soleus (A), TA (B), biceps (C), and triceps (D) collected during 10%, 30%, and 50% MVC for soleus and TA and 20% for biceps and triceps.

MVT, the average distributions of MUAP RMS amplitude are 0.43 ± 0.20 in the TA and 0.41 ± 0.24 in the SOL. For the muscles in the upper limb, the average distributions of MUAP RMS amplitude is 0.47 ± 0.15 in the BIC and 0.47 ± 0.23 in the TRI at 20% MVT. For the TA and SOL the distribution of MUAP amplitudes is skewed to the right, across all contraction levels and speeds. The median MUAP amplitudes for the SOL are 0.28, 0.33, and 0.39 at 10%, 30%, and 50%. The median MUAP amplitudes for the TA are 0.17, 0.27, and 0.43 at 10%, 30%, and 50%. The median MUAP amplitude for the BIC and TRI are 0.45 and 0.38, respectively. The skewness and kurtosis for these distributions is listed in Table 3.3. In the SOL, there is a significant increase in the median MUAP amplitude between 10% and 50% ($p < 0.001$) and 30% and 50% contraction levels ($p < 0.001$). The median MUAP amplitude for the TA also increases from 10% to 30% ($p < 0.001$), from 10% to 50% ($p < 0.001$), and from 30% to 50% ($p < 0.001$). However, the large sample size and number of degrees of freedom may play a role in the strength of significance seen.

Table 3.3: MUAP amplitude distributions

Muscle	%MVT	Skewness	Kurtosis
Biceps	20	0.90	4.11
Triceps	20	0.60	2.12
Soleus	10	1.70	6.76
	30	1.91	9.40
	50	0.82	3.26
TA	10	1.14	3.54
	30	1.14	5.18
	50	0.43	2.38

3.5 Discussion

By comparing the number of motor units decomposed in various muscles and different effort levels and contraction speeds, this study highlights some of the protocol dependent limitations inherent in the current implementation of high-density surface EMG decomposition. In

particular, the action potentials of lower-threshold motor units seem more difficult to discriminate during relatively fast ramp contractions at high contraction levels.

Based on the current understanding of motor unit properties and previous fine wire findings, we would expect that the number of units recruited would be skewed toward lower threshold units for all four muscles (Milner-Brown *et al.*, 1972; Kukulka & Clamann, 1981; Feiereisen *et al.*, 1997; Oya *et al.*, 2009). However, as seen in Figure 3.3 our results show that low threshold motor units can be decomposed well during slower contractions at lower effort levels, but, as the contraction speed and effort level increase the number of low threshold motor units decomposed was reduced. Instead, at higher contraction speeds and torque levels we see broader distributions of recruitment thresholds. Recruitment threshold distributions (Table II) show that except for the TA at 10% MVT, every MVT level for the SOL and TA show broad distribution (Kurtosis < 3.0).

The results in Figure 3.4 show that surface decomposition produced a wide range of MUAP amplitudes. A larger number of smaller amplitude units were decomposed in the SOL and TA, when compared with the BIC and the TRI, evidenced by skewness to the right (Table III). As muscle contraction level increases, larger units are recruited (Somjen *et al.*, 1965). Additionally, it has been shown that later recruited units have larger MUAP amplitudes (Del Vecchio *et al.*, 2018; Martinez-Valdes *et al.*, 2018). Our results show that in both the SOL and TA, MUAP amplitudes significantly increase during contractions of higher effort level and speed.

This study shows that surface EMG decomposition is capable of recording a wide range of motor units across multiple muscles, and across several different levels of contraction. These results confirm that although surface EMG decomposition is an improved method to decompose larger number of motor units than more traditional methods such as fine wire electrodes, there are

still limitations. These data demonstrate higher contraction speeds and/or intensities will bias the detection towards units with larger MUAP amplitudes. It is possible that interference from the number of motor units active may be playing a large role in preventing the decomposition of as many low threshold units, and previous work has shown that small deep units may not decompose as well (Holobar *et al.*, 2009). It is also possible that the speed of contraction has affected the decomposition algorithms ability to capture smaller units during high contraction levels. Because the duration of ramps stayed constant for all the contraction levels, the speed of contraction varied from 1% to 5% MVT per second. During high contraction speed, the muscle length changes more rapidly and it has been shown that shortening of muscle length during dynamic contractions changes MUAP shapes, introducing a non-stationarity into the decomposition (Negro *et al.*, 2016). These changes can negatively affect decomposition algorithms ability to discriminate motor units. To achieve better stability during high speed contractions, the algorithm can be modified to follow changes in MUAP shapes (Glaser & Holobar, 2019).

In conclusion, surface EMG decomposition is a useful tool to examine large number of motor units simultaneously across varying contraction levels and muscles. The current protocol compares recruitment thresholds and MUAP amplitudes from different contraction levels, but the results cannot be generalized due to varying speed of contraction. However, these results provide evidence that investigators should be aware that protocols involving high contraction speed may limit the capability of decomposition algorithm to discriminate the activity of motor units with smaller MUAP amplitudes. Future work will aim to improving the algorithm to increase the number of units with smaller MUAP amplitudes detected at high contraction levels. Additionally, further experiments will focus on decomposed units collected during varying contraction levels at a fixed, slower contraction speed.

4. Impact of parameter selection on estimated of motoneuron excitability using paired motor unit analysis

4.1 Abstract

Objective. Noninvasive estimation of motoneuron excitability in human motoneurons is achieved through a paired motor unit analysis (ΔF) that quantifies hysteresis in the instantaneous firing rates at motor unit recruitment and derecruitment. The ΔF technique provides insight into the magnitude of neuromodulatory synaptic input and persistent inward currents. While the ΔF technique is commonly used for estimating motoneuron excitability during voluntary contractions, computational parameters used for the technique vary across studies. A systematic investigation into the relationship between these parameters and ΔF values is necessary. *Approach.* We assessed the sensitivity of the ΔF technique to several criteria commonly used in selecting motor unit pairs for analysis and methods used for smoothing the instantaneous motor unit firing rates. Using high-density surface EMG and convolutive blind source separation, we obtained a large number of motor unit pairs (5,409) from the triceps brachii of ten healthy individuals during triangular isometric contractions. *Main Results:* We found an exponential plateau relationship between ΔF and the recruitment time difference between the motor unit pairs and an exponential decay relationship between ΔF and the derecruitment time difference between the motor unit pairs, with the plateaus occurring at approximately 1s and 1.5s, respectively. Reduction or removal of the minimum threshold for rate-rate correlation of the two units did not affect ΔF values or variance. Removing motor unit pairs in which the firing rate of the control unit was saturated had no significant effect on ΔF. Smoothing filter selection had no substantial effect on ΔF values and ΔF variance; however, filter selection affected the minimum recruitment and derecruitment time

differences. *Significance.* Our results offer recommendations for standardized parameters for the ΔF approach and facilitate interpretation of findings from studies that implement the ΔF analysis but use different computational parameters.

4.2 Introduction

Initial investigations of motoneuron firing patterns proposed that the firing rate of a motoneuron bears a linear relation to the net excitatory synaptic input that the motoneuron receives. However, in recent decades, studies have shown that this relationship is non-linear due to the influence of monoaminergic neuromodulatory synaptic inputs (Bennett *et al.*, 1998; Lee *et al.*, 2003). Serotonin (5-HT) and norepinephrine (NE) are robust monoaminergic neuromodulators that act through G-protein coupled receptors to dramatically change motoneuron excitability by adjusting the response of the motoneuron to excitatory and inhibitory ionotropic input (Heckman & Enoka, 2012). These monoamines have a prominent effect on motoneuron dendrites by activating persistent inward currents (PICs), comprised of slow L-type Ca+ currents and fast persistent Na+ currents, which evoke a sustained depolarization in the cell (Hounsgaard *et al.*, 1984; Bennett *et al.*, 1998). This depolarization leads to amplified and prolonged responses in motoneuron output in relation to excitatory synaptic inputs, creating the distinctive firing patterns we see in motoneurons.

There is a small but growing body of recent work in humans that is beginning to reveal the importance that PICs have in both typical and pathological motor control. In the intact nervous system, the influence of PICs likely varies among muscles throughout the body and may be crucial in the control of muscles with different functions. For example, because the prolonged motoneuron output elicited by PICs is advantageous for muscles that must be activated for extended periods,

postural and anti-gravity muscles are likely to have larger PICs than muscles specialized for fine motor control (Binder & Powers, 2001; Heckman & Enoka, 2012; Wilson *et al.*, 2015). Additionally, abnormal neuromodulatory synaptic input and/or PICs may underlie motor deficits seen in pathological states. In individuals with chronic spinal cord injury, uncontrolled muscle spasms and hyperactive reflexes have been linked to PICs elicited by constitutively active serotonin receptors (Gorassini *et al.*, 2004; Li *et al.*, 2004; Murray *et al.*, 2010; Murray *et al.*, 2011). In individuals with chronic stroke, increased monoaminergic drive and PICs may be partially responsible for hyperactive stretch reflexes and for facilitating the upper extremity flexion synergy (McPherson *et al.*, 2008; Mottram *et al.*, 2009; McPherson *et al.*, 2018a; McPherson *et al.*, 2018b; McPherson *et al.*, 2018c; Karbasforoushan *et al.*, 2019). Weakness associated with sepsis may be related to impaired PICs, as serotonin agonist-induced PICs have also been shown to ameliorate motor neuron firing deficits in a preclinical model of sepsis (Nardelli *et al.*, 2017). This work in pathological populations emphasizes the role that neuromodulatory inputs and PICs play in the control of movement and the importance of their study. Nonetheless, much is still unknown and further study of neuromodulatory inputs and PICs is necessary.

Although PICs cannot be directly measured from human motoneurons, experimental techniques have been developed to estimate the size of PICs in humans via motor unit recordings. Currently, the standard method for estimating PIC amplitude (thus allowing for inference of neuromodulatory synaptic input) is the ΔF technique developed by Gorassini and colleagues (Gorassini *et al.*, 2002). With this technique, PIC amplitude is estimated by quantifying motor unit recruitment/de-recruitment hysteresis (ΔF) using pairs of motor units firing during slow linear "triangle" contractions. The hysteresis of the higher threshold motor unit, as compared to a lower

threshold unit, is thought to represent the decrease in excitatory synaptic input between the level of input at motor unit recruitment and the level of input at motor unit derecruitment. Such a decrease would then be indicative of the contribution of the PIC to motor unit firing. The ΔF metric has been validated through both animal and simulation work (Powers *et al.*, 2008; Powers & Heckman, 2015) and has shown sensitivity to increased monoaminergic drive in humans given amphetamines (Udina *et al.*, 2010).

Conventionally, the ΔF technique requires that motor unit pairs meet certain criteria based on assumptions related to the underlying physiology. For example, the difference in recruitment time between the control (lower threshold) and test (higher threshold) unit must be long enough to ensure that the PIC in the control unit is fully active before test unit recruitment. The control and test units must have sufficient correlation of their firing rates (i.e., the instantaneous firing rate time series of each motor unit, calculated as the inverse of the inter-spike interval of the time series of motor unit action potentials), as the firing rate of the control unit is used as an approximation of the ionotropic excitatory synaptic input to the test unit. Firing rate saturation in the control unit may also bias the ΔF calculation and is often controlled for in these analyses. Despite the use of these standard criteria, the specific parameter values for each criterion vary across studies. Further, there are differences in computational factors across studies, such as the type of filter used to provide a smoothed instantaneous motor unit firing rate time series.

The purpose of the present study is to determine the sensitivity of the ΔF technique to differences in 1) minimum recruitment and derecruitment time difference, 2) minimum rate-rate slope correlation, 3) control unit firing rate modulation, and 4) filter selection. Such a robust sensitivity analysis is now possible as we can obtain spike trains from large populations of motor

units using high-density surface EMG (HD-sEMG) decomposition approaches (Holobar & Zazula, 2007; Chen & Zhou, 2015; Negro *et al.*, 2016). Previous work with ΔF has largely used intramuscular recordings and has therefore been limited by the number of motor units that can feasibly be recorded. Here, we present motor unit data obtained using convolutive blind source separation of HD-sEMG signals (Negro *et al.*, 2016) recorded from the human triceps.

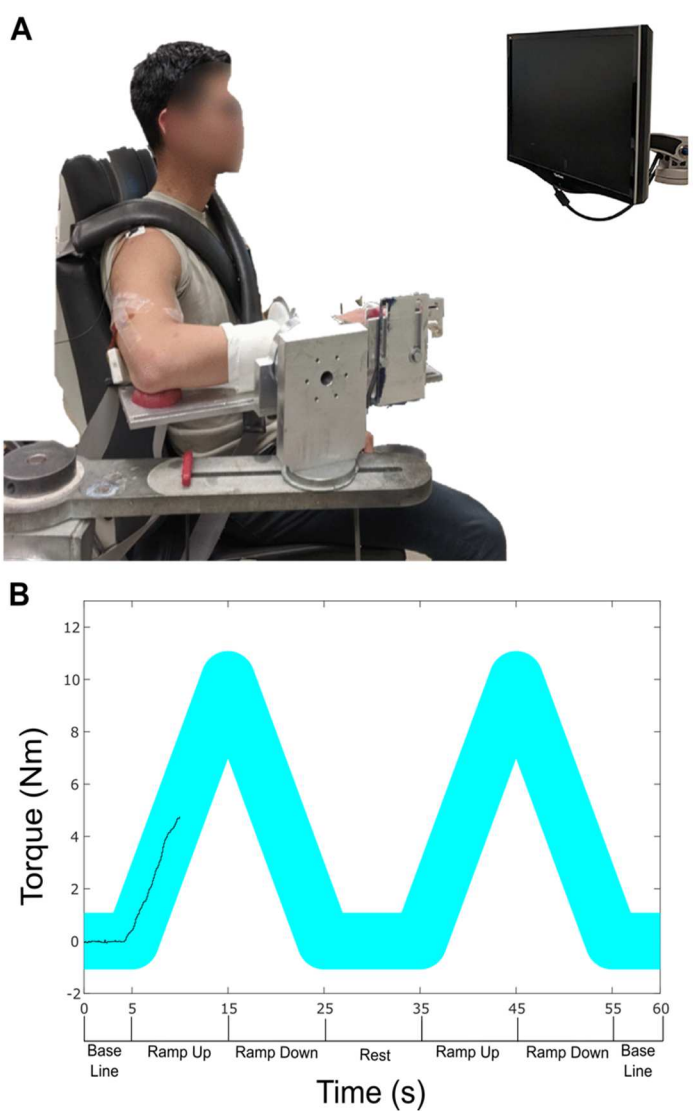

Figure 4.1: Experimental apparatus and visual feedback
Isometric joint torque recording device with high-density surface EMG grids on the biceps brachii and triceps brachii (A). An example of the visual feedback provided to a subject, with the desired torque profile as the wide cyan line, and the generated torque as the black line, along with a timeline of key phases of a typical trial below the x-axis. (B).

4.3 Methods

4.3.1 Participants

Ten adults (3 female, 7 male) ranging in age from 22 to 31 (mean ± SD age: 26.2 ± 2.4) completed the study. For inclusion in this study all participants were required to have: (1) no known neurological injury or disease, (2) no muscular impairment of upper extremity motor function, and (3) no significant visual or auditory impairments. All participants provided written

informed consent prior to participation in this experiment which was approved by the Institutional Review Board of Northwestern University.

4.3.2 Experimental Apparatus

Participants were seated in a Biodex experimental chair (Biodex Medical Systems, Shirley, NY) and secured with shoulder and waist straps to minimize trunk movement. In order to measure isometric elbow torques, the participant's dominant forearm was placed in a fiberglass cast and rigidly fixed to a six degree-of-freedom load cell (JR3, Inc., Woodland, CA). The six degree-of-freedom load cell had an input range of 1115 N for forces in the x and y directions, 2230 N for forces in the z direction, and 127 Nm for torques about the x, y, and z axes. The data recorded across all participants had a maximum force of 539.8 N, and a maximum torque of 83.0 Nm. The arm was positioned at a shoulder abduction angle of 75º and an elbow flexion angle of 90º. The fingers were secured to a custom hand piece at 0º wrist and finger (metacarpophalangeal) flexion/extension (Stienen *et al.*, 2011; Miller & Dewald, 2012; Miller *et al.*, 2014b) (Figure 4.1).

Forces and torques measured at the forearm-load cell interface were recorded at 1024 Hz and, along with limb segment lengths and joint angles, converted into elbow flexion and extension torques using a Jacobian based algorithm implemented by custom MATLAB software (The MathWorks).

Multi-channel surface EMG recordings were collected in single differential mode from the lateral head of the triceps brachii using a grid of 64 electrodes with 8mm inter-electrode distance (GR08MM1305, OT Bioelettronica, Inc., Turin, IT) (Figure 4.1). For 2 of the 10 participants, EMG data were collected using the EMG-USB2+ signal amplifier (OT Bioelettronica, Inc., Turin, IT). For other 8 participants, EMG data were collected on the Quattrocento signal amplifier (OT

Bioelettronica, Inc., Turin, IT), the newer model of the EMG-USB2+. EMG signals were amplified (Quattrocento: x150; EMG-USB2+: x1k-x10k), band-pass filtered (10-500Hz) and sampled at 2048 Hz. For the data collected using the EMG-USB2+, the gain was manually set to maximize signal amplitude without saturating the A/D board (+/- 5V). Data recorded on the Quattrocento had a maximum range of 3.85mV (Quattrocento input range: 33mVpp). Because the EMG recordings and the force/torque recordings were collected on separate computers, a 1 second TTL pulse was transmitted to both computers for use as a marker, and each trial was temporally synced offline using cross-correlation of the TTL pulses.

4.3.3 Protocol

First, participants were asked to generate maximum voluntary torques (MVTs) in the direction of elbow extension. Real-time visual feedback of torque performance was provided on a computer monitor. Trials were repeated until three trials in which the peak torque was within 10% of each other were collected. If the final trial had the highest peak torque, a subsequent trial was collected. Participants were provided with enthusiastic vocal encouragement during MVT trials and were given adequate rest breaks between trials to prevent fatigue.

Experimental trials entailed the generation of triangular isometric torque ramps using real-time visual feedback of elbow flexion/extension torque, shown in Figure 4.1B. Participants were instructed to gradually increase their elbow extension torque to ~20% MVT over 10 seconds and then gradually decrease their torque back to 0% MVT over the subsequent 10 seconds. To facilitate accurate completion of the task, the desired time-torque profile was displayed on the monitor with an overlay of real-time torque performance. Each trial consisted of either two or three ramps in succession, with ten seconds of rest between ramps and five seconds of baseline at the beginning

and end of each trial, where no torque generation was required. Participants were given at least several minutes of rest between trials. Participants were given several practice trials with verbal coaching to become comfortable with the task, followed by five to six experimental trials that were used for subsequent analysis. Torque traces were visually inspected. Trials that did not exhibit smoothly increasing torque from 0% to 20% and smoothly decreasing torque 20% to 0% MVT over the appropriate timeline were discarded, as were trials that exhibited any sudden increases or decreases in torque.

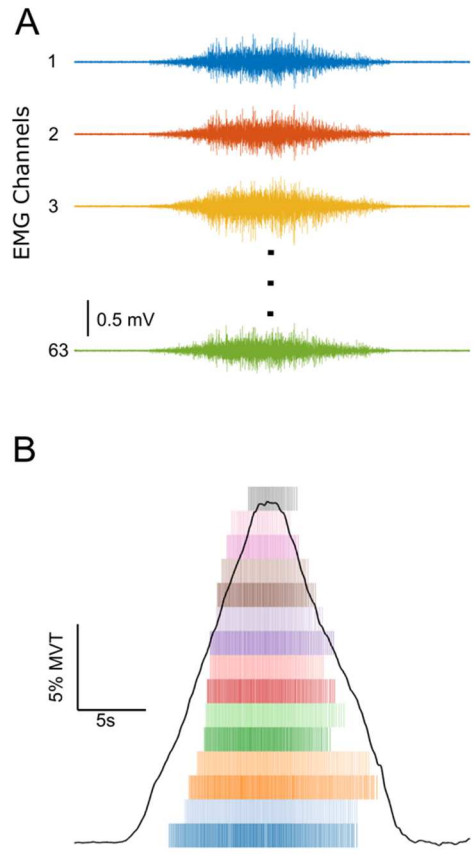

Figure 4.2: Raw EMG and MU decomposition
Raw EMG traces from the high-density electrode placed on the triceps brachii of one participant (A). Elbow extension torque trace and a spike raster plot of MU firings from the same trial (B).

4.3.4 Motor unit decomposition and selection

All surface EMG channels were visually inspected and channels showing substantial artifacts, noise, or saturation of the A/D board were removed (typically zero to five channels were removed per trial). The remaining surface EMG channels were decomposed into motor unit spike trains based on convolutive blind source separation (Negro *et al.*, 2016) and successive sparse deflation improvements (Martinez-Valdes *et al.*, 2017). The silhouette threshold for decomposition was set to 0.85. However, even with this high threshold of decomposition accuracy, the blind source separation algorithm may still extract some solutions which deviate from physiological motor unit

firing patterns. To address these errors, we supplemented the automatic decomposition with visual inspection of the motor unit firings. When potential errors were noted, a local re-optimization of the decomposition parameters was performed by experienced investigators with the use of a custom-made graphical user interface. This approach has been previously applied (Boccia *et al.*, 2019) and provides a high degree of accuracy in the estimated discharge patterns. While the automatic blind source separation does not produce any duplicate motor units, the visual inspection and iterative improvement process occasionally leads to duplicate units due to the separation of merged motor units or removal of erroneous firing times. For this reason, after the visual inspection, all duplicate motor units were detected by cross-correlation and the unit with a higher coefficient of variation in the interspike intervals was eliminated. The instantaneous motor unit firing rates were calculated as the inverse of the interspike intervals of the motor unit spike trains. Figure 4.2 displays raw EMG traces (A), along with the decomposed motor unit spike trains (B).

4.3.5 Paired Motor Unit Analysis

The ΔF technique is a paired motor unit analysis that quantifies the effects of PICs on motoneuron firing patterns by measuring the discharge hysteresis of a higher threshold motor unit (test) with respect to the firing rate of a lower threshold motor unit (control) (Gorassini *et al.*, 2002). Specifically, the ΔF value of the test motor unit is calculated as the difference in the firing rate of the control motor unit between the time of recruitment and derecruitment of the test motor unit. Figure 4.3 illustrates this method of analysis.

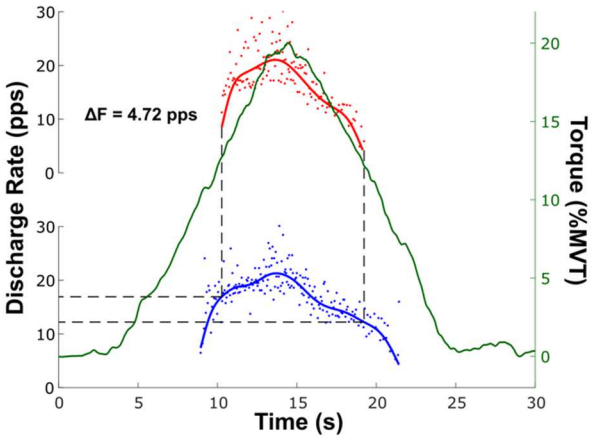

Figure 4.3: ΔF Calculation
An example of the ΔF technique where the change in firing rate of the control unit (blue) is measured at the recruitment (16.93 pps) and derecruitment (12.21 pps) of the test unit (red) taken from the triceps brachii of one participant. The solid blue and red lines represent the smoothed firing rates. The solid green line shows the torque trace for this trial, plotted against the right y-axis.

The ΔF technique first considers every combination of motor unit pairs in which the lower threshold control unit fires through both recruitment and derecruitment of the higher threshold test unit. The test unit must fire for at least 2 s to ensure the PIC can be fully activated (Stephenson & Maluf, 2011). Then, the motor unit pairs must meet additional criteria to be appropriate for further analysis.

Criteria commonly used for the ΔF technique are the following: (1) a minimum time difference between recruitment of the motor unit pairs, (2) a minimum rate-rate slope (reflecting

sufficient shared synaptic input), and (3) sufficient rate modulation in the control unit. Here, we assess the sensitivity of the ΔF calculation to various parameter values of these criteria.

4.3.5.1 Recruitment time difference: The criterion of a minimum recruitment time difference between the control and test motor units is based on the idea that the PIC in the control unit must be fully activated prior to the recruitment of the test unit. Thus, any further changes in the control unit firing rate will reflect a change in excitatory synaptic drive rather than changes in the activation of its PIC. Early work required a minimum of 2 s between recruitment of the control and test unit based on initial literature showing the PIC can take up to 2 s to fully activate (Hounsgaard & Kiehn, 1989; Bennett *et al.*, 2001a; Li *et al.*, 2004). However, simulation work by Powers and Heckman (Powers & Heckman, 2015) has suggested that the effect of recruitment time difference on ΔF and its variance across motor unit pairs diminishes greatly after 0.5 s.

4.3.5.2 Derecruitment time difference: The minimum derecruitment time difference between the control and test units may also have a substantial effect on ΔF due to the rapid decrease in firing rate typical of motor units at derecruitment. Previous work has not investigated the effect of derecruitment time difference on the ΔF analysis; however, deactivation of the PIC in the control unit very close in time to deactivation of the test unit may lead to overestimation of PICs.

4.3.5.3 Rate-rate relationship: The ΔF calculation relies on the assumption that both the control and test unit share substantial synaptic input as quantified using correlation of their rate-rate relationship (firing rate of the test unit as a function of the firing rate of the control unit during test unit firing). A consistent minimum for the rate-rate correlation has not been established. The initial threshold of $r^2 \geq 0.7$ used by Gorrassini and colleagues (Bennett *et al.*, 2001a; Gorassini *et al.*, 2002) has been used extensively (Udina *et al.*, 2010; Stephenson & Maluf, 2011; Wilson *et al.*,

2015). However, other work has used more lenient limits on rate-rate correlation including $r^2 \geq 0.6$ (Mottram *et al.*, 2009) and $r^2 \geq 0.5$ (Powers *et al.*, 2008), and $r^2 \geq 0.3$ (Zijdewind *et al.*, 2014). We investigated the effect of 8 different rate-rate correlation minima ($r^2 > 0$, 0.25, 0.5, 0.7, 0.75, 0.8, 0.85, 0.9) on the ΔF calculation.

4.3.5.4 Rate modulation of the control unit: If the firing rate of the control unit does not reflect the net ionotropic excitatory synaptic drive (e.g., due to decreased rate modulation of that unit), then the PIC amplitude using the ΔF method could be underestimated. Rate modulation in the control unit is here defined as the range of firing rates of the control unit during the time the test unit is active. Previous work (Stephenson & Maluf, 2011; Wilson *et al.*, 2015) has excluded motor unit pairs in which the rate modulation of the control unit is within 0.5 pps of the calculated ΔF, to ensure rate saturation of the control unit is not limiting ΔF. Here we evaluated the effect of removing motor unit pairs which showed control unit saturation on the ΔF calculation.

4.3.5.5 Filter selection: Variation in computational methods used to prepare motor unit firing patterns for the ΔF analysis may affect the results. Gorassini and colleagues' original implementation of the ΔF method fit a 5^{th}-order polynomial to the instantaneous firing rates (Gorassini *et al.*, 2002) while previous motor unit work has filtered instantaneous firing rates using a Hanning window (De Luca & Erim, 1994; De Luca *et al.*, 1996; De Luca & Contessa, 2012) or a Gaussian window (Powers *et al.*, 2008). Due to the use of these smoothing methods in previous ΔF and other motor unit analyses, we have chosen to investigate the effect of these methods on the ΔF results. These smoothing methods have different effects on the firing patterns, particularly as a result of edge effects at motor unit recruitment and derecruitment. The shape of Hanning and Gaussian filters produce sharper downward edges, while the 5^{th}-order polynomial is more sensitive

to doublets and errors, which may disproportionally skew the polynomial fit at recruitment and derecruitment. Here we compare ΔF values, as well as the relationship between recruitment/derecruitment time difference and ΔF, calculated using a 1s Hanning window, a 2 s Hanning window, a 2 s Gaussian window, and a 5th order polynomial to smooth instantaneous firing rates.

4.3.6 Statistical Analysis

Values are presented as mean ± SD. For group means, the mean ΔF was calculated for each participant before averaging across participants. A paired t-test was used to determine whether group mean ΔF was different when removing motor unit pairs with control unit rate saturation compared to not removing those pairs. Separate one-way repeated measures ANOVAs were used to determine the effect of filter type on ΔF values and on the individual participant variance in ΔF. When the effect of filter was significant, post-hoc tests were conducted to compare values between each pair of filter types using the Tukey correction for multiple comparisons. All statistical tests were calculated using GraphPad Prism (version 8.2.0 for macOS, GraphPad Software, San Diego, California USA). Statistical significance was set at $p < 0.05$.

4.3.7 Approach to sensitivity analysis

We first examined the effect of recruitment and derecruitment time difference on ΔF using 3 different rate-rate correlation thresholds and a 2s Hanning window. The Hanning window was chosen to start because it has been used extensively by our group and others (De Luca & Erim, 1994; De Luca & Contessa, 2012) to smooth motor unit firing patterns. For the subsequent analysis of the effect of various rate-rate correlation thresholds, we applied the recruitment and

derecruitment time difference parameters obtained from the first analysis. Then, the recruitment and derecruitment time difference and rate-rate correlation parameters were used for both the analyses of control unit saturation and filter selection.

4.4 Results

In total, 1576 motor unit spike trains were decomposed from the triceps brachii of 10 participants. Each participant completed at least 8 isometric elbow extension triangle contractions with an average yield of 10.4 ± 4.3 motor units per trial. We considered 5,409 motor unit pairs for the ΔF analysis. A small number of these pairs (106) were excluded because the test unit was active for less than 2 s.

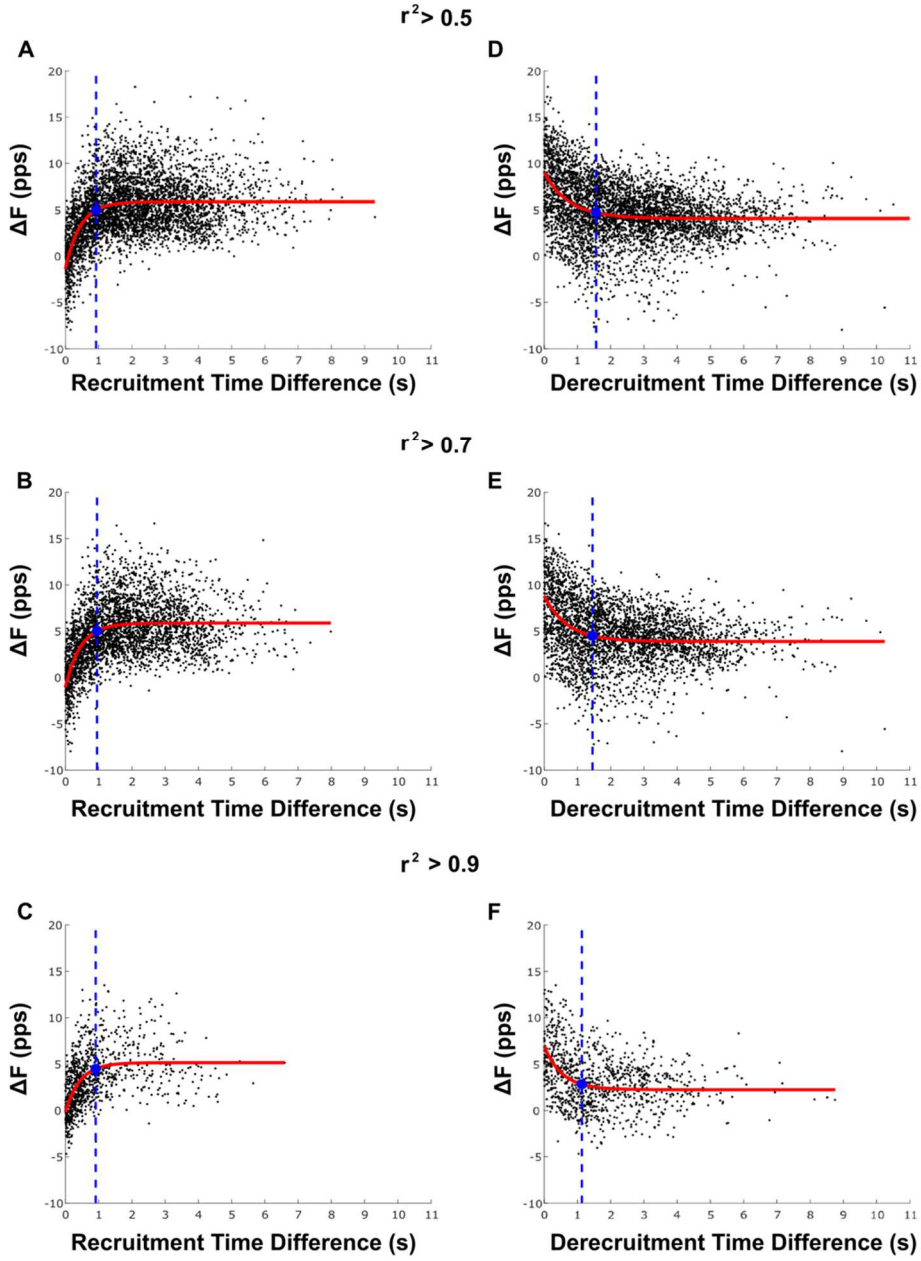

Figure 4.4: Recruitment and Derecruitment time difference

The relationship between recruitment time difference (A,B,C) and ΔF as well as derecruitment time difference (D,E,F) and ΔF is shown for 3 different rate-rate correlation thresholds. The red lines denote exponential plateau (A,B,C) or decay (D,E,F) fits. The blue filled circles indicate where the exponential model is 87.5% from the value at t = 0 to the asymptote value. The blue dotted lines indicate the minimum recruitment/derecruitment time difference used for further analyses.

4.4.1 Relation of ΔF values to recruitment and derecruitment time difference

Figure 4.4 a-c shows the relationship between ΔF values and the time difference between control and test unit recruitment with three different thresholds for rate-rate correlation ($r^2 > 0.5$, 0.7, 0.9). With all three rate-rate correlation thresholds, the ΔF values demonstrated an exponential plateau behavior, rapidly increasing along with recruitment time difference values before plateauing. This exponential relationship has not been previously presented in the literature, but was more apt for our data than the previously demonstrated linear and second order polynomial fits (Stephenson & Maluf, 2011; Wilson *et al.*, 2015). To approximate the minimum recruitment time difference at which ΔF values no longer varied, we fit the data using an exponential plateau function and identified where the exponential fit had grown 3 half-lives, reaching 87.5% of its asymptotic value. This resulted in a recruitment time difference cutoff of 0.92 s, 0.95 s, and 0.91 s for the motor unit pairs with $r^2 > 0.5$, 0.7, and 0.9, respectively.

Figure 4.4 d-f shows the relationship between ΔF values and the time difference between test and control unit derecruitment, with 3 different thresholds for rate-rate correlation ($r^2 > 0.5$, 0.7, 0.9). A decaying exponential plateau function was used to fit the data, and the minimum derecruitment time difference was determined as the point where the exponential fit had decayed 87.5% from the value at derecruitment time difference = 0 to its asymptotic value. The minimum derecruitment time difference was 1.56 s, 1.45 s, and 1.13 s for the motor unit pairs with $r^2 > 0.5$, 0.7, and 0.9, respectively.

Based on these results, we restricted our following analyses to motor unit pairs with at least 1 s difference between control and test unit recruitment times and 1.5 s difference between test and

control unit derecruitment times, which yielded 3,041 motor unit pairs (304.1 ± 178.4 pairs per participant) across all contractions.

4.4.2 Dependence of ΔF on rate-rate correlation

The average number and percentage of motor unit pairs with rate-rate correlation values above each threshold ($r^2 > 0$, 0.25, 0.5, 0.7, 0.75, 0.8, 0.85, 0.9) are shown in Table 4.1. The percentage of retained motor unit pairs decreased dramatically when the r^2 threshold increased beyond 0.5, dropping from 76.1% (2,320 motor unit pairs) with $r^2 > 0.5$ to 49.8% (1,602 motor unit pairs) with $r^2 > 0.7$ to only 6.5% (197 motor unit pairs) with $r^2 > 0.9$.

Figure 4.5 A shows the relationship between group mean ΔF value and each rate-rate correlation threshold. Figure 4.5 B displays the group mean individual participant variance in ΔF across the different thresholds for rate-rate slope correlation. At the majority of the rate-rate slope correlation thresholds (below 0.85), both the group mean ΔF values and group mean individual

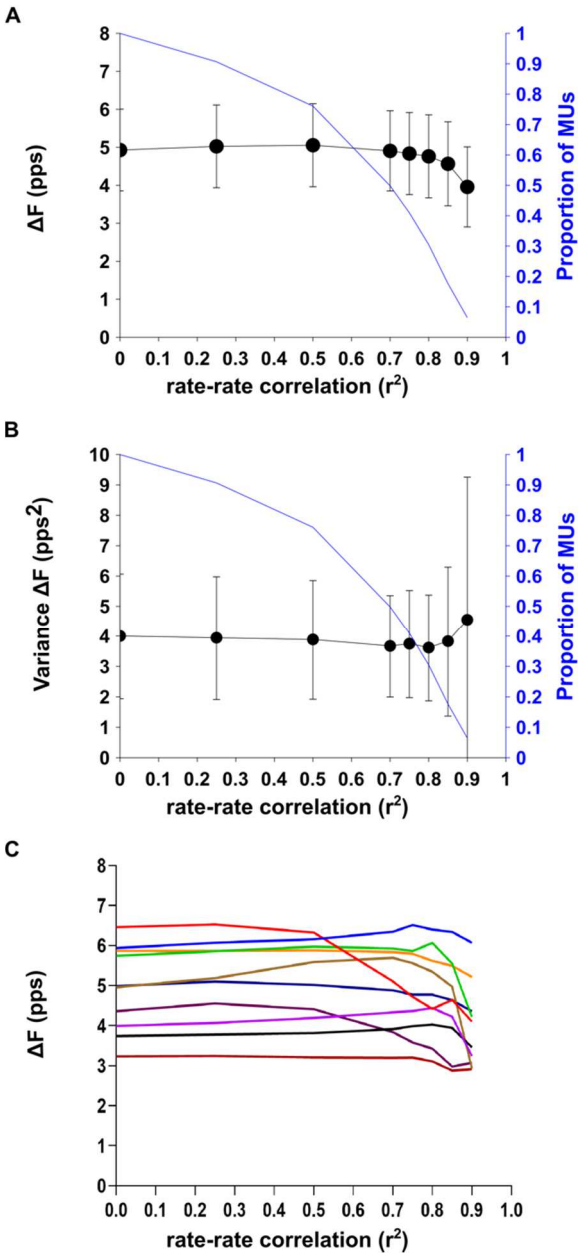

Figure 4.5: Rate-Rate correlation
The group mean ±SD ΔF values (A) and group mean ± SD individual participant variance in ΔF (B) across three different thresholds for rate-rate correlation. The relationship between ΔF and rate-rate correlation threshold for each of the 10 participants is shown in part C.

participant variance remained constant. The group mean ΔF values of ~5 pps are comparable to results from previous work that calculated ΔF in the triceps brachii using motor unit data obtained using intramuscular EMG decomposition (Wilson, Thompson et al. 2015). At the strictest r^2 thresholds ($r^2 > 0.85$ and $r^2 > 0.9$), the group mean ΔF value decreased, and the group mean individual participant variance increased.

Figure 4.5 C shows the relationship between ΔF value and minimum rate-rate correlations for each participant. ΔF values for all participants were relatively stable for r^2 thresholds of up to 0.5. For three participants, ΔF decreased markedly with higher r^2 thresholds whereas values for the other participants fluctuated to a lesser degree.

Table 4.1: Motor unit pairs at various rate-rate correlation thresholds (group mean ± SD)

Minimum r^2	Number of pairs	% of pairs
0.00	304.1 ± 178.4	100 ± 0.0
0.25	276.6 ± 164.8	90.7 ± 0.1
0.50	232.0 ± 146.7	76.1 ± 0.1
0.70	160.2 ± 124.2	49.8 ± 0.2
0.75	133.1 ± 110.8	40.9 ± 0.2
0.80	98.8 ± 83.9	30.5 ± 0.2
0.85	55.8 ± 49.7	17.6 ± 0.1
0.90	19.7 ± 17.5	6.5 ± 0.0

Similar ΔF values and variance were obtained when using no rate-rate correlation threshold as were obtained when using threshold of $r^2 > 0.7$ that has been most commonly used in the literature. Based on this consistency, as well as the higher number of motor unit pairs afforded by removing the rate-rate correlation restriction, we removed the rate-rate correlation criterion in our following analyses.

4.4.3 Dependence of ΔF on control unit firing rate modulation

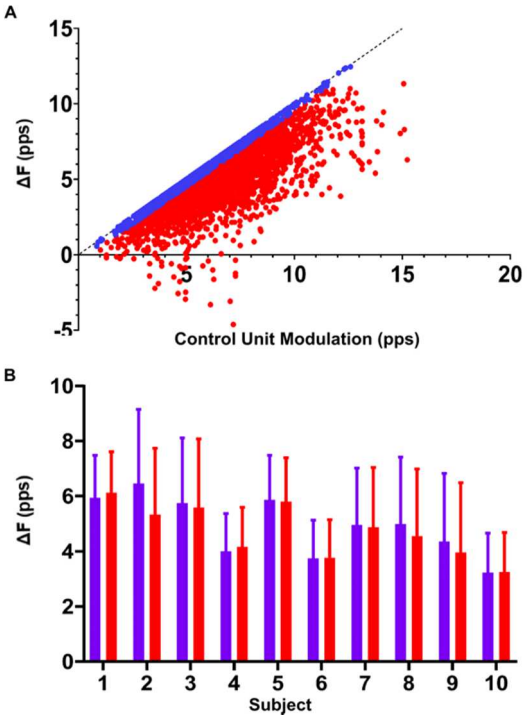

Figure 4.6: Control Unit Saturation
A: The relationship between ΔF and control unit firing rate modulation. Motor unit pairs matching the criteria for control unit saturation are shown in blue. B: The mean ± SD ΔF per subject before (purple) and after (red) the removal of motor unit pairs with control unit saturation.

The maximum ΔF value of a motor unit pair is limited by the amount of rate modulation in the control unit during test unit firing. In order to avoid underestimation of ΔF due to insufficient rate modulation in the control unit, previous studies have removed motor unit pairs in which the ΔF value was within 0.5 pps of the control unit rate modulation (Stephenson & Maluf, 2011; Wilson *et al.*, 2015). Figure 4.6 A shows the relationship between ΔF and the firing rate modulation of the control unit; motor unit pairs that fit the criteria for control unit saturation are shown in blue. The group mean ΔF was 4.9 ± 1.1 pps before removal of pairs which exhibited control unit saturation, and the group mean ΔF was 4.7 ± 1.0 pps following the removal of those pairs. There was no significant change in subject mean ΔF after removal of pairs that fit the saturation criterion ($p = 0.17$). Figure 4.6 B shows the mean ΔF per subject before and after the removal of motor unit pairs that exhibited possible saturation.

4.4.4 Effect of filter selection on ΔF results

The ΔF technique requires filtering of instantaneous motor unit firing rates to provide smoothed continuous firing rates. Figure 4.7 A shows the change in each subject's mean ΔF across

4 different filter methods. The group mean ΔF was 5.1 ± 1.1 pps for the 1 s Hanning window, 4.9 ± 1.1 pps for the 2 s Hanning window, 4.9 ± 1.1 pps for the 2 s Gaussian window, and 5.0 ± 1.1 pps for the fifth-order polynomial fit. The one-way repeated measures ANOVA revealed a significant effect of filter type on ΔF ($P < 0.0001$, $F(3,27) = 11.96$). Post-hoc tests revealed that the 1 s Hanning window resulted in mean ΔF values that were significantly higher than those obtained using the 2s Hanning window (+ 0.18, $p = 0.002$), the 2 s Gaussian window (+ 0.25, $p < 0.0001$), and the fifth-order polynomial (+ 0.15, $p = 0.011$). However, these increases are unlikely to be meaningful given their small magnitudes. The remaining comparisons were not significantly different.

Figure 4.7 B shows the relationship between each participant's variance in ΔF values and filter type. The mean individual participant variance was 4.4 ± 2.3 pps^2 for the 1 s Hanning window, 4.0 ± 2.0 pps^2 for the 2 s Hanning window, 3.9 ± 2.0 pps^2 for the 2 s Gaussian window, and 4.9 ± 2.3 pps^2 for the fifth-order polynomial fit. The one-way repeated measures ANOVA revealed a significant effect of filter type on individual participant variance in ΔF ($P < 0.0001$, $F(3,27) = 20.20$). Post-hoc tests revealed that the fifth-order polynomial resulted in individual participant variances that were higher than for the 1 s Hanning window (+0.47, $p = 0.01$), the 2 s Hanning window (+0.88, $p < 0.0001$), and the 2 s Gaussian window (+0.98, $p < 0.0001$). The 1 s Hanning window led to more variability than the 2 s Hanning window (+0.41, $p = 0.034$) and the 2 s Gaussian window (+0.51, $p = 0.006$). There was no significant difference in variability between the 2 s Hanning window and the 2 s Gaussian window ($p = 0.10$).

Figure 4.7 C shows the relationship between ΔF and recruitment time difference for each filter type. Based on the previous analysis of ΔF vs. recruitment time difference using a 2 s Hanning

window (Figure 4.4), these relationships were modeled as exponential plateau functions. The recruitment time difference at which the exponential fit reached 87.5% of its asymptotic value was smaller for the data smoothed with the 1 s Hanning window (0.50 s) than with the 2 s Hanning window (0.87 s), 2 s Gaussian window (0.91 s), and the fifth-order polynomial, (1.82s). Additionally, ΔF calculated using a fifth order polynomial was less sensitive to the recruitment time difference parameter, with a range of 2.36 pps for the exponential function across the range of observed recruitment time differences, compared to 7.70 pps, 7.53 pps, and 7.39 pps for the 1 s Hanning window, 2 s Hanning, and 2 s Gaussian window, respectively.

Figure 4.7 D shows the relationships between ΔF and derecruitment time difference, modeled using an exponential decay function. The derecruitment time difference at which the exponential fit had decayed 87.5% from the value at derecruitment time difference = 0 to its asymptotic value was similar for the data smoothed with a 1 s Hanning window, 2 s Hanning window, and 2 s Gaussian window (1.78 s, 1.63 s, and 1.65 s, respectively) but was much later for the data smoothed with the fifth-order polynomial (4.09 s). As with recruitment time difference, the fifth order polynomial was least sensitive to the derecruitment time difference parameter. The range of the exponential decay function was 4.02 pps compared with 4.90 pps for the 1 s Hanning window, 5.11 pps for the 2 s Hanning window, and 5.04 pps for 2 s Gaussian.

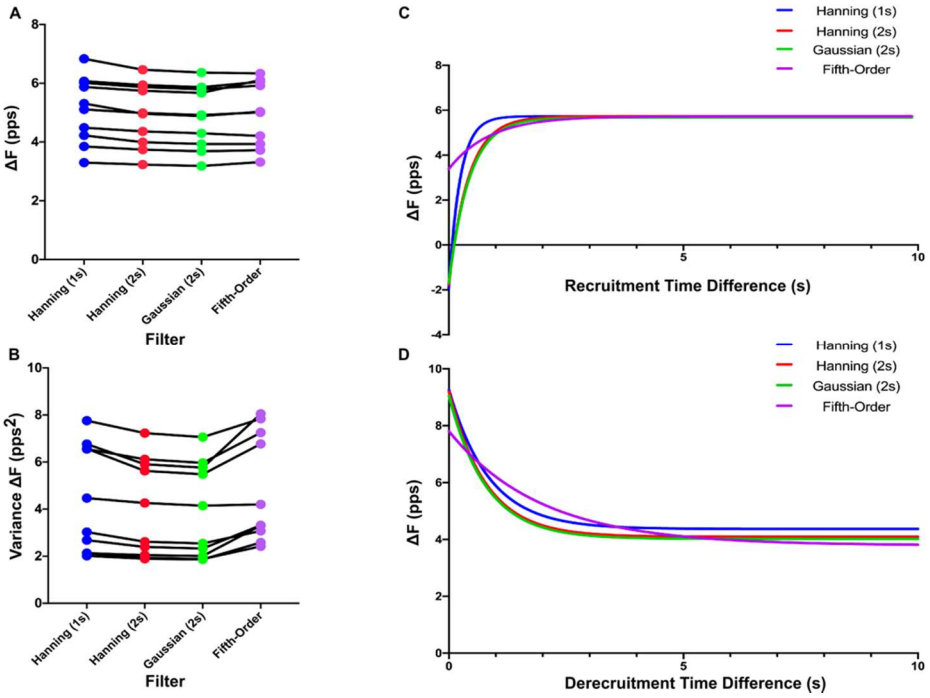

Figure 4.7: Filter Effects on ΔF
Mean ΔF (A) and variance in ΔF (B) for each participant plotted across four filter types. An exponential plateau function showing the relationship between ΔF and recruitment time difference (C) and derecruitment time difference (D) for the same four filter types.

4.5 Discussion

In this study we quantified the relationship between values of ΔF and the methods used to calculate them. By utilizing HD-sEMG and motor unit decomposition, we were able to obtain a much larger sample of motor unit pairs than previous studies, enabling us to systematically explore the sensitivity of the ΔF calculation to different computational parameters.

4.5.1 Effect of recruitment and derecruitment time difference on ΔF

The ΔF technique requires that the PIC of the control unit be active for the duration of test unit firing, to ensure the control unit firing rate varies linearly in response to changes in net excitatory input. If the PIC in the control unit has not been fully activated before the recruitment

of the test unit ΔF may be underestimated. Previous studies have controlled for this by discarding motor unit pairs with recruitment time differences below a certain minimum, however, these thresholds vary across studies from 0.5 to 2 s.

In alignment with previous work (Powers *et al.*, 2008; Stephenson & Maluf, 2011; Wilson *et al.*, 2015), we observed a reduction in ΔF values for motor unit pairs with closely recruited control and test units. Further, we found an exponential plateau relationship between ΔF and recruitment time difference (Figure 4.4). While previous work has modeled this relationship with linear (Wilson *et al.*, 2015) or quadratic (Stephenson & Maluf, 2011) fits, data from the current study demonstrated an exponential plateau function. Because we measured a vastly larger number of motor unit pairs across a wider range of recruitment time differences compared with previous studies, we were able to characterize this relationship in a robust manner, which may explain the differences in type of model fit. Based on the exponential plateau relationship, we identified that a recruitment time difference of ~ 1 s is an appropriate minimum for use in the ΔF calculation. This time course is similar to that of PIC activation recorded from intracellular recordings in rat motoneurons (Bennett *et al.*, 2001a).

Examining the relationship between ΔF and the derecruitment time difference of the test and control units, an exponential decay relationship was observed. When control units that are derecruited closely after the test unit are included in the ΔF calculation, the ΔF value may be overestimated. This finding suggests that the effect of derecruitment time difference on ΔF should be considered and/or controlled for in future studies. The increased ΔF for motor unit pairs with short derecruitment time differences is likely due to the deceleration of the control unit firing rate that typically occurs just prior to derecruitment. PIC inactivation near derecruitment could be one

contributor to this rapid deceleration, as could prolongation of the after hyperpolarization (Wienecke *et al.*, 2009). Additionally, the edge effects of filters used to smooth instantaneous firing rates may enhance the deceleration near derecruitment. A reduced derecruitment time difference may be due to PIC induced onset/offset hysteresis in the test unit, and is accurately reflected by an increase in ΔF. However, the tail end of the control unit may not be an accurate reflection of synaptic input.

4.5.2 Relation between ΔF and rate-rate slope correlation

As the ΔF technique uses the control unit as an estimate of the excitatory synaptic drive to the test unit, previous studies use only motor unit pairs that have a strong correlation between their firings rates. Previous work has commonly used rate-rate correlation thresholds of $r^2 > 0.5$-0.7.

The present study found that reducing or removing the minimum threshold for rate-rate slope correlation did not affect ΔF value or its variance. These results are consistent with findings from the decerebrate cat (Powers *et al.*, 2008). As previously posited, one possible explanation for these results is that the ΔF calculation only measures the control unit firing at two points, test recruitment and derecruitment (Powers *et al.*, 2008). Differences in modulation of the test and control unit that do not occur at test recruitment and derecruitment would affect the rate-rate slope correlation, but not the ΔF value, as long as the control unit is a sensitive indicator of synaptic input at the onset and offset of discharge of the test unit.

While ΔF values were stable across lower minimum correlation thresholds, our results suggest putting stricter limitations on firing rate correlation leads to a decrease in ΔF value and an increase in variance. The increased variance is likely due to the substantially reduced number of motor units available for these analyses. Selection bias may also play a role in the reduced ΔF

values observed with higher rate-rate correlation threshold. Motor unit pairs with higher firing rate correlation are often recruited closely together, which can lead to reduced ΔF if a sufficient minimum recruitment time difference is not used. Additionally, only test units with minimal PIC-induced firing rate nonlinearities would have a sufficiently high correlation with control units that have fully activated PICs, limiting the selection to units with lower ΔF.

The ability to relax the rate-rate correlation threshold without affecting ΔF values may enable a more robust implementation of the ΔF technique in pathological conditions that may alter motor unit firing rate correlation, such as individuals with chronic spinal cord injury (Zijdewind *et al.*, 2014).

4.5.3 Effect of control unit firing rate modulation on ΔF

Due to the nature of the ΔF calculation, the ΔF value for any motor unit pair is limited by the firing rate modulation of the control unit while the test unit is active. Limited rate modulation in the control unit relative to the excitatory synaptic input may lead to an underestimation of ΔF. To address this possible underestimation, previous work has excluded motor unit pairs in which the rate modulation of the control unit during test unit firing was within 0.5 pps of ΔF (Stephenson & Maluf, 2011; Wilson *et al.*, 2015).

The present study found that removing possibly saturated motor unit pairs had no significant effect on group mean ΔF. This result is consistent with findings from intramuscular recordings (Wilson *et al.*, 2015) and suggest that control unit saturation does not have a substantial influence on ΔF value. However, identifying possibly saturated control units using the current method (Stephenson & Maluf, 2011), may also lead to underestimation of ΔF. Pairs with saturated control units often have higher ΔF values due to the mathematical constraints inherent in this

method for determining saturation. One possible solution is to quantify rate modulation in the control unit using a method that is independent of the ΔF calculation. Additionally, the ΔF technique only requires that the control unit be a sensitive indicator of synaptic input at the recruitment and derecruitment time of the test unit, and saturation of the control unit that does not occur at test unit onset or offset would not affect ΔF values.

4.5.4 Influence of smoothing method on ΔF

The ΔF calculation requires a smoothed instantaneous firing rate time series for each motor unit. A variety of different smoothing methods have been previously used, and the method chosen to smooth the instantaneous firing rates may influence the ΔF calculation.

While our results show a significant effect of filter type on ΔF value, the range of group mean ΔF across the smoothing methods (0.25 pps) was negligible relative to the magnitude of ΔF and the only filter to differ from the rest was a 1 s Hanning window. Filter type also had a significant effect on individual participant variance in ΔF, which was highest when using the fifth-order polynomial. This could be attributed to due to this filter's increased sensitivity to doublets and erroneous spikes, particularly at onset and offset, when compared to Hanning or Gaussian filters. Additionally, some units displayed non-physiological increases in firing rates at recruitment or derecruitment when smoothed using the fifth-order polynomial.

There is also an effect of filter type on the ΔF vs. recruitment/derecruitment time difference relationship. When a fifth-order polynomial is used, ΔF varies to a lesser extent across recruitment time difference values compared with the other filter types. Additionally, data smoothed using the shorter 1 s Hanning window reached a plateau in ΔF value at a shorter recruitment time difference than data smoothed using the longer 2 s Hanning and Gaussian windows. These results suggest

that a portion of the observed relationship between recruitment time difference and ΔF is due to the smoothing of instantaneous firing rates, in addition to the rapid firing rate acceleration associated with PIC activation. Data smoothed with the fifth-order polynomial were also less sensitive to derecruitment time difference, though to a lesser extent than recruitment time difference. There was minimal difference between smoothing firing rates with the shorter 1 s Hanning window and the 2 s Hanning or Gaussian window. This is possibly due to the slower time course and smaller magnitude of the effect of derecruitment time difference on ΔF compared with recruitment time difference.

4.6 Conclusions, limitations, and future directions

Previous studies utilizing the ΔF technique have required motor unit pairs to meet certain criteria based on physiological assumptions. This study assessed the relationship between ΔF values and the commonly used criteria and smoothing filters. The data presented here indicate that the following methodological considerations may enable more accurate estimation of PIC amplitude using the ΔF technique: (1) the control unit should be recruited a sufficient time (~1 s) before the test unit to avoid underestimation of ΔF; (2) the control unit should also be derecruited a sufficient time (~1.5 s) after the test unit to avoid overestimation of ΔF; (3) reduction or removal of rate-rate correlation restrictions does not affect ΔF values or variance; (4) Filter selection for smoothing instantaneous firing rates has little effect on ΔF values, however, the fifth-order polynomial showed increased individual participant variance compared with the Hanning and Gaussian filters, and therefore may not be the best smoothing option. Additionally, filter selection may affect the minimum recruitment and derecruitment time difference function shown in Figure 4.4 for the Hanning window, and therefore a suitable minimum value should be determined for the

specific filters being used; (5) Removal of possibly saturated control units had no effect on ΔF values. *Limitations and Future Work:* This work was conducted in one muscle of young healthy participants which may affect the generalizability of findings. It is possible that the relationships between ΔF and the criteria and filters investigated here may vary in different muscles or populations. Additionally, while this work evaluated the influence of several common smoothing filters on ΔF, there are a number of additional smoothing methods, as well as a larger range of filter window lengths, that could still be explored. Future work will continue to compare methods for the comprehensive quantification of PICs in humans. The results of this robust sensitivity analysis allow for comparison between the paired motor unit analysis and any novel methods to characterize PIC behavior.

5. Estimates of persistent inward currents (PICs) are reduced in upper limb motor units of older adults

5.1 Abstract

Aging is a natural process that causes alterations in the neuromuscular system, which contribute to weakness and reduced quality of life. Reduced firing rates of individual motor units (MUs) likely contribute to weakness, but the mechanisms underlying reduced firing rates are not clear. Persistent inward currents (PICs) are crucial for the initiation, gain control, and maintenance of motoneuron firing, and are directly proportional to the level of monoaminergic input. Since the concentration of monoamines (i.e. serotonin and norepinephrine) are reduced with age, we sought to determine if estimates of PICs are reduced in older (>60 years old) compared to younger adults (<35 years old). We decomposed MU spike trains from high-density surface electromyography over the biceps brachii and triceps brachii during isometric ramp contractions to 20% of maximum. Estimates of PICs (i.e. ΔF) were computed using the paired MU analysis technique. Regardless of the muscle, peak firing rates of older adults were reduced by ~1.6 pulses per second (pps) ($P = 0.0292$), and ΔF was reduced by ~1.9 pps ($P < 0.0001$), compared to younger adults. We further found that age predicted ΔF in older adults ($P = 0.0261$), resulting in a reduction of ~1pps per decade, but there was no relationship in younger adults ($P = 0.9637$). These findings suggest that PICs are reduced in older adults, and, further, age is a significant predictor of estimates of PICs in older adults. Reduced PIC magnitude represents one plausible mechanism for reduced firing rates, weakness, and reduced function in older individuals.

5.2 Introduction

Aging is a natural process that causes alterations within the neuromuscular system, which can have severe consequences on health and quality of life in older adults (McNeil & Rice, 2018). Even in the absence of disease, there is age-related loss of muscle or lean mass (i.e. sarcopenia), and, perhaps more importantly, age-related loss of strength (i.e. dynapenia). Emerging evidence suggests that dynapenia is a significant contributor to quality of life in the elderly (Mitchell *et al.*, 2012). Indeed, biophysical properties of the muscle play a role in the reduced force generating capacity, but neural factors are likely to contribute as well.

There is a progressive loss in the number of motor units (MUs) with age (McNeil *et al.*, 2005), which comprise the muscle fibers and their parent motoneurons (Heckman & Enoka, 2012). As such, death of motoneurons is widely accepted as a precursor for many of the age-related adaptations in the nervous system (McNeil & Rice, 2018). Following death of motoneurons, the nervous system displays astounding plasticity, as evidenced by the reinnervation of orphaned muscle fibers by axonal sprouting (Gordon *et al.*, 2004), a process known as MU remodeling (Hepple & Rice, 2016). Since it is speculated that the loss of larger/faster motoneurons precedes the loss of smaller/slower type motoneurons (Kanda & Hashizume, 1989), reductions in MU firing rates are typically ascribed to this mechanism. Dalton et al. (Dalton *et al.*, 2010) previously showed that the firing rates of both biceps brachii (BIC) and triceps brachii (TRI) MUs are reduced across a wide range of contraction intensities in older, compared to young, adults. They suggested that the relatively higher proportional loss of higher threshold motoneurons may play a role in the age-related decline in firing rates, but alterations in the biophysical properties of the motoneurons are also likely to contribute.

Altered intrinsic motoneuron excitability may play a major role in age-related changes in motoneuron firing patterns. Although motoneurons were once believed to integrate their synaptic inputs passively, many studies have demonstrated that this integration is a highly active process due to voltage-sensitive ion channels in their dendrites (Heckman *et al.*, 2008a; Heckman *et al.*, 2008b). Persistent inward currents (PICs) amplify and prolong excitatory synaptic input to the motoneuron (Lee & Heckman, 1998a, 2000), which are the result voltage-gated slow activating L-type Ca^{2+} and fast activating persistent Na^{+} currents (Heckman *et al.*, 2008b). PICs are activated near threshold and can amplify synaptic currents by as much as 3-5 fold (Binder & Powers, 2001), and the level of PIC activation is highly dependent on the neuromodulatory drive from the monoaminergic system (i.e. serotonergic and noradrenergic drive) (Lee & Heckman, 1998a, 2000). In addition, PICs are reduced with antagonist muscle afferent input (i.e. reciprocal inhibition), illustrating a role for inhibition in the control of PIC activity (Heckman *et al.*, 2008a; Powers *et al.*, 2012). Therefore, changes in levels of monoaminergic drive, intrinsic motoneuron excitability (i.e. monoamine receptor or ion channel function), and inhibition may alter MU firing patterns, as well as estimates of PICs, with age (Johnson *et al.*, 2017).

Furthermore, recent work has called for the investigation of PIC estimates in the aging neuromuscular system (Latella, 2021). The function of two primary monoaminergic nuclei in the brainstem, the raphe nuclei and locus coeruleus, have been shown to deteriorate with age (Shibata *et al.*, 2006; Pagano *et al.*, 2017). This deterioration likely results in reduced monoaminergic drive, and consequently reduced activation of PICs.

Fortuitously, recent advances in technology have enabled us to sample from large populations of concurrently active MUs, by using high-density surface electromyography (HD-

sEMG) array electrodes and blind source separation algorithms (Holobar & Zazula, 2007; Negro *et al.*, 2016) with great success (Yavuz *et al.*, 2015; Del Vecchio *et al.*, 2018; Thompson *et al.*, 2018; Cogliati *et al.*, 2020; Del Vecchio *et al.*, 2020; Hassan *et al.*, 2020; Kim *et al.*, 2020; Martinez-Valdes *et al.*, 2020). This non-invasive technology has created an opportunity to further study the age-related alterations in the neuromuscular system by sampling from many concurrently active MUs. Using this technology allows us to gain better appreciation of the population behaviour and provide more insights about the control of large portions of the motor pool, which was difficult to achieve with intramuscular EMG approaches.

In this study, we examined whether the MU firing characteristics in a large population of concurrently active MUs differed between a group of younger and older adults. More specifically, we compared MU firing patterns of the elbow flexor and extensors during triangular isometric contractions. We hypothesized that since previous work has shown MU firing rates are reduced in older adults, we would observe reductions in peak firing rates of both BIC and TRI MUs, as well as estimates of PIC magnitude (i.e. ΔF), in the older group. In addition, since healthy younger adults are unlikely to have an impairment in PIC function, we investigated the relationship between age and estimates of PICs in both groups separately. We hypothesized that there would be no relationship between age and estimates of PICs in the younger group, however there would be a negative relationship between age and estimates of PICs in the older group.

5.3 Methods

5.3.1 Participants

In order to compare MU firing behaviour between healthy younger and older individuals, we recruited 10 younger (26 [2.87] years old, 3 female) and 10 older (67 [4.40] years old, 2 female) adults. At the time of testing, all participants were free of neurological, motor, and muscular impairments. All participants provided written informed consent in accordance with the Declaration of Helsinki, which was approved (STU00084502-CR0003) by the Institutional Review Board of Northwestern University.

5.3.2 Experimental Apparatus

The experimental apparatus, protocol, and data processing methods utilized is similar to those used in a previous experiment in our lab (Hassan *et al.*, 2020). Participants were secured in a Biodex chair (Biodex Medical Systems, Shirley, NY) with their dominant upper limb rigidly fixed to a six degree-of-freedom load cell with a fiberglass cast (JR3, Inc., Woodland, CA). The casted arm was positioned at a shoulder abduction angle of 75º and an elbow flexion angle of 90º. An illustration of the experimental setup is shown in Figure 1.

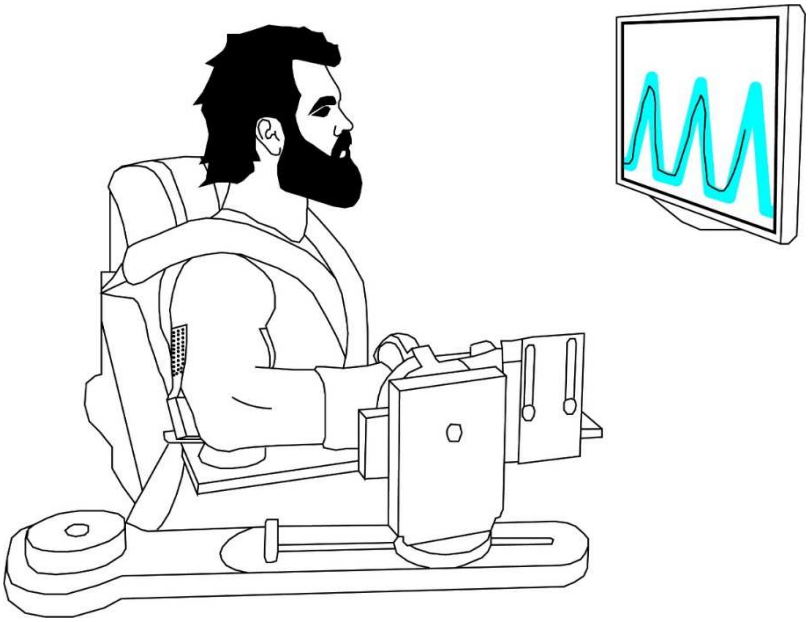

Figure 5.1: Illustration of the experimental setup.
High-density surface electromyography (HD-sEMG) arrays were placed on the lateral head of the TRI and along the muscle belly of the BIC.

High-density surface EMG (HD-sEMG) arrays (64 electrodes, 13x5, 8mm I.E.D., GR08MM1305, OT Bioelettronica, Inc., Turin, IT) were placed on the BIC and the lateral head of the TRI on the casted limb. HD-sEMG data were sampled (2048 Hz), amplified (x150), and band-pass filtered (10-500Hz) using a Quattrocentro signal amplifier (OT Bioelettronica, Inc., Turin, IT). A reference electrode was placed on the acromion process of the casted arm. Prior to collecting experimental data, real-time HD-sEMG recordings were checked visually to ensure high signal-to-noise ratios.

Torque was sampled at 1024 Hz with a forearm-load cell interface. The limb segment lengths and joint angles were converted into elbow flexion and extension torques using a Jacobian based algorithm implemented by a custom MATLAB software (MathWorks). As EMG and force/torque recordings were collected using separate computers, a 1 second TTL pulse was transmitted to both computers for data alignment. Each trial was temporally synced offline using cross-correlation of the TTL pulses.

5.3.3 Experimental Protocol

Participants were initially asked to produce their maximum voluntary torques (MVTs) in the directions of elbow flexion or extension. A wall-mounted computer monitor placed directly in front of participants provided real-time feedback of torque performance. MVT trials were repeated until three trials in which the peak torque was within 10% of each other were collected. If the last trial had the highest peak torque, an additional MVT trial was collected. Participants were verbally encouraged during MVT trials to ensure peak torque performance and were given adequate rest between trials to prevent muscle fatigue.

Each of the subsequent experimental trials consisted of three triangular isometric elbow extension/flexion torque ramps, separated by 10 seconds of rest. Each ramp required participants to increase torque (2% MVT/s) to 20% MVT over 10 seconds, and then decrease (-2% MVT/s) to 0% MVT over the next 10 seconds. During all trials, real-time torque feedback, as well as the desired experimental torque profile, were provided to the participants. In order to avoid fatigue, a minimum of 2 minutes of rest was given to participants between trials. Trials that did not exhibit a smooth increase of torque from 0% to 20% MVT and a smooth decrease of torque from 20% to 0% MVT over the desired timeframe were discarded, as were trials that display any sudden jerks in torque.

5.3.4 Data Analysis

MU Decomposition & Variables of Interest

After data acquisition, each EMG channel of the surface array was manually inspected and any channels with substantial artifacts, noise, or analog to digital saturation were removed. A convolutive blind-source separation algorithm (Negro *et al.*, 2016) with a silhouette threshold of 0.85 was used to decompose HD-sEMG into individual MU spike trains. All decomposed MU spike trains were visually inspected for each participant and trial through a custom-made graphical user interface in MATLAB. Any minor errors were corrected by local re-optimization of decomposition parameters in a manner similar to recent studies using the same blind source separation algorithm (Boccia *et al.*, 2019; Afsharipour *et al.*, 2020; Del Vecchio *et al.*, 2020; Hassan *et al.*, 2020; Martinez-Valdes *et al.*, 2020). Instantaneous MU firing rates were calculated as the inverse of the interspike intervals of each MU spike train and smoothed using a 2 second Hanning window using a custom-written MATLAB script.

Peak, total duration, and total range of smoothed decomposed MU firing rates were extracted through custom written MATLAB scripts for each muscle. MU range and duration during the ascending and descending phases of torque production were also extracted (see Figure 2). Further, to provide a measure of the symmetry of MU firing throughout the ascending and descending phases of torque, we calculated a ratio of the MU firing duration using the following formula:

$$Duration\ Ratio = \frac{(Duration_{ascending} - Duration_{descending})}{Duration_{total}} \quad (1)$$

The duration ratio produced values between -1 and 1, with a MU that was only active on the ascending limb having a value of 1 (leftward shift; less hysteresis), and a MU that was only active on the descending limb producing a value of -1 (rightward shift; more hysteresis).

Estimating Persistent Inward Currents (PICs)

The effects of persistent inward currents (PICs) on motoneuronal firing patterns can be appreciated through MU onset-offset hysteresis. The best approximation of this hysteresis, Delta F (ΔF), is calculated as the difference in the smoothed firing rate of a reporter (lower threshold) MU between the times of recruitment/derecruitment of a test (higher threshold) MU (Gorassini *et al.*, 2002). All ΔF values used throughout this study are "unitwise" mean values. That is, the average of ΔF values obtained for each test unit from all possible reporter units (see Figure 2). Criteria for inclusion of ΔF values from MU pairs were that the test MU was 1) recruited at least 1 second after the control unit to ensure full activation of PIC, and 2) derecruited at least 1.5 seconds prior to the control MU to prevent ΔF overestimation (see Hassan et al. (Hassan *et al.*, 2020) for more details on utilizing ΔF for paired MU analysis).

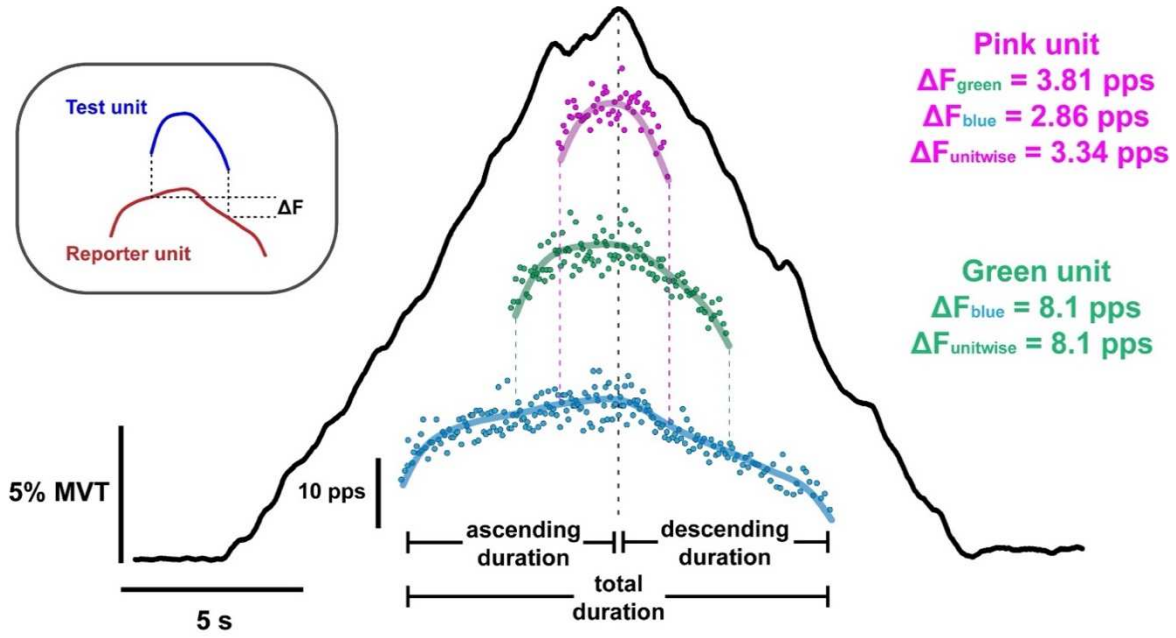

Figure 5.2: Motor Unit Analyses
Top left shows the paired MU analysis method used to estimate persistent inward current magnitude, which quantifies the onset-offset hysteresis (i.e. ΔF) of a higher threshold (test unit; blue) MU with respect to a lower threshold (reporter unit; red). In the center, a typical extension torque trace (black line) from one younger participant is shown. Underneath the torque ramp, 3 out of the 12 decomposed MU firing patterns are shown. Each point indicates the instantaneous firing rate for each interstimulus interval, and the thick coloured lines indicate the smoothed firing rates of each MU. At the ends of the green and pink unit are vertical dotted lines that extend downward to the units below them (i.e. recruited at lower torque), which helps indicate the onset and offset of firing with respect to their reporter units. Individual ΔF values obtained from each reporter unit, and the mean of those values (ΔF unitwise) is shown for each test unit. The vertical black dotted line indicates peak torque in this ramp for ease of viewing the time point between ascending and descending duration.

5.3.5 Statistical Analysis

All data was imported into GraphPad (version 9.0.1 for Windows, GraphPad Software, San Diego, California USA) where descriptive statistical analyses were performed. Hedge's g effect

sizes (ES) were calculated to provide a standardized effect for the mean differences between the younger and older subjects for each variable. Mean and standard deviation values for each variable reported are group means, which represent the average and error of the individual means computed for each participant.

We detail the effects of healthy aging on MU firing characteristics using linear mixed effects models. More specifically, we take into consideration all of our data points rather than averaging across them and basing our analysis on the mean within an individual trial or subject (Giboin *et al.*, 2020). All of these analysis were performed in R (R Core Team 2020, R Foundation for Statistical Computing, Vienna, AUT) using the lme4 package (Bates & Maechler, 2015) and significance was calculated using the lmerTest package (Kuznetsova *et al.*, 2017), which applies Satterthwaite's method to estimate degrees of freedom and generate p-values for mixed effects models by comparing the full model including the effect of interest against a null model excluding the effect of interest.

We used linear mixed effects models to determine if age group (categorical) and muscle were significant predictors for our MU variables. We employed age group (younger vs. older), muscle (BIC vs TRI), and their interaction as fixed effects. As random effects, we included a random intercept for each subject as well as a random slope accounting for the muscle within each subject. Effects estimated from the linear mixed effects models are presented as parameter estimates ± SE.

In order to avoid the bimodal distribution of ages created by our selective sampling of healthy younger and older adults, we used separate generalized linear mixed effects models (computed by the MuMIn R package (Barton, 2018) to identify significant relationships between

ΔF and age in the younger and older groups. This was done to assess the degree to which the age of the subjects in each group could account for variance in ΔF. Specifically, we analyzed whether age was able to predict ΔF. For each age group, we included age (continuous variable), muscle (TRI vs. BIC), and their interaction as fixed effects. As random effects, we included a random intercept for each subject as well as a random slope accounting for the muscle within each subject. Variance accounted for by the model is reported as conditional R^2GLMM values, whereas variance accounted for by only the fixed effects is reported as marginal R^2GLMM values (Nakagawa & Schielzeth, 2013; Johnson, 2014; Nakagawa & Schielzeth, 2017).

5.4 Results

In the ten younger participants, decomposition yielded 1002 MU spike trains from the BIC, and 1211 MU spike trains from the TRI. In the ten older participants, decomposition yielded 533 MU spike trains from the BIC, and 827 from the TRI. All participants completed a minimum of 10 submaximal torque ramps in the directions of EF and EE. An average of 6.2 (3.81) and 9.0 (4.99) MUs per trial were decomposed from the BIC and TRI, respectively, of younger participants, and 4.4 (1.60) and 6.7 (3.39) MUs per trial were decomposed from the BIC and TRI, respectively, of older participants. Following the visual inspection and removal of erroneous spike times, the mean silhouette values of the decomposed motor units were 0.91 (0.05) from the BIC and 0.90 (0.05) from the TRI of the younger participants. The mean silhouette values from the older participants was 0.91 (0.04) from the BIC and 0.93 (0.05) from the TRI. An example of smoothed MU firing rate patterns of decomposed TRI MUs in a single trial from one younger and older individual are shown in Figure 3, which shows many of the features that will be quantified below.

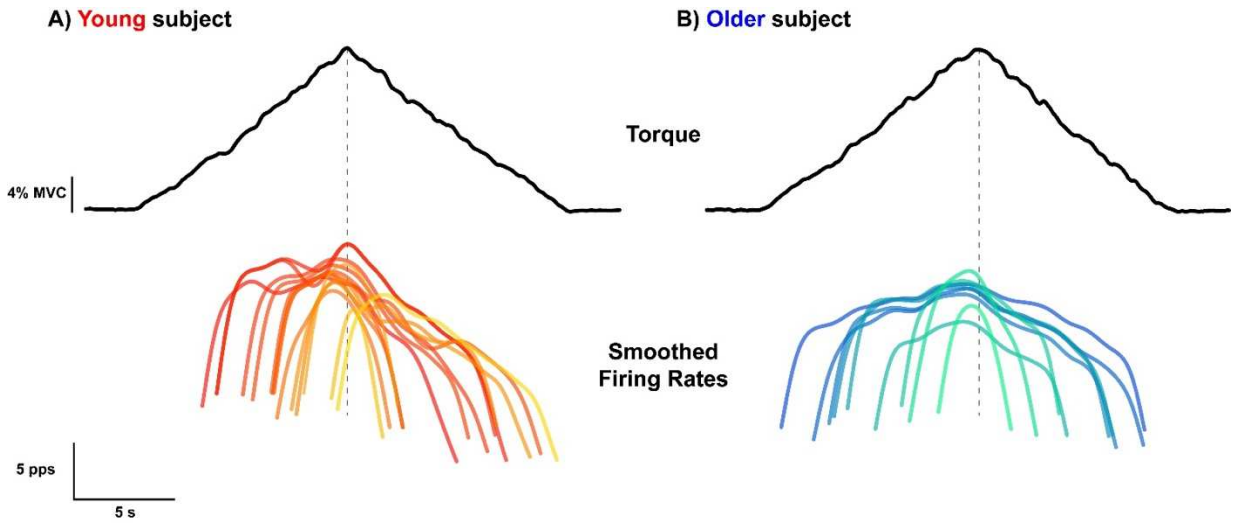

Figure 5.3: Motor unit traces during elbow extension
Single trial elbow extension torque (top; black traces) and smoothed firing rates of all decomposed triceps brachii MUs (bottom; coloured traces) for a younger (left; A) and an older (right; B) participant. Smoothed firing rates are darker at lower thresholds, and lighter for higher thresholds for both participants.

5.4.1 Comparison of peak MU firing rates

The peak firing rates from BIC and TRI MUs are shown in Figure 4. In this, and in the following figures, each data point represents the mean value from all MUs collected from one subject during the submaximal EF torque ramps (BIC data) or submaximal EE torque ramps (TRI data). In congruence with previous findings (Dalton *et al.*, 2010), older

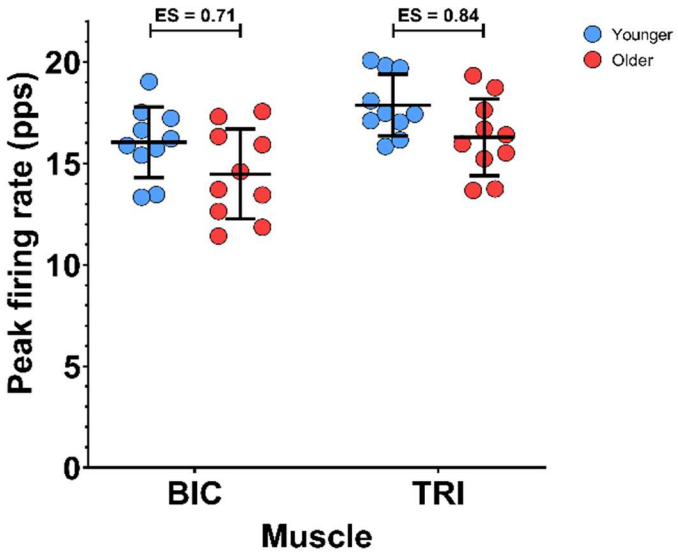

Figure 5.4: Peak firing rate in older and younger adults
Individual participant means (younger = blue; older = red) and group mean and SD (black) for the peak firing rate of BIC (biceps brachii) MUs during a 20% elbow flexion ramp, and TRI (triceps brachii) MUs during a 20% elbow extension ramp.

participants had reduced peak firing rates compared to younger participants. Group mean peak firing rates for the younger participants were higher than observed in the older participants in both the BIC (16.0 [1.74] pps vs 14.5 [2.22] pps, *ES = 0.71*) and the TRI (17.9 [1.52] pps vs 16.3 [1.90] pps, *ES = 0.84*). A linear mixed effects model revealed that both age group (χ^2 *[1] = 4.7564, P = 0.0292*) and muscle (χ^2 *[1] = 15.731, P < 0.0001*) were significant predictors of peak firing rate, but the interaction between the two variables was not significant (*P = 0.9980*). Peak MU firing rates were lowered by 1.6 (0.72) pps (*P = 0.0412*) in older participants, and were 1.8 (0.38) pps (*P = 0.0001*) higher in TRI, compared to BIC.

5.4.2 Range of MU firing rates

Figure 5A shows the range of MU firing rates from BIC and TRI MUs. The group mean range of firing rates from the younger participants were higher than the MU firing rate ranges in the older participants in both BIC (12.0 [1.45] pps vs 9.4 [1.66] pps, *ES = 1.48*) and TRI (13.6 [1.22] pps vs 10.5 [1.97] pps, *ES = 1.70*). Age group (χ^2 *[1] = 7.7509, P = 0.0053*) and muscle (χ^2 *[1] = 15.570, P < 0.0001*) were both significant predictors of firing rate range; the interaction of age group and muscle was not significant (*P = 0.8687*). The range of MU firing rates was 1.7 (0.60) pps (*P = 0.0091*) higher in younger participants than older participants, and 1.5 (0.32) pps (*P = 0.0001*) higher in MUs from the TRI than the BIC.

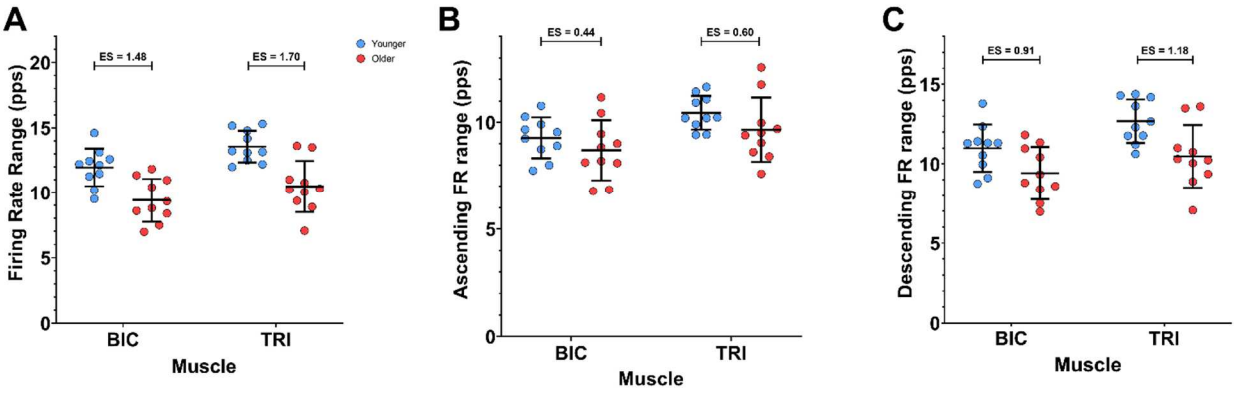

Figure 5.5: Firing rate range in older and younger adults
Participant means (younger = blue; older = red), along with group mean and SD (black) , for the range of MU firing rates during the full ramp (A), the ascending limb of the ramp (B), and the descending limb of the ramp (C). BIC (biceps brachii) data is from elbow flexion ramps, and TRI (triceps brachii) data is from elbow extension ramps.

The observed range of MU firing rates for the ascending and descending limbs of the torque ramps are displayed in Figure 5B and 5C, respectively. During the ascending torque phase, the group mean firing rate range in the younger participants was 9.3 (0.96) pps in the BIC and 10.4 (0.79) pps in the TRI. While in the older participants, the group mean firing rate range was 8.7 (1.41) pps in the BIC and 9.7 (1.50) pps in the TRI. In the BIC, the effect size of the difference in firing rate range on the ascending limb between younger and older participants was *0.44*, and in the TRI the effect size was *0.60*. However, age group was not a significant predictor ($P = 0.1112$) nor was the interaction between muscle and age group ($P = 0.7546$). Muscle was the only significant predictor of MU firing rate range over the ascending limb of the torque ramp ($\chi^2\ [1] = 10.9590,\ P = 0.0009$). The ascending limb firing rate range was 1.1 (0.29) pps higher in the TRI than in the BIC ($P = 0.0014$).

During the descending torque phase, the group mean MU firing rate ranges were higher in the younger participants compared to the older participants for both muscles (BIC: 11.0 [1.49] pps vs 9.4 [1.66] pps, *ES = 0.91*; TRI: 12.7 [1.37] pps vs 10.5 [1.97] pps, *ES = 1.18*). Both age group (χ^2 *[1] = 7.7199, P = 0.0055*) and muscle (χ^2 *[1] = 10.856, P = 0.0010*) were significant predictors of descending limb firing rate range, in our model. The interaction between age group and muscle was not significant (*P = 0.4002*). During the descending torque ramps, the firing rate range was 1.9 (0.62) pps higher in younger participants (*P = 0.0083*), as compared to older participants, and 1.4 (0.37) pps higher in the TRI (*P = 0.0015*), as compared to the BIC.

Similar to the peak firing rates, older participants showed a reduced range of MU firing rates overall, as well as a reduction in firing rate range on the descending limb. However, the firing rate range during the ascending portion of the torque ramp was not significantly affected by aging. The difference in firing rate range between younger and older participants can be appreciated in an example of smoothed firing rates from the TRI of one younger and one older participant in Figure 3.

5.4.3 Estimates of persistent inward currents using ΔF

Subject mean values for the ΔF calculation are shown in Figure 6. Group means for ΔF were substantially higher in the younger participants than in the older participants in the BIC (4.1 [1.35] pps vs 2.3 [0.84] pps, *ES = 1.47*) and in the TRI (5.2 [0.94] pps vs 3.2 [1.10] pps, *ES = 1.84*). Age group (χ^2 *[1] = 18.326, P < 0.0001*) and muscle (χ^2 *[1] = 17.796, P < 0.0001*) were both significant predictors for ΔF, in our model, however the interaction between those variables was not significant (*P = 0.2848*). ΔF was reduced by 1.9 (0.36) pps in the older participants (*P < 0.0001*), and 1.3 (0.24) pps lower in the BIC than in the TRI (*P < 0.0001*).

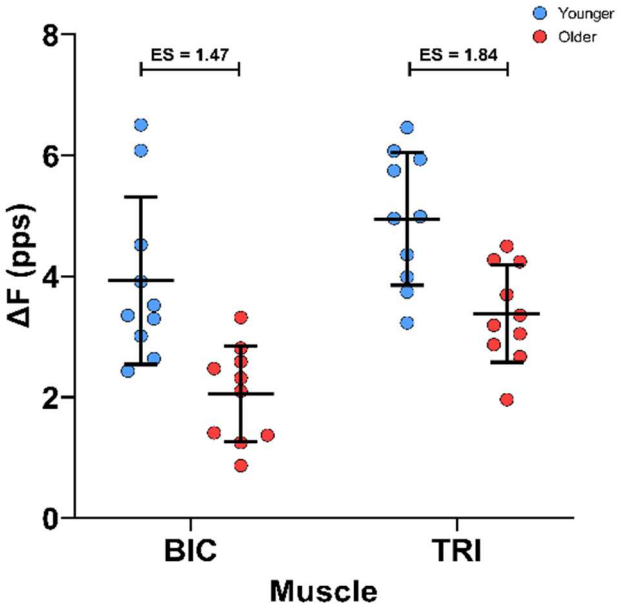

Figure 5.6: ΔF in older and younger adults
ΔF from the BIC (biceps brachii) during elbow flexion and TRI (triceps brachii) during elbow extension. Participant means in color (younger = blue; older = red), with the black bars denoting group mean and SD.

We then determined whether any relationship existed between the reported age of participants and ΔF within each of these age groups. In Figure 7, ΔF is plotted as a function of participant age along with regression lines from our model. In the younger participants, the generalized linear mixed effects model accounted for 31.96% of the variance in ΔF, with the fixed effects of muscle and age accounting for 5.28% of the variance. Muscle was a significant predictor of ΔF (χ^2 *[1] = 5.3981, P = 0.0202*), however, age was not a significant predictor of ΔF in the

younger participants (χ^2 *[1] = 0.0021, P = 0.9637*). The interaction between age and muscle was also not a significant predictor (χ^2 *[1] = 0.3742, P = 0.5407*).

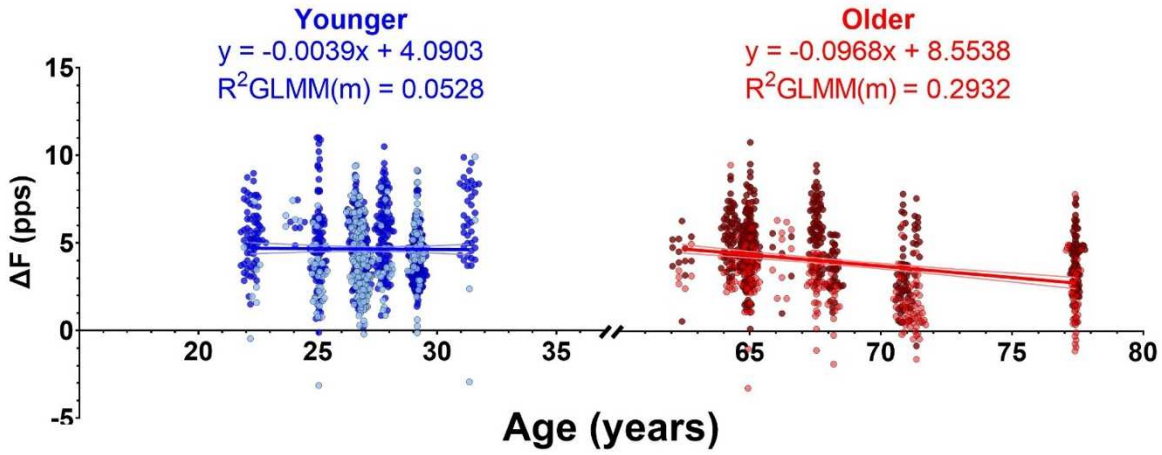

Figure 5.7: The relationship between ΔF and age
From the younger (blue; left) and older (red; right) group of participants. The lines indicate individual generalized linear mixed effects models. We show only the overall slope of the model, which includes fixed effects of age and muscle. For clarity of display, individual participants are not distinguished from one another, however the random effect in the model does account for the variability within each participant. Dark and light data points indicate ΔF values from TRI (triceps brachii) and BIC (biceps brachii) MUs, respectively. Some jitter was added to the data points x-value (age) for clarity of display. Equations derived from the model are displayed for the younger and older participants along with the marginal R^2GLMM, which indicates the variance accounted for by our fixed effects of muscle and age.

In the older participants, the model accounted for 45.98% of the observed variance in ΔF, with the fixed effects accounting for 29.32% of the variance. Both muscle (χ^2 *[1] = 14.75, P = 0.0001*) and age (χ^2 *[1] = 4.9504, P = 0.0261*) were significant predictors of ΔF, but the interaction between them was not (χ^2 *[1] = 0.8031, P = 0.3702*). Greater reductions in ΔF were associated with increasing age, in the older participants (-0.097 [0.041] pps/year, *P = 0.0473*). In summary, ΔF was reduced in older participants compared to younger participants and a negative relationship existed between age and ΔF in the older participants, but not in the younger participants.

5.4.5 MU firing duration

Provoked by the reduction in firing rate hysteresis in older participants (i.e. reduced ΔF), we investigated whether the duration of the MU firing differed between age groups; the subject and group means for all MU duration variables are plotted in Figure 8. On the ascending limb of the ramp (Figure 8A), the group means for MU firing duration were shorter in the younger participants than in the older participants (see Figure 3 for example) in both the BIC (3.6 [0.99] s vs 4.6 [0.82] s, *ES = 0.97*) and in the TRI (4.1 [0.78] s vs 5.1 [0.83] s, *ES = 1.10*). Our model found age group (χ^2 *[1] = 9.3990, P = 0.0022*) and muscle (χ^2 *[1] = 4.5555, P = 0.0328*) were both significant predictors of firing duration on the ascending limb of the torque ramp, while the interaction between the two variables was not significant (*P = 0.9224*). Ascending limb firing duration was increased by 1.0 (0.30) s in the older participants (*P = 0.0039*), compared to younger participants, and 0.5 (0.22) s longer in TRI MUs than BIC MUs (*P = 0.0401*).

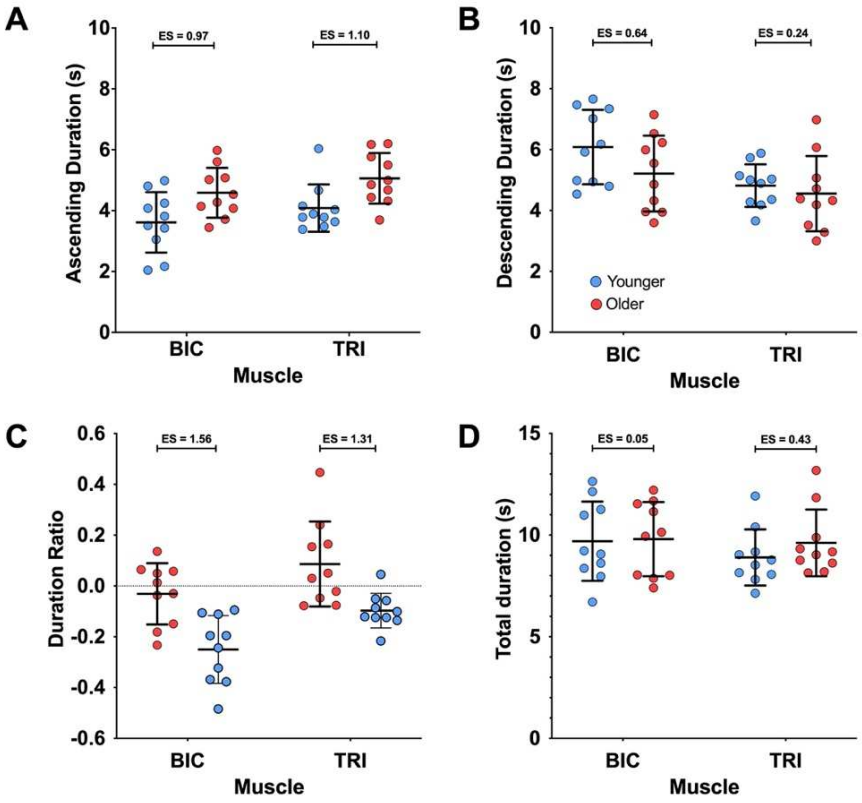

Figure 5.8: Motor unit firing duration in older and younger adults
Participant means (color) and group means (black), showing the firing duration of MUs for the full torque ramp (A), the ascending limb of the torque ramp (B), and the descending limb of the torque ramp (C).

On the descending limb of the torque ramps (Figure 8B), the group means for MU firing duration were longer for the younger participants than the older participants in both muscles (BIC: 6.1 [1.22] s vs 5.2 [1.24] s, *ES = 0.64*; TRI: 4.8 [0.70] s vs 4.6 [1.24] s, *ES = 0.24*). Muscle was revealed to be a significant predictor of firing duration on the decreasing torque ramp (χ^2 *[1] = 7.4705, P = 0.0063*), but age group was not a significant predictor (*P = 0.1765*) and the interaction of age group and muscle was not significant (*P = 0.3589*). Descending limb firing duration was 1.0 (0.33) s longer in BIC MUs than in TRI MUs.

The duration ratios (Figure 8C) were lower for the younger adults than older adults in both the BIC (-0.25 [0.13] s vs -0.03 [0.12] s, *ES = 1.56*) and in the TRI (-0.10 [0.07] s vs 0.09 [0.17] s, *ES = 1.31*), indicative of greater duration of firing on the ascending limb of the torque ramp in older adults, compared to the descending limb (i.e. leftward shift or less hysteresis). Our model found that both age group (χ^2 *[1] = 14.003, P = 0.0002*) and muscle (χ^2 *[1] = 13.090, P = 0.0003*) were both significant predictors of duration ratio, however, the interaction between age and muscle was not significant (*P = 0.5528*). The duration ratio was 0.20 (0.05) higher in the older adults than the younger adults, and 0.14 (0.03) higher in TRI MUs than in BIC MUs.

Total MU firing duration was similar between age groups and muscles (Figure 8D). The group means for total MU firing duration in the younger participants was 9.7 (1.95) s in the BIC and 8.9 (1.38) s in the TRI. In the older participants, the group mean for MU firing duration was 9.8 (1.83) s in the BIC and 9.6 (1.64) s in the TRI. The effect sizes between younger and older participants are *0.05* for the BIC and *0.43* in the TRI. However, the linear mixed effects model found that age group (*P = 0.3534*), muscle (*P = 0.3182*), and the interaction between age group and muscle (*P = 0.5084*) were not significant predictors of MU firing duration.

In summary, older participants had an increased duration of firing on the ascending limb of the torque ramp and an increased ratio of firing on the asendinng limb of the torque ramp, but the overall firing duration and the firing duration on the descending limb of the torque ramp was similar to younger participants. As shown in Figure 3, a longer duration of firing during the ascending phase of the ramp without a difference during the descending phase of the ramp or total duration of firing indicates a leftward shift, and more symmetrical pattern of firing.

5.5 Discussion

The present study aimed to investigate the effects of healthy aging on the MU firing patterns from the biceps brachii (BIC) and triceps brachii (TRI) by comparing younger and older healthy adults. In agreement with previous literature, we have found lower peak firing rates in both the BIC and TRI of older adults. Further, and perhaps most novel, we found substantial and significant reductions in estimates of persistent inward currents (PICs; ΔF) in older adults irrespective of muscle. In older adults, we also found that age was a significant predictor of ΔF (i.e. ΔF decreased with respect to age); however, there was no such relationship in the younger group. Additional characteristics of MU firing patterns support the notion of reduced onset-offset hysteresis, such as reduced firing rate range during the descending phase of the ramp and a leftward shift in MU firing in older compared to younger adults. These findings suggest that MU firing patterns in older people exhibit less PIC activity, which may have implications for motor control.

5.5.1 Reduced motor unit firing rates in older people

Reductions in MU firing rates in older adults here are similar to those reported in previous studies. For example, using intramuscular EMG, Dalton et al (Dalton *et al.*, 2010) found that mean firing rates are reduced in both the BIC and TRI across a variety of voluntary effort levels. The difference between younger and older adults was substantial (~45%) at high levels of effort for both muscles, but the differences at 25% MVC were modest and similar in magnitude to what we observed. Indeed, firing rates have been shown to be reduced in older adults in other studies as well, with larger differences at higher contraction intensities (Kamen *et al.*, 1995; Connelly *et al.*, 1999; Kamen & Knight, 2004; Barry *et al.*, 2007; Kirk *et al.*, 2018; Kirk *et al.*, 2019).

Organizational changes to the MUs following age-related loss of motoneurons (Doherty *et al.*, 1993) could play a role in the observed reductions in firing rate. With re-modelling there are changes in MU twitch contraction times such that twitch fusion occurs at a lower rate (Bellemare *et al.*, 1983; Newton *et al.*, 1988; Connelly *et al.*, 1999; Roos *et al.*, 1999). However, investigations into motoneuron loss with age have shown a very moderate loss in individuals below the age of 60 (Tomlinson & Irving, 1977). As the mean age of the older participants in this group is only 67.8, some of our sample may not have substantial loss of motoneurons, and the subsequent reorganization of the motor pool would lead to only modest reductions of firing rates.

Changes in the pattern or level of excitatory synaptic input to the motoneurons are also likely to contribute to the observed reduction in firing rates with age. For instance, excitatory post-synaptic potential (i.e. EPSP) amplitudes, as estimated with peristimulus time histograms, in response to transcranial magnetic stimulation of the motor cortex, are reduced by ~50% in older people (> 55 years old). Hypoexcitability of the corticospinal pathway corresponds with weakness in older adults (Clark *et al.*, 2015), and ~33% of the variance in weakness in seniors can be accounted for by measures of corticospinal excitability (i.e. motor evoked potential amplitudes) and inhibition (i.e. corticospinal silent period). Stretch reflexes are also reduced with aging, suggesting that homonymous 1a input from muscle spindles is reduced (Bryndum & Marquardsen, 1964; Milne & Williamson, 1972), and slowed (i.e. longer half relaxation times) with advancing age (Carel *et al.*, 1979), which could be due to a combination of changes in muscle spindle sensitivity (Swash & Fox, 1972), Ia-motoneuronal transmission, and/or spinal motoneuron excitability (Geertsen *et al.*, 2017). Interestingly, the Hoffman (H-) reflex, which bypasses the muscle spindles by direct peripheral nerve stimulation, is also reduced with age, providing further

support for Ia-motoneuronal transmission and/or spinal motoneuron excitability alterations with age (deVries *et al.*, 1985; Scaglioni *et al.*, 2003). Reductions in any combination of the above mentioned excitatory input would surely result in reduced MU firing rates in older adults.

Inhibitory spinal circuits can also affect descending input and/or Ia afferent input to spinal motoneurons via inhibitory interneurons. Older adults also have reduced indices of reciprocal inhibition, both at the spinal (Kido *et al.*, 2004) and cortical levels (Hortobagyi *et al.*, 2006), which may alter the commands to agonist-antagonist muscle pairs. Although the effects of aging on Ia presynaptic inhibition at rest are unclear (Butchart *et al.*, 1993; Morita *et al.*, 1995; Earles *et al.*, 2001), there is a decrease in the amount of modulation of Ia presynaptic inhibition with increasing contraction intensity in older adults (Butchart *et al.*, 1993), which would lead to differences in the pattern of inhibition and have profound effects on the balance of excitation, inhibition, and neuromodulation (Johnson *et al.*, 2017) required to perform a task. The imbalance of inhibition and excitation could therefore play a role in the reduced firing rates we observed in our older adults.

MU firing rates are highly dependent upon the biophysical properties of the parent motoneurons, and age-related changes of such properties can lead to reductions in firing rates. Spike after-hyperpolarization (AHP) duration is increased in aged rodents (Cameron *et al.*, 1991; Kalmar *et al.*, 2009) and cats (Morales *et al.*, 1987). Similarly, AHP duration increases gradually with age (Piotrkiewicz *et al.*, 2007), and when compared directly, AHP is longer in older compared to younger adults (Christie & Kamen, 2010), which can contribute to reductions in MU firing rates. Other biophysical properties that are altered with age can affect recruitment and repetitive firing of MUs, such as increases in the input resistance (Chase *et al.*, 1985; Morales *et al.*, 1987; Kalmar

et al., 2009), and reduced rheobase current (Morales *et al.*, 1987; Kalmar *et al.*, 2009), suggesting that aged motoneurons are less excitable. Indeed motoneuron recruitment gain is reduced with age, as evidenced in a recent investigation by Nielsen and colleagues (Nielsen *et al.*, 2019). Therefore, changes to the biophysical properties of the motoneurons likely contribute to the reduced firing rates we observed in older adults.

Not only were peak firing rates reduced in the current investigation, but older adults also showed a compressed range of MU firing rates. This compressed range of firing can arise from similar mechanisms that underlie the reductions in peak firing rates, but it is interesting to note that the firing rate range during the ascending phase of the contraction was similar for both younger and older adults. That is, the rate modulation from the onset of firing to peak firing was similar (see Figure 5B). On the contrary, the reduction in overall firing rate range (~1.7 pps) seen in older participants, is primarily attributed to the reduction in firing rate range seen on the descending limb of the torque ramp (~1.9 pps). The reduced firing range seen on the descending limb (I.e. reduced hysteresis) of the torque ramps is most likely related to a decrease in PIC activity, which brings us to the next topic of our discussion; reduced estimates of PICs in older adults.

5.5.2 Reduced estimates of PICs in older people

We have shown that ΔF is substantially lower, regardless of muscle, in the upper limb of older adults, compared to younger adults. Further, in our older group, we found that increasing age was associated with reductions in ΔF (see Figure 7). In addition, the relative firing duration of motor units is shifted to the left in older adults, such that the duration of firing is symmetrical during the ascending and descending phases of the ramp contraction, indicating less onset-offset hysteresis. Although ΔF and the leftward shift in firing patterns are an indirect estimate of PIC

activity, they do support our hypothesis that PICs are reduced older people. Such age-related changes in estimates of PICs are most likely due to either changes in 1) monoaminergic input to the motoneurons, 2) the amount or pattern of inhibition, and/or 3) Na+ or Ca2+ channel function.

The overall leftward shift in the firing patterns of older individuals provides further insights into the effects of aging on MU firing. Based on the reduced ΔF and reduced firing rate range on the descending limb in the older adults, we expected to see a reduced duration of firing on the descending limb in those participants. Instead, we found an increased duration ratio, which was driven by a duration of firing on the ascending limb of the torque ramps in older participants, without significant changes to the overall duration and descending duration of firing. This could suggest that motor units in older participants were recruited earlier than those from younger participants. Indeed, this would be similar to other reports that have shown a lower average recruitment threshold for motor units recorded from older compared to younger adults (Erim *et al.*, 1999; Klass *et al.*, 2005, 2008; Fling *et al.*, 2009; Pascoe *et al.*, 2011). Most intriguing though is the fact that the firing patterns of older individuals were more symmetrical (~approximately equal time on the ascending and descending portion of the ramps – see Figure 3 and Figure 8C), indicating less hysteresis, a behaviour that is a hallmark of PICs.

Schwindt and Crill (Schwindt & Crill, 1980) first discovered PICs in motoneurons by blocking K^+ currents in anesthetized preparations, but by using un-anesthesthetized decerebrate preparation, Hounsgaard and colleagues (Hounsgaard *et al.*, 1984; Hounsgaard & Kiehn, 1989) showed that PICs emerged in the presence of serotonin (5HT) or norepinephrine (NE), meaning that PICs are a natural consequence of endogenous neurotransmitters. Although important for initiation of repetitive firing, the component of the PIC mediated by Na+ is not responsible for the

long-lasting prolongation of firing due to the inactivation time constant of just a few seconds (Lee & Heckman, 1998a; Binder & Powers, 2001). Instead, it is the component mediated by L-type Ca2+ channels that causes prolonged self-sustained firing and profound onset-offset hysteresis (Lee & Heckman, 2001; Harvey *et al.*, 2006; Kuo *et al.*, 2006), in particular, the Ca2+V1.3 channels show little or no inactivation (Moritz *et al.*, 2007; Binder *et al.*, 2020). This "self-sustained" firing, or simply maintained motoneuron firing with decreased synaptic input, was emphasized as being quite important for postural behaviours because sustained force generation can be maintained without the need for sustained descending input (Hounsgaard *et al.*, 1984; Hounsgaard & Kiehn, 1989). Therefore, the functional role of PICs in normal human behaviours can easily be appreciated (Heckman *et al.*, 2008b). With a reduction in PIC-related prolongation of motoneuron firing, simple tasks would require greater synaptic input to maintain activities such as standing or carrying objects. Since the aging process is associated with reduced excitatory input to motoneurons, the role of PICs in maintaining forces required for everyday activities may be increased with advancing age.

Initial attempts to understand PIC effects of human MU firing behaviour focused on self-sustained firing or "bi-stability"(Kiehn & Eken, 1997). In such experiments, MUs are tracked during low-level voluntary efforts and an additional source of synaptic input (i.e. vibration) causes the recruitment of an additional MU (test unit) that maintains firing after the additional input is removed (Gorassini *et al.*, 1998). MUs can then be classified as either having PICs, or not, based on the occurrence of test units that maintain firing after the additional synaptic input is removed. Using this approach, Kamen and colleagues (Kamen *et al.*, 2006) showed that older individuals have a similar occurrence (23.1%) of MUs that exhibit self-sustained firing as younger adults

(22.8%). As such, and contrary to the findings in our current investigation, they concluded that PIC-like behaviour does not seem to be affected by the aging process. They did, however, report that the mean drop-out torque of newly recruited MUs was slightly higher for older adults (3.26% maximal voluntary contraction (MVC) vs 2.43% MVC), although variability was high and therefore no statistical differences were reported. It is important to note that the occurrence of self-sustained firing may not be the be-all-end-all method to quantify whether PICs are present during voluntary motor behaviour in humans. This is because PICs almost certainly contribute to motoneuron firing during all voluntary behaviours, because without the amplification effects of PICs, the small currents produced by descending and sensory inputs are too weak to have much of an effect on motonneuron firing (Binder & Powers, 2001). More important to the understanding of human motor output is the magnitude of PICs, rather than the presence.

Hysteresis of MU firing rates, on the other hand, has proven to be the most consistent hallmark for non-invasive estimation of the magnitude of PICs in humans, as was first realized by Gorassini, Bennett and colleagues (Bennett *et al.*, 2001a; Gorassini *et al.*, 2002). The now standard paired-MU analysis technique (ΔF) has been subject to rigorous investigations interested in the accuracy of these estimates (Bennett *et al.*, 2001a; Bennett *et al.*, 2001b; Powers *et al.*, 2008; Revill & Fuglevand, 2011; Powers & Heckman, 2015; Afsharipour *et al.*, 2020; Hassan *et al.*, 2020). Bennett and colleagues (Bennett *et al.*, 2001a; Bennett *et al.*, 2001b) used parallel MU and intracellular recordings in rat motoneurons to clearly demonstrate that ΔF reflects features of PICs. With advances in technology, these estimates of PICs have been obtained across hundreds of MUs (Afsharipour *et al.*, 2020; Hassan *et al.*, 2020; Kim *et al.*, 2020; Trajano *et al.*, 2020), which likely provides a better overall estimation of PIC magnitude across the entire motor pool. Even though

MUs of older adults in our experiment certainly displayed onset-offset hysteresis (i.e. positive ΔF values overall), the magnitude of this hysteresis was markedly reduced compared to the sample of younger adults that were recruited. In fact, estimates of PICs (ΔF) were reduced by ~40%, with very large effect sizes (all ES > 1.45). In addition, the age of individuals was a significant predictor of ΔF, suggesting that PICs may deteriorate with age at a rate of ~1pps/decade, but only in older adults.

The magnitude of PICs is directly proportional to the level of NE and 5HT (Lee & Heckman, 1998a, 2000), which are monoamines released from the from the caudal raphe nucleus and locus coeruleus, respectively. These monoaminergic nuclei of the brainstem deteriorate with age (Shibata *et al.*, 2006; Pagano *et al.*, 2017), and in particular, the age-related reduction in locus coeruleus structural integrity is associated with impaired cognitive and behavioural function (Liu *et al.*, 2020), as well as reductions in central pain modulation (Grashorn *et al.*, 2013; Damien *et al.*, 2018). Deterioration of these nuclei could also lead to reductions in neuromodulatory drive to motorneurons, reducing PIC activity, which would ultimately explain some of the reductions observed in ΔF. NE-mediated effects are likely predominantly due to degradation of the locus coeruleus because older rodents maintain only ~30% NE nuclei compared to ~90% 5HT nuclei (Tatton *et al.*, 1991). Despite the evidence that a greater proportion of raphe nuclei are maintained with age, spinal 5HT is greatly reduced (Johnson *et al.*, 1993; Ko *et al.*, 1997). Therefore, the potential of 5HT-mediated effects with the aging process are more likely to occur peripherally. With aging, there is increased circulation of cytokines (so-called “inflamm-aging”) (Michaud *et al.*, 2013), which affect 5HT receptors and increase re-uptake of 5HT (Steinbusch *et al.*, 2021). In

sum, less availability of monoamines would result in reduced PIC magnitude at the same relative effort, which is what we observed as a reduction in ΔF.

PICs are also highly sensitive to inhibitory inputs (Hultborn *et al.*, 2003; Kuo *et al.*, 2003; Heckman *et al.*, 2008a; Hyngstrom *et al.*, 2008; Revill & Fuglevand, 2017). Thus, changes to the amount or pattern of inhibition may lead to reduced estimates of PICs as estimated by ΔF. As mentioned above, there are age-related alterations in spinal and supraspinal inhibitory circuits (Butchart *et al.*, 1993; Kido *et al.*, 2004; Hortobagyi *et al.*, 2006) that could modify the synaptic input to motoneurons. While difficult to measure, the temporal pattern of inhibitory commands can also affect the ΔF estimate (Powers *et al.*, 2012; Johnson *et al.*, 2017). Push-pull inhibition, where inhibition varies inversely with excitation, can lead to reductions in MU hysteresis (Powers *et al.*, 2012). It, therefore, remains possible that the pattern of the inhibitory commands is altered with age to compensate for the various structural and functional changes in the neuromuscular system (Hepple & Rice, 2016; McNeil & Rice, 2018) associated with the aging process and may contribute to our observed reductions in ΔF.

Alterations in the integrity and function of 5HT/NE receptors and voltage sensitive ion channels must also be considered in relation to age-related changes in the nervous system. Basic (i.e. larger and longer AHP, lower rheobase, greater input resistance) and rhythmic (i.e. slower minimum and maximum steady-state firing frequencies and lower f-I slopes) motoneuron properties are consistent with reduced motoneuron excitability in very old (>30 months) rodents. However, Kalmar et al (Kalmar *et al.*, 2009) also showed an increased incidence of PIC-like behaviour in very old rodent motoneurons, which they suggested to have resulted from increased 5HT and NE receptor sensitivity to residual endogenous monoamines (Harvey *et al.*, 2006) as a

compensatory mechanism to counteract the reduced motoneuron excitability. Although this increased incidence of PIC may seem to contradict our findings, this type of analysis simply determines the relative number of motoneurons that have hysteresis in response to current injection to the soma, whereas we quantified the average magnitude of hysteresis during voluntary activation (i.e. axo-dendritic synaptic input). L-type Ca2+ channels are concentrated in the dendritic tree, far away from the soma, meaning that the levels of injected current may have underestimated PICs in a healthy younger motoneuron receptor hypersensitivity due to the inability to activate PICs from the soma (Bennett *et al.*, 1998; Lee & Heckman, 1998a). Aging may also result in changes in the expression of receptor subtypes or the downstream signaling of various receptors. Indeed, there are age-related reductions in the duration of Ca2+-mediated plateau potentials in striatal neurons (Dunia *et al.*, 1996), and more generally, deregulated Ca2+ is an active component of healthy aging that can increase the risk of cell death and neurodegenerative disorders (Nikoletopoulou & Tavernarakis, 2012). As such, it is difficult to pinpoint the exact monoaminergic receptor or ion channel dysfunction that may contribute to the observed reductions in estimated PICs during voluntary contractions with aging.

5.5.3 Methodological considerations

Since this experiment was conducted in a non-invasive fashion, we were unable to directly determine the PIC magnitude. Instead, we relied on the best estimation of PICs available in humans (i.e. ΔF), which has undergone rigorous scrutiny to ensure accuracy of the estimates (Bennett *et al.*, 2001a; Bennett *et al.*, 2001b; Powers *et al.*, 2008; Revill & Fuglevand, 2011; Powers & Heckman, 2015; Afsharipour *et al.*, 2020; Hassan *et al.*, 2020). Nonetheless, it is difficult to determine whether the reduction in ΔF is the result of alterations in monoaminergic drive, the

amount or pattern of inhibition, and/or changes to the monoaminergic receptor sensitivity or ion channel function. This delineation will require further work.

Overall, the MUs decomposed in the older participants had longer durations on the ascending phase of the ramp, suggesting a lower relative threshold of units decomposed for older adults. This relatively lower recruitment torque could lead to a ceiling effect in terms of how much hysteresis those units could exhibit. However, as the average duration of MU firing on the descending limb was 5.2 s and 4.6 s for the BIC and TRI respectively in the older participants with the descending limb of the torque ramp being 10 seconds long, we do not believe the reduced ΔF observed was due to early derecruitment due to the time constraints of the task.

5.5.4 Practical considerations

In the words of Power and colleagues (Power *et al.*, 2016) – "If you don't use it, you'll likely lose it." Whether this holds true for PICs is unclear at the moment, although Latella (Latella, 2021) recently made a compelling argument for studying the efficacy of strength training to mitigate the effects of aging on MU firing behaviour. Indeed, the work of Power and colleagues (Power *et al.*, 2010) suggests that estimates of MU numbers are greater in masters runners compared to their sedentary counterparts. Further, strength training-induced plasticity of motoneurons is not limited to younger adults. AHP duration is longer in older compared to younger adults, but that duration can be reduced with strength training in both age groups (Christie & Kamen, 2010). Thus, it remains possible that strength training, which necessitates high levels of effort (likely utilizing high levels of monoaminergic drive), could mitigate deterioration of monoaminergic function and/or PIC behaviour seen in older adults.

5.6 Conclusion

The present study compared the firing patterns of MUs from the elbow extensors and flexors of healthy younger and older adults during isometric ramp contractions. Irrespective of muscle, age was a significant predictor of peak firing rate and firing rate hysteresis, such that both were reduced in older adults. In addition to the differences observed between age groups, the age of individuals within the older group predicted a ~1pps per decade reduction in ΔF, a non-invasive estimate of PIC magnitude across the motor pool. This reduced estimate of PIC magnitude likely arises from reductions in monoaminergic input, alterations in the amount or pattern of inhibition, and/or alterations in monoamine receptor or ion channel function. It remains unclear whether alterations in firing rate hysteresis are a compensatory adjustment or impairment that occurs with aging, however, it remains possible that physical training may be able to mitigate such changes.

6. Estimates of persistent inward currents are increased bilaterally, yet motoneuron firing rates are only reduced in the paretic upper limb post-hemiparetic stroke

6.1 Abstract

Individuals who have survived a stroke exhibit motor deficits including paresis, hypertonia, and a loss of independent joint control. Increased use of bulbospinal motor control pathways, including neuromodulatory drive and the resulting persistent inward currents (PICs), have been linked to the observed motor deficits seen post-stroke. Our goal was to understand how the changes in neural drive that occur following a stroke affect the motor unit firing patterns in the upper limb. We quantified motor unit firing rate, rate modulation, and estimated PIC amplitude (ΔF) during isometric ramp contractions in the directions of elbow flexion and elbow extension in both the paretic and non-paretic upper limb of stroke survivors, as well as neurologically-intact control participants. Motor units from the paretic biceps and triceps of stroke participants showed reductions in both peak firing rate and rate modulation, as compared to motor units from the non-paretic limb and control participants. We found ΔF was increased in both muscles and in both the paretic and non-paretic limbs of stroke participants, as compared to controls. These results suggest a broad increase in neuromodulatory drive occurs post-stroke, with the intact ionotropic connections to the non-paretic motor pools limiting the effect of this diffuse monoaminergic drive on the motor unit firing rates and on the observed motor deficits.

6.2 Introduction

Long term motor deficits are common in the upper limbs of individuals who have survived a stroke, and often interfere with activities of daily living. These impairments include paresis (Colebatch & Gandevia, 1989; Beer *et al.*, 1999; Canning *et al.*, 2004), hypertonia and associated spasticity (O'Dwyer *et al.*, 1996; Zackowski *et al.*, 2004; Sommerfeld *et al.*, 2012), and a loss of independent joint control (Dewald *et al.*, 1995; Dewald & Beer, 2001; Sukal *et al.*, 2007). These motor impairments are postulated to be the result of an increased dependence on indirect corticobulbospinal pathways and their multi-segmental spinal ionotropic projections (McPherson *et al.*, 2018a; Karbasforoushan *et al.*, 2019). In particular, the reticulospinal tract has been consistently suggested as a compensatory neural pathway which plays a major role in the observed motor deficits (Ellis *et al.*, 2012).

The reduction in corticospinal integrity, and subsequent compensatory utilization of these indirect motor pathways, may lead to alterations in the ionotropic drive to muscles in individuals with stroke. Brainstem motor pathways, including the often-implicated corticoreticulospinal tract, may not be able to provide sufficient excitation to the motor pool due to the reduced frequency content (Grosse & Brown, 2003; Blouin *et al.*, 2007) and smaller EPSPs generated through these pathways (Riddle *et al.*, 2009; Baker, 2011). This reduced ability to fully activate the muscle is evident in the impaired voluntary activation seen post-stroke (Garmirian *et al.*, 2019). Further, the upregulation of bulbospinal pathways may alter the pattern of inhibitory drive to the muscle during active movement.

In combination with the greater reliance on ipsilateral corticoreticulospinal projections, there is evidence for upregulation of the reticular formation following the loss of corticoreticular

input from the lesioned hemisphere (Fisher *et al.*, 2012), resulting in increased metabotropic neuromodulatory inputs to the spinal cord post hemiparetic stroke (McPherson *et al.*, 2008; McPherson *et al.*, 2018b; McPherson *et al.*, 2018c). Descending monoaminergic drive from the reticular formation can modulate the sensitivity of motoneurons and interneurons to excitatory input (Heckman *et al.*, 2008b). Previous work has found increased tonic vibration reflexes in the biceps brachii of stroke survivors, suggesting an increased neuromodulatory drive (McPherson *et al.*, 2008; McPherson *et al.*, 2018c). However, the distribution of neuromodulatory drive across flexors and extensors, and between the paretic and non-paretic arm in hemiparetic stroke has not been studied yet.

The purpose of this study is to investigate how both ionotropic and metabotropic neural drive are altered in both elbow flexor and extensor muscles in the paretic and non-paretic upper extremities following a stroke. This will be accomplished through analyses of motor unit firing patterns of the biceps brachii and triceps brachii including firing rate and rate modulation, and estimates of PICs. We hypothesize that alterations in motor unit firing rate will be due to both the reduced ionotropic corticospinal drive to the motor pool and the increased use of compensatory pathways to activate these units. As the non-paretic limb retains intact corticospinal projections, we expect the alterations in motor unit firing rate to be restricted to the paretic limb. Specifically, we hypothesize that motor units from the paretic biceps and triceps of stroke participants will show reductions in both firing rate and firing rate modulation, due to reductions in corticospinal drive. Furthermore, we expect to see increased discharge hysteresis in biceps and triceps motor units from both the paretic and non-paretic motor units, due to an upregulation of monoaminergic drive

following stroke. This is projected to be bilateral, affecting both flexor and extensor muscles in the upper limb.

6.3 Methods

6.3.1 Participants

A total of 22 individuals (stroke, 11; control, 11) took part in this study. Demographic information for participants is listed in Table 6.1. Control participants were within the same age range and were required to meet the following inclusion criteria: (1) no known neurological injury or disease, (2) no muscular impairment of upper extremity motor function, and (3) no significant visual or auditory impairments. Stroke participants were required to meet the following inclusion criteria: (1) Paresis confined to one side, (2) At least one year post-stroke, (3) Absence of muscle tone abnormalities and motor or sensory impairment in the non-paretic limb, (4) Absence of severe wasting or contracture of the paretic upper limb, (5) Absence of severe cognitive or affective dysfunction, (6) Absence of severe concurrent medical problems, and (7) Absence of brainstem lesions as determined from clinical or radiological reports. Prior to participation in this experiment, all participants provided written informed consent which was approved by the Institutional Review Board of Northwestern University.

Table 6.1: Demographic information of participants

	Stroke	*Control*
Age	60.91 (6.14)	65.45 (6.62)
Gender	10 male; 1 female	9 male; 1 female
Fugl-Meyer Score	29.90 (15.67)	N/A

6.3.2 Experimental Apparatus

The experiment was carried out using a custom apparatus designed to collect isometric torques from the shoulder and elbow joints simultaneously, which has been used previously (Hassan *et al.*, 2020). Participants were seated in a Biodex chair and comfortably secured with waist and shoulder straps to prevent trunk movement. The participant's arm was positioned at a shoulder abduction angle of 75º and an elbow flexion angle of 90º and with the forearm rigidly fixed to a six degree-of-freedom load cell (JR3, Inc., Woodland, CA), using a fiberglass cast. A Jacobian-based algorithm allowed for the calculation of joint torques at the elbow and shoulder using the forces and torques collected from the load cell, limb segment lengths, and upper limb

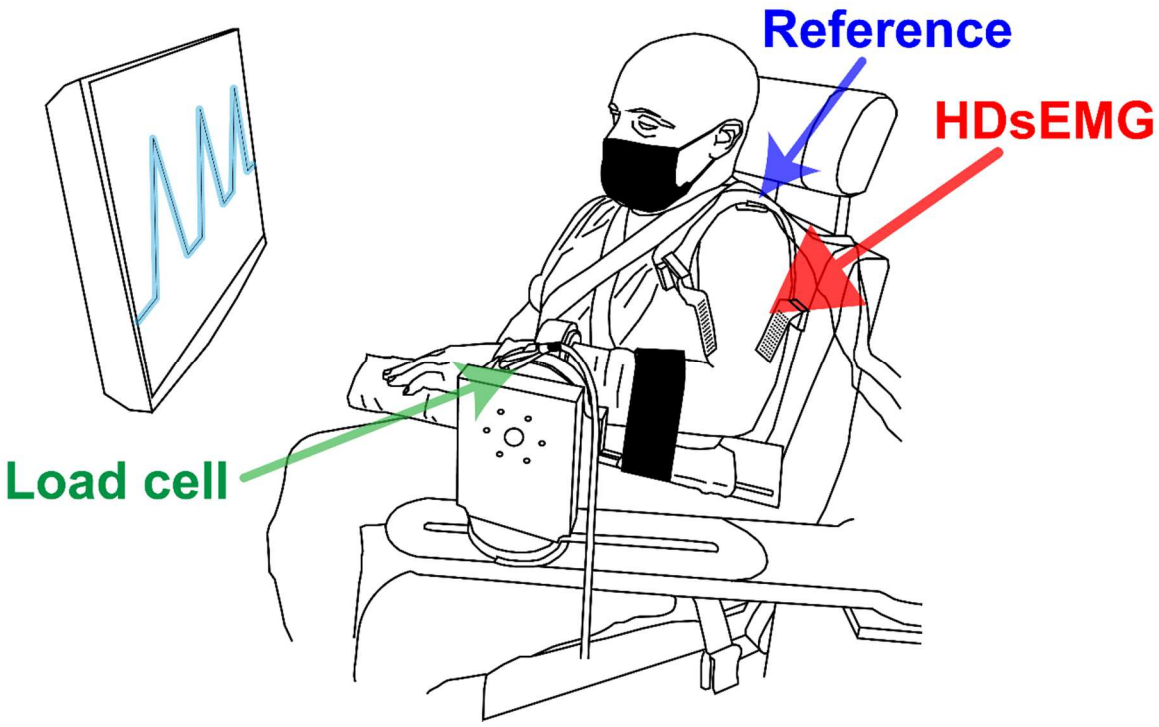

Figure 6.1: An illustration of the experimental setup.
Participants are seated in a biodex chair with their forearm secured to a 6 degree-of-freedom loadcell. High-density EMG electrode grids are placed on the lateral head of the triceps brachii, and along the muscle belly of the biceps brachii. Real-time visual feedback of task performance was provided via a computer monitor in front of the participant.

joint angles. Force and torque data were collected at 1024 Hz using custom MATLAB software (The MathWorks).

HD-sEMG was collected from the biceps and triceps brachii using multi-electrode grids with 64 channels per muscle and an 8 mm inter-electrode distance (GR08MM1305, OT Bioelettronica, Inc., Turin, IT). EMG data were recorded at 2048 Hz, amplified (x150), and band-pass filtered (10-500 Hz) using a Quattrocento signal amplifier (OT Bioelettronica, Inc., Turin, IT). For synchronization of the EMG and torque recordings, a 1 second TTL pulse was included as a separate channel on both recordings. The experimental apparatus is shown in Figure 1.

6.3.3 Experimental Procedure

Each stroke survivor participated in two experimental sessions, one each for the paretic and non-paretic limb, and each healthy control subject participated in one experimental session with their dominant limb.

Maximum voluntary torque contractions. To allow for comparisons across limbs and across subjects, isometric torque ramps were conducted at matched effort levels with respect to maximum voluntary torque (MVT). Accordingly, MVTs were collected in the directions of shoulder abduction (SABD), elbow flexion (EF), and elbow extension (EE) from the paretic and non-paretic limbs of stroke participants, and from the dominant limb of healthy control participants. Directions were randomized, and MVT trials in each direction were repeated until three trials with peak torque within 10% of each other were obtained. If the largest torque was obtained during the last trial, subsequent trials were collected to ensure an accurate MVT. During the MVT trials, participants

received visual feedback of their torque in the intended direction along with vigorous vocal encouragement from the experimenter.

Submaximal isometric torque ramps. Participants generated triangular isometric torque ramps in the directions of EF and EE by gradually increasing torque in the intended direction to 20% of their MVT over 10 seconds, and then gradually relaxing their torque back down to rest over the following 10 seconds. To aid in participant's accurate completion of this task, they were provided with real-time visual feedback of their torque trace superimposed over an image of the desired time-torque profile and each participant conducted several practice trials to acclimate to the task and the visual feedback. Participants completed four to six trials of isometric torque directions in each EF and EE, with each trial consisting of 3 ramps in one torque direction. Trials included 10 seconds of rest between ramps, along with 5s of rest at the beginning and end of each trial; participants also received several minutes of rest in between each trial. As the motor unit analyses conducted in this paper rely on smooth torque traces, all torque traces were visually inspected and any ramps which did not match the desired time-torque profile or did not show smoothly increasing and decreasing torque were removed from the following analyses.

6.3.4 Data Analysis

Motor unit decomposition. Motor unit decomposition for this experiment was carried out using similar methods as previous work from our group. Below is a brief description of the motor unit decomposition process, but further details on these methods are provided in previous papers (Hassan *et al.*, 2020).

All EMG channels were visually inspected and those with substantial noise, artifacts, or saturation were not included for decomposition. Decomposition of the high-density EMG was carried out using a convolutive blind source separation algorithm (Negro *et al.*, 2016; Martinez-Valdes *et al.*, 2017), with a silhouette threshold of 0.85. To correct for any non-physiological discharge times extracted by the decomposition algorithm, decomposed motor unit pulse trains were visually inspected and any errors were corrected using a local reoptimization of the decomposition parameters; this approach has been extensively utilized in recent years (Boccia *et al.*, 2019; Hassan *et al.*, 2019; Afsharipour *et al.*, 2020; Del Vecchio *et al.*, 2020; Martinez-Valdes *et al.*, 2020). The errors observed were primarily missed spikes, producing firing rates half of the mean rate, or multiple spikes at one time point, producing firing rates two to three times the mean rate. Motor unit firing rates were calculated as the inverse of the interspike intervals obtained from the decomposed motor unit spike trains and smoothed using a 2 s Hanning window.

Estimation of persistent inward currents. The amplitude of persistent inward currents (PICs) were estimated from the motor units collected from both the biceps and triceps using ΔF, a paired motor unit analysis. For this analysis the PIC amplitude of a higher threshold motor unit (test unit) is estimated based on the difference in firing rate of a lower threshold unit (control unit) at the time of recruitment and derecruitment of the test unit (Gorassini *et al.*, 2002).

Test and control motor unit pairs selected for the ΔF analysis had to meet certain criteria. To ensure that the PIC of the control unit is fully activated, the test unit must be recruited at least 1 s after the control unit. To prevent overestimation of ΔF the control unit must be derecruited at least 1.5s after the test unit. For these analyses we placed no restriction on the rate modulation of the control unit or on the rate-rate relationship between the test and control units. These parameters

have been selected in alignment with previous investigations into the ΔF technique (Hassan *et al.*, 2020).

Quantification of rate modulation. Rate modulation is calculated here as the firing rate response to an increase in descending input. As the descending excitatory input to the motor units cannot be measured directly, torque about the elbow joint was used as a surrogate for the descending input. We excluded the acceleration phase near motor unit recruitment, as the activity in this phase is similar across most motor units, and changes in the smoothed firing rate during acceleration are primarily due to the onset of the PIC and edge effects of the smoothing filter. A bilinear fit of the firing rate with respect to torque on the ascending limb of the torque ramp was used to determine the acceleration and rate saturation phases of motor unit firing. Rate modulation was quantified as the slope of the linear fit of the firing rate with respect to torque from the end of the acceleration phase to the peak of the torque ramp. In order to ensure motor units completed the acceleration phase and had a substantial rate saturation phase, motor units recruited less than three seconds prior to peak torque or those recruited after peak torque were not included in these analyses.

Many muscles can contribute to the net torque seen at the elbow. To avoid the confounding effects of activity from other muscles at the elbow joint, motor unit rate modulation was also quantified with respect to the EMG amplitude of the muscle of interest. The EMG signals from all channels used for the decomposition were rectified and summed for each contraction. This rectified EMG signal was used as a proxy for descending input in a similar manner as described for torque, above. However, as EMG data was not collected for max contractions, the EMG values

were normalized to the maximum EMG amplitude seen during the submaximal torque ramps (nEMG).

6.3.5 Statistical Analysis

Mean values presented for each group are averages of the means of each participant in the group. Group values are presented as mean (SD) unless otherwise noted. Cohen's *d* was used to estimate effect sizes (ES) for all comparisons between groups (Cohen, 1992). Group means, standard deviations, and effect size were calculated using GraphPad by Prism (version 9.0.1 for Windows, GraphPad Software, San Diego, California USA).

Three linear mixed effects models were used to make comparisons between: 1) the paretic and non-paretic limb of the stroke participants, 2) the non-paretic limb of the stroke participants and the dominant limb of control participants, and 3) the paretic limb of the stroke participants and the dominant limb of control participants. To investigate differences across between limbs of the stroke participants the model included main effects of limb, muscle, and the interaction effect of muscle-by-limb, along with 2 random factors (a random subject intercept and a random slope accounting for the effect of muscle within a subject). Similar models were used to compare the results between stroke participants and healthy controls. These models used a fixed non-repeated factor of group (non-paretic/paretic vs. control) and a repeated fixed factor of muscle, along with the same random factors as the model between limbs of stroke subjects. To ensure the data met the assumptions of normality and homoscedasticity, model residuals were visually inspected using Q-Q plots and residual plots across the range of fitted values.

In cases where the interaction between muscle and limb/group was found to have a significant effect, 4 pairwise comparisons were conducted using simplified linear models on subsets of the data. These pairwise models investigated either a main effect of limb/group for each muscle independently, or a main effect of muscle on each limb/group independently. The pairwise linear models include only one of limb, group, or muscle as a fixed effect and subject as a random effect.

Effects estimated from the linear mixed effects model are presented as model estimate (SE). *P*-values were obtained using likelihood ratio tests of the full model including the effect of interest against a null model excluding the effect of interest. Linear mixed effects analyses were conducted using *lme4* (Bates & Maechler, 2015) in R (R Core Team 2020, R Foundation for Statistical Computing, Vienna, AUT) and statistical significance was set at $\alpha = 0.05$ for all comparisons.

6.4 Results

Decomposition of EMG recordings from the paretic limb of 11 stroke subjects discriminated 643 motor unit spike trains from the biceps and 774 motor unit spike trains from the triceps, with an average yield of 5.2 (3.53) and 7.8 (6.31) spike trains per trial from the biceps and triceps, respectively. In the non-paretic limb of 7 stroke subjects, the decomposition yielded 435 motor unit spike trains from the biceps and 645 from the triceps, with an average of 4.0 (2.91) spike trains per trial from the biceps and 6.1 (4.62) from the triceps. From 11 control subjects, 565 motor unit spike trains were decomposed from biceps EMG and 850 motor unit spike trains were decomposed from triceps EMG; an average of 4.3 (1.57) motor unit spike trains were decomposed

from each bicep ramp, and 6.3 (3.52) were decomposed from each triceps ramp, from the control participants.

6.4.1 Motor unit firing rates

The peak firing rates of biceps and triceps motor units from both stroke and control participants are shown in Figure 6.2A. In the biceps, the group mean peak motor unit firing rate was 12.3 (2.49) pps in the paretic limb of stroke participants, 14.9 (2.11) pps in the non-paretic limb, and 14.2 (2.30) pps in control participants. The effect size of the difference between the peak firing rates in the paretic and non-paretic limbs (ES_{PvNP}) was 1.15, the effect size of the difference between the non-paretic and control limbs (ES_{NPvC}) was 0.33, and the effect size of the difference between the paretic and control limbs (ES_{PvC}) was 0.80. From the triceps, the group mean peak firing rates were 13.5 (2.87) pps in the paretic limb of stroke participants, 16.2 (2.97) pps in the non-paretic limb ($ES_{PvNP} = 0.94$), and 16.2 (1.85) pps in the control participants ($ES_{NPvC} = 0.02$; $ES_{PvC} = 1.12$).

A linear mixed effects model revealed that limb ($P < 0.0001$) and muscle ($P = 0.0307$) were significant predictors of peak firing rate in stroke participants. Peak motor unit firing rates were 3.2 (0.15) pps higher in the non-paretic than the paretic limb of stroke subjects, and 1.7 (0.71) pps higher in the triceps than the biceps. Comparing the non-paretic and control motor units, muscle was a significant predictor of peak firing rate ($P = 0.0016$), with peak firing rates 2.0 (0.75) pps higher in triceps motor units than biceps motor units. In the model comparing paretic and control motor units, the main effects of group ($P = 0.0129$) and of limb ($P = 0.0013$) were both significant. Peak motor unit firing rates were 2.3 (1.21) pps lower in the paretic limb than control

limb, and 2.0 (0.59) pps higher in the triceps than the biceps. The full results from these three models are found in section I of Table 6.2A below.

The range of the motor unit firing rates are shown in Figure 6.2B. The group mean firing rate ranges for biceps motor units were 9.2 (1.72) pps for the paretic limb, 10.5 (1.59) pps for the non-paretic limb ($ES_{PvNP} = 0.81$), and 10.1 (1.85) pps for the control limb ($ES_{NPvC} = 0.24$; $ES_{PvC} = 0.52$). Group mean firing rate ranges for triceps motor units were 9.4 (2.40) pps in the paretic limb, 11.2 (2.71) pps in the non-paretic limb ($ES_{PvNP} = 1.81$), and 11.6 (1.64) pps in control participants ($ES_{NPvC} = 0.18$; $ES_{PvC} = 1.07$).

Limb ($P < 0.0001$) and the interaction between limb and muscle ($P = 0.0064$) were significant predictors of firing rate range in comparisons between the paretic and non-paretic limb. A linear model comparing firing rate range in the control and non-paretic limbs found muscle to be a significant predictor ($P = 0.0035$), with triceps motor units showing a 1.5 (0.59) pps higher range of firing rates. The model comparing the paretic limb of stroke participants with control participants revealed significant main effects of muscle ($P = 0.0273$) and the interaction of muscle and group ($P = 0.0247$) on motor unit firing rate range. The full results from these three models are found in section II of Table 6.2A below.

For the models which revealed a significant interaction between muscle and limb / group, we completed pairwise comparisons on subsets of the data. The paretic biceps had a decreased firing rate range of 1.9 (0.15) pps compared to the non-paretic biceps, and the paretic triceps displayed a reduction in firing rate range of 2.4 (0.13) compared to the non-paretic triceps. The paretic triceps also displayed a reduction of firing rate range of 2.0 (0.73) pps compared to the control limb. In the non-paretic limb, the triceps had a firing rate range of 0.8 (0.15) pps higher

than the biceps. Similarly in the control limb the triceps displayed a firing rate range of 1.5 (0.12) higher than the biceps. The full results from the pairwise linear mixed models are provided in Table 6.2B.

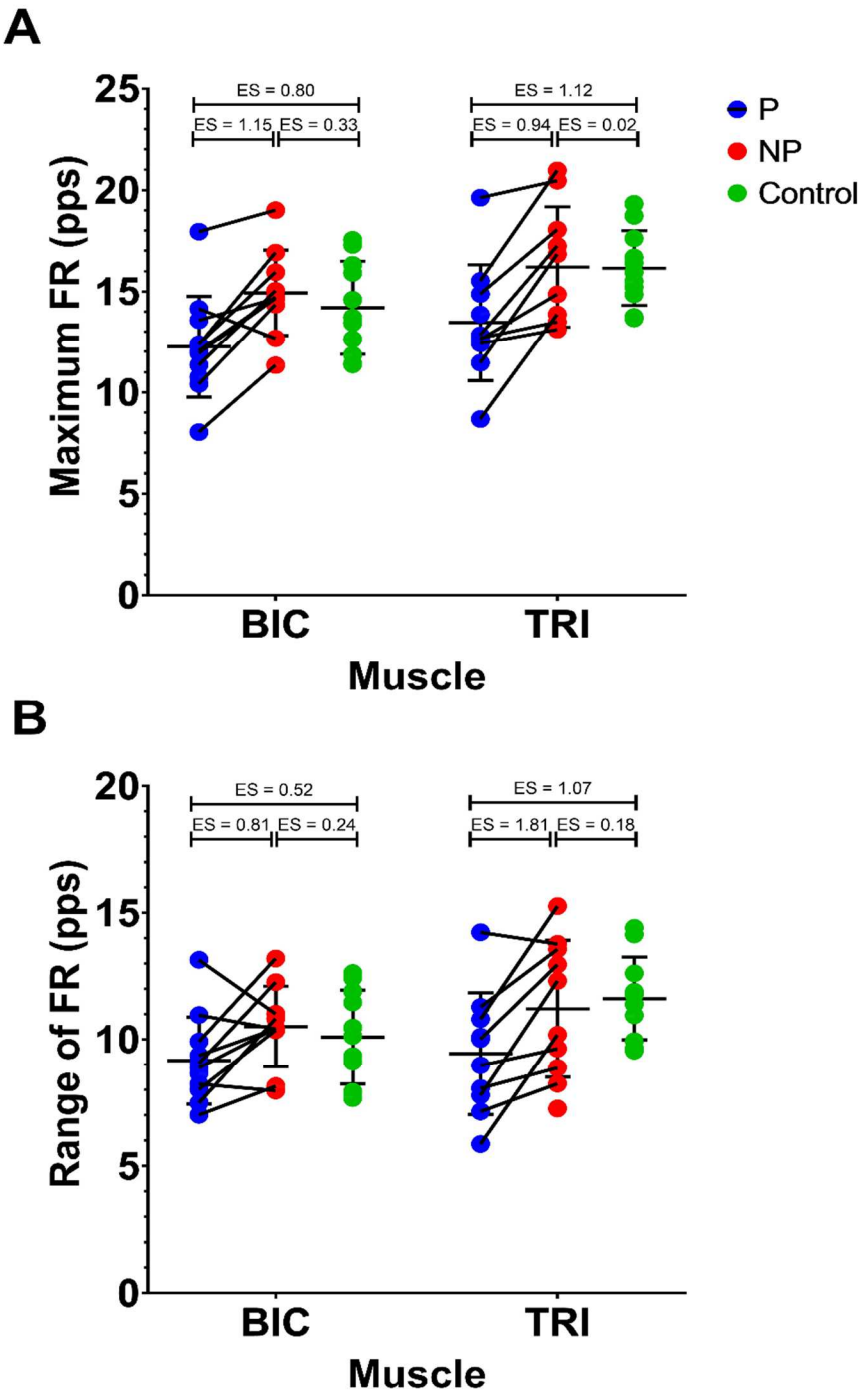

Figure 6.2: Range and peak firing rate in stroke and control participants
Subject means (colors) along with group mean ± SD (black) for the peak motor unit firing rate (A), and range of firing rates (B) during the submaximal torque ramps. In this and all following figures, individual participant means are shown for illustrative purposes, the linear model utilizes data from all motor units

Table 6.2A: Results from the 3 linear mixed effects models comparing firing rate across muscle and limb / group

I) Peak FR				
Comparison	Fixed effects	$\chi^2(1)$	*P*	Estimate (SE)
P - NP	Interaction	0.06	0.8003	
	Limb	**824.85**	**<0.0001**	**-3.17 (0.15) pps**
	Muscle	**4.67**	**0.0307**	**1.65 (0.71) pps**
NP - C	Interaction	0.04	0.8357	
	Group	0.63	0.4273	
	Muscle	**9.98**	**0.0016**	**1.96 (0.75) pps**
P - C	Interaction	1.27	0.2599	
	Group	**6.19**	**0.0129**	**-2.29 (1.21) pps**
	Muscle	**10.32**	**0.0013**	**1.96 (0.59) pps**
II) Range FR				
Comparison	Fixed effects	$\chi^2(1)$	*P*	Estimate (SE)
P - NP	**Interaction**	**7.42**	**0.0064**	**See Table 2B**
	Limb	**450.08**	**<0.0001**	**See Table 2B**
	Muscle	1.05	0.3055	**See Table 2B**
NP - C	Interaction	0.27	0.6032	
	Group	1.03	0.3103	
	Muscle	**8.52**	**0.0035**	**1.53 (0.59) pps**
P- C	**Interaction**	**5.05**	**0.0247**	**See Table 2B**
	Group	1.21	0.2719	See Table 2B
	Muscle	**4.87**	**0.0273**	**See Table 2B**

Table 6.2B: Model results for the pairwise comparisons for firing rate range

I) Range FR: P v NP			
Muscle	Group	Estimate (SE)	*P*
BIC	**P-NP**	**-1.85 (0.15) pps**	**<0.0001**
TRI	**P-NP**	**-2.38 (0.13) pps**	**<0.0001**
TRI-BIC	P	0.20 (0.11) pps	0.0743
TRI-BIC	**NP**	**0.77 (0.15) pps**	**<0.0001**
II) Range FR: C v P			
Muscle	Group	Estimate (SE)	*P*
BIC	P-C	-0.42 (0.73) pps	0.5730
TRI	**P-C**	**-1.97 (0.86) pps**	**0.0333**
TRI-BIC	**C**	**1.49 (0.12) pps**	**<0.0001**
TRI-BIC	P	0.20 (0.11) pps	0.0743

6.4.2 Estimates of PIC amplitude

Group mean ΔF values are shown in Figure 6.3. For the paretic biceps the group mean ΔF was 3.7 (0.78) pps, the non-paretic biceps group mean ΔF was 3.8 (1.01) pps ($ES_{PvNP} = 0.15$), and the control biceps group mean ΔF was 2.0 (0.76) pps ($ES_{NPvC} = 1.98$; $ES_{PvC} = 2.12$). In the triceps, the group mean ΔF was 3.9 (0.77) pps in the paretic limb, 4.3 (0.88) pps ($ES_{PvNP} = 0.57$) in the non-paretic limb, and 3.2 (1.09) pps ($ES_{NPvC} = 1.15$; $ES_{PvC} = 0.72$) in the control participants.

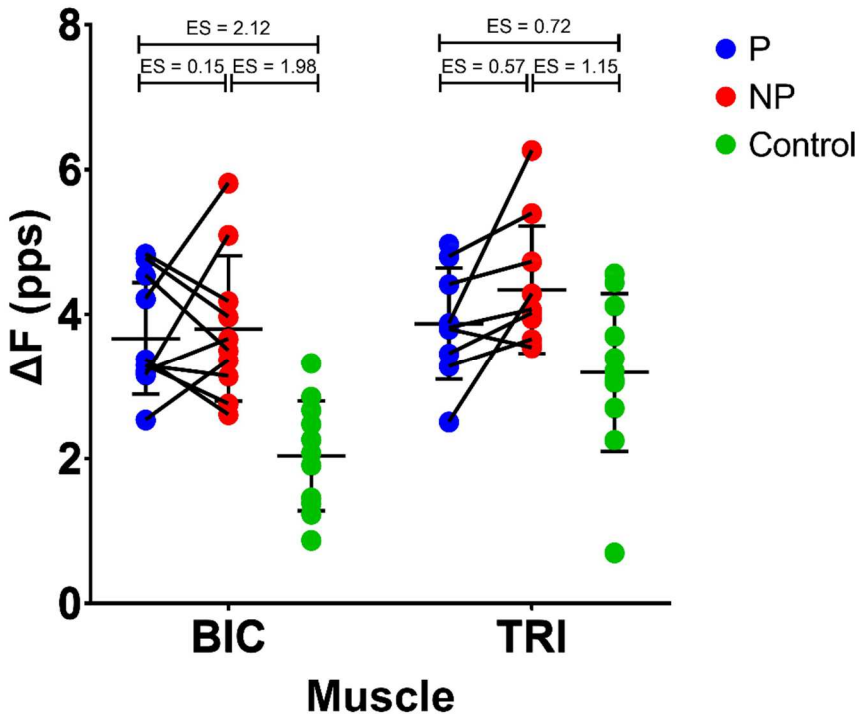

Figure 6.3: ΔF estimates in stroke and control participants
Subject means (colors) and group mean ± SD (black) for ΔF estimates of PIC amplitude for the paretic, non-paretic, and control limbs for the biceps and triceps, during EF and EE ramps, respectively.

In the model comparing the paretic and non-paretic limbs of stroke participants, the main effects of limb (*P = 0.0627*), muscle (*P = 0.1800*), or the interaction (*P = 0.2470*) between limb and muscle were not significant predictors of ΔF. The effects of group (*P = 0.0002*), muscle (*P = 0.0002*), and the interaction between muscle and group (*P = 0.0456*) on ΔF were significant in the model of non-paretic and control limbs. Similarly, in the model comparing the paretic and control limbs, group (*P = 0.0002*), muscle (*P = 0.0081*), and the interaction between group and muscle (*P = 0.*0276) were significant predictors of ΔF. The full results from these models are shown in Table 6.3A.

Pairwise comparisons revealed ΔF was 1.7 (0.35) pps higher in the non-paretic biceps than in the control limb, and 1.0 (0.42) pps higher in the non-paretic triceps than in the control limb. Similarly, ΔF was 1.7 (0.32) pps higher in the paretic biceps than in the control limb, and 0.63 (0.31) pps higher in the paretic triceps than in the control limb. For all 3 limbs tested, ΔF was significantly higher in the triceps than in the biceps. ΔF was 1.6 (0.10) pps higher in the control

triceps than biceps, 0.5 (0.13) pps higher in the non-paretic triceps than biceps, and 0.5 (0.11) pps higher in the paretic triceps than biceps. The full results from the pairwise linear mixed models are provided in Table 6.3B.

Table 6.3A: Results from the 3 linear mixed effects models comparing ΔF across muscle and limb / group

ΔF				
Comparison	Fixed effects	$\chi^2(1)$	*P*	Estimate (SE)
P - NP	Interaction	1.34	0.2470	
	Limb	3.47	0.0627	
	Muscle	1.80	0.1800	
NP - C	**Interaction**	**4.00**	**0.0456**	**See Table 3B**
	Group	**13.99**	**0.0002**	**See Table 3B**
	Muscle	**14.33**	**0.0002**	**See Table 3B**
P - C	**Interaction**	**4.86**	**0.0276**	**See Table 3B**
	Group	**13.72**	**0.0002**	**See Table 3B**
	Muscle	**7.01**	**0.0081**	**See Table 3B**

Table 6.3B: Model results for the pairwise comparisons for firing rate range

I) ΔF: C v NP			
Muscle	Group	Estimate (SE)	*P*
BIC	**NP-C**	**1.71 (0.35) pps**	**0.0001**
TRI	**NP-C**	**1.01 (0.42) pps**	**0.0268**
TRI-BIC	**C**	**1.58 (0.10) pps**	**<0.0001**
TRI-BIC	**NP**	**0.49 (0.13) pps**	**0.0003**
II) ΔF: C v P			
Muscle	Group	Estimate (SE)	*P*
BIC	**P-C**	**1.68 (0.32) pps**	**<0.0001**
TRI	**P-C**	**0.63 (0.31) pps**	**0.0440**
TRI-BIC	**C**	**1.58 (0.10) pps**	**<0.0001**
TRI-BIC	**P**	**0.46 (0.11) pps**	**<0.0001**

6.4.3 Slope of motor unit firing rate modulation

Figure 6.4A shows the group means for motor unit firing rate slope with respect to torque. From biceps motor units, the paretic limb showed a group mean rate modulation slope of 4.6 (2.62 x 10^{-2}) pps/%MVT, the non-paretic limb displayed a slope of 0.18 (0.12) pps/%MVT (ES_{PvNP} = *1.57*), and the control participants had a rate modulation slope of 0.24 (0.11) pps/%MVT (ES_{NPvC} *= 0.48;* ES_{PvC} *= 2.42*). In triceps motor units, the group mean rate modulation slope was 0.98 (64.2 x 10^{-3}) pps/%MVT in the paretic limb, 0.18 (0.06) pps/%MVT (ES_{PvNP} *= 2.79*) in the non-paretic limb, and 0.18 (0.12) pps/%MVT (ES_{NPvC} *= 0.03;* ES_{PvC} *= 1.89*) in the control limb.

Limb was a significant predictor of rate modulation slope with respect to torque (*P* < *0.0001*) in comparisons between arms of stroke subjects, with the non-paretic limb associated with

an increased rate modulation slope of 0.14 (0.02) pps/%MVT. The linear model comparing the non-paretic and control data found that none of the main effects of group ($P = 0.5880$), muscle ($P = 0.1580$), and the interaction between group and muscle ($P = 0.4131$) were significant. In the model comparing rate modulation slope from the paretic and control motor units the main effects of both group ($P < 0.0001$) and muscle ($P = 0.0163$) were significant. Rate modulation in the control limb was 0.19 (0.03) pps/%MVT higher than in the paretic limb, and rate modulation in the triceps was 0.06 (0.03) pps/%MVT higher than the biceps. Table 6.4A displays the full statistical results from these models.

Motor unit rate modulation was also calculated with respect to nEMG, and the subject and group means for this calculation are shown in Figure 6.4B. The group means for rate modulation slope with respect to nEMG were 2.4 (2.19×10^{-2}) pps/nEMG in the paretic biceps, 5.9 (3.41×10^{-2}) pps/nEMG in the non-paretic biceps ($ES_{PvNP} = 1.22$), and 7.6 (2.04×10^{-2}) pps/nEMG in the control biceps ($ES_{NPvC} = 0.61$; $ES_{PvC} = 2.46$). In the triceps the group mean was -2.2 (2.64×10^{-2}) pps/nEMG in the paretic limbs, 6.4 (3.32×10^{-2}) pps/nEMG in the non-paretic limbs ($ES_{PvNP} = 2.86$), and 6.4 (3.18×10^{-2}) pps/nEMG in the control limbs ($ES_{NPvC} = 0.01$; $ES_{PvC} = 2.95$).

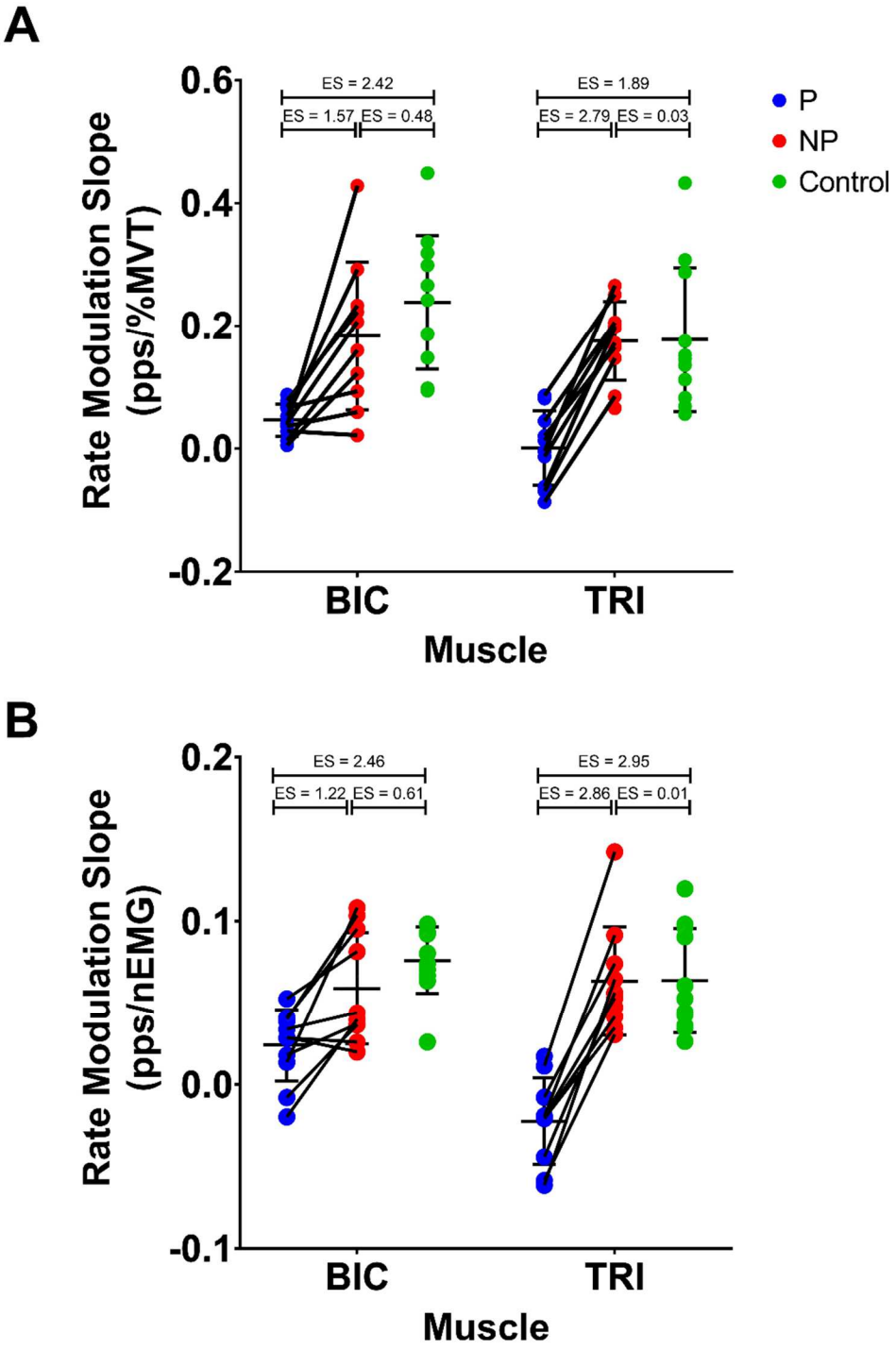

Figure 6.4: Rate modulation in stroke and control participants
Rate modulation slope calculated with respect to normalized torque (A), and normalized EMG amplitude (B) for the paretic, non-paretic, and control motor units. Individual participant means are in color, with the group means and standard deviation in black.

A linear mixed effects model comparing the paretic and non-paretic limbs of stroke participants revealed significant main effects of limb ($P < 0.0001$), muscle ($P = 0.0328$) and the interaction of muscle and limb ($P < 0.0001$) on motor unit rate modulation slope with respect to nEMG. Table 4A displays the full statistical results from this model. In the pairwise comparisons of triceps motor units, the paretic limb displayed a reduction of rate modulation by 8.8 (0.80×10^{-2}) pps/nEMG compared to the non-paretic limb. In pairwise comparisons between muscles of the same limb, the paretic triceps displayed rate modulation of 5.7 (0.85×10^{-2}) pps/nEMG lower than the paretic biceps, however, the non-paretic triceps displayed rate modulation of 1.8 (0.84×10^{-2}) pps/nEMG higher than the non-paretic biceps. The full results from the pairwise linear mixed models for the paretic and non-paretic limb data are provided in section I of Table 6.4B.

The linear model comparing the control and non-paretic limbs found the main effects of group ($P = 0.1691$), muscle ($P = 0.5788$), and the interaction of muscle and group ($P = 0.1714$) were not significant predictors of rate modulation with respect to nEMG; the full statistical results from this model are shown in Table 6.4A.

The model comparing the paretic limb of stroke participants with control participants revealed significant main effects of group ($P < 0.0001$), muscle ($P = 0.0119$), and the interaction of muscle and group ($P = 0.0419$) on rate modulation slope over nEMG, with the full statistical details of the model shown in Table 6.4A. Pairwise linear comparisons showed rate modulation slope with respect to EMG was significantly decreased by 8.4 (1.25×10^{-2}) pps/nEMG in the paretic triceps compared to the control triceps. Rate modulation slope was also significantly decreased in the paretic triceps as compared to the paretic biceps, as discussed above. The full

results from all pairwise linear mixed models comparing the paretic and control limb data are provided in section II of Table 6.4B.

Table 6.4A: Results from the 3 linear mixed effects models comparing motor unit rate modulation across muscle and limb / group

I) Rate Modulation with respect to normalized torque				
Comparison	Fixed effects	$\chi^2(1)$	*P*	Estimate (SE)
P - NP	Interaction	0.71	0.3994	
	Limb	**114.34**	**<0.0001**	**-0.14 (0.021) pps/%MVT**
	Muscle	1.76	0.1852	
NP - C	Interaction	0.67	0.4131	
	Group	0.29	0.5880	
	Muscle	1.99	0.1580	
P - C	Interaction	0.20	0.6439	
	Group	**23.39**	**<0.0001**	**-0.19 (0.031) pps/%MVT**
	Muscle	**5.77**	**0.0163**	**0.06 (0.028) pps/%MVT**
II) Rate Modulation with respect to nEMG				
Comparison	Fixed effects	$\chi^2(1)$	*P*	Estimate (SE)
P - NP	**Interaction**	**31.10**	**<0.0001**	**See Table 4B**
	Limb	**73.88**	**<0.0001**	**See Table 4B**
	Muscle	**4.56**	**0.0328**	**See Table 4B**
NP - C	Interaction	1.87	0.1714	
	Group	1.89	0.1691	
	Muscle	0.31	0.5788	
P- C	**Interaction**	**4.14**	**0.0419**	**See Table 4B**
	Group	**23.17**	**<0.0001**	**See Table 4B**
	Muscle	**6.33**	**0.0119**	**See Table 4B**

Table 6.4B: Model results from all pairwise comparisons for rate modulation with respect to nEMG

I) Rate Modulation with respect to nEMG: P v NP			
Muscle	Limb	Estimate (SE)	*P*
BIC	P-NP	-1.61 (1.04) X 10^{-2} pps/nEMG	0.1208
TRI	**P-NP**	**-8.82 (0.80) X 10^{-2} pps/nEMG**	**<0.0001**
TRI-BIC	**P**	**-5.68 (0.85) X 10^{-2} pps/nEMG**	**<0.0001**
TRI-BIC	**NP**	**1.82 (0.84) X 10^{-2} pps/nEMG**	**0.0315**
II) Rate Modulation with respect to nEMG: C v P			
Muscle	Group	Estimate	*P*
BIC	P-C	-2.46 (2.32) X 10^{-2} pps/nEMG	0.3037
TRI	**P-C**	**-8.35 (1.25) X 10^{-2} pps/nEMG**	**<0.0001**
TRI-BIC	C	-1.10 (0.60) X 10^{-2} pps/nEMG	0.0613
TRI-BIC	**P**	**-5.68 (0.85) X 10^{-2} pps/nEMG**	**<0.0001**

6.5 Discussion

This study compared the motor unit firing patterns from the biceps and triceps brachii of the paretic and non-paretic limbs of stroke survivors along with the dominant limb of healthy control individuals in a similar age range. We found a reduction in motor unit firing rate in the paretic biceps and triceps, in comparison to the biceps and triceps of the non-paretic and control limbs. The range of motor unit firing was also reduced in the paretic biceps and triceps compared to the non-paretic limb, and the firing range of the paretic triceps, but not the paretic biceps, was reduced in comparison to motor units from healthy control participants. ΔF estimates of PIC amplitude were higher in both the paretic and non-paretic biceps and triceps as compared to the control biceps and triceps. We found reduced firing rate modulation slope with respect to torque in both muscles in the paretic limb as compared to the non-paretic and control limbs, however, rate modulation with respect to nEMG, only showed reductions in rate modulation in the paretic triceps.

6.5.1 Motor unit firing rate is reduced in the paretic limb

We observed reductions in both peak motor unit firing rate and firing rate range, in both the paretic biceps and triceps of stroke survivors, in comparison to their non-paretic limbs and the limbs of healthy control participants. Previous work has shown reductions in motor unit peak firing rates in the paretic biceps brachii in comparison to the non-paretic limb (Gemperline *et al.*, 1995; Mottram *et al.*, 2014). These studies showed lower firing rates even when matched to the same absolute torque level. However, there exists limited information regarding motor unit firing patterns from the triceps brachii following stroke. Relative weakness is comparable in elbow

flexors and extensors of the paretic limb (Colebatch & Gandevia, 1989; Garmirian *et al.*, 2019). Reduced voluntary activation during elbow extension is of a similar magnitude to elbow flexion (Garmirian *et al.*, 2019). Together, these suggest an inability to fully activate elbow flexors and extensors following stroke.

Decreases in motor unit firing rates following stroke in other muscles has been linked to stroke-induced interruption of the corticospinal drive (Rosenfalck & Andreassen, 1980; Gemperline *et al.*, 1995; Mottram *et al.*, 2014). Stroke survivors may utilize a combination of any remaining corticofugal resources from the lesioned hemisphere along with brainstem pathways activated via cortico-bulbar connections from the non-lesioned hemisphere. This mechanism is also the likely cause for the reductions in firing rate in triceps firing rate shown here.

6.5.2 Estimates of PIC amplitude are increased in the biceps and triceps of both the paretic and non-paretic limbs

Our results showed an increase in ΔF at both elbow flexors and extensors in both limbs of the stroke participants. These results suggests that the level of monoaminergic drive may be increased systemically following stroke. Previous work has shown that the descending monoaminergic projections have diffuse connections and affects multiple motoneuron pools simultaneously (Skagerberg & Bjorklund, 1985), and increasing the excitability of one motor pool through monoaminergic input, may result in increased excitability of multiple pools including agonists and antagonists, and motor pools acting at multiple joints (Prochazka, 1989). Additionally, there is evidence that a portion of serotonergic projections to the spinal cord cross to the contralateral side at the level of termination (Skagerberg & Bjorklund, 1985), providing a possible avenue for the bilateral increase in ΔF observed here.

Increases in metabotropic drive seen in stroke may be due to a decreased corticobulbar drive to the monoaminergic brainstem nuclei from the lesioned hemisphere (Fisher *et al.*, 2012). The effect of an increase in monoaminergic drive may amplify the reduced descending excitatory input to enable sufficient voluntary activation of the motor pool via weaker bulbospinal ionotropic inputs.

However, if a systemic increase in monoaminergic drive occurs post-stroke, this begs the question: why does the non-paretic limb not exhibit symptoms of this increased motoneuron excitability like hypertonia and spasticity? One possible explanation is the utilization of inhibitory drive to modulate the increased neuromodulatory drive. The diffuse nature of descending monoamines has been hypothesized to be modulated through inhibition in order to achieve a precise pattern of motoneuron excitability (Heckman *et al.*, 2008a; Heckman *et al.*, 2008b). Additionally, the PIC has been shown to be extremely sensitive to inhibition (Hultborn *et al.*, 2003; Kuo *et al.*, 2003). Stroke survivors still retain corticospinal and corticobulbospinal connections to the non-paretic limb, and may use these resources to provide inhibition to the motoneuron pools and prevent PIC related hyperexcitability. Additionally, previous work suggests that the exaggerated stretch reflexes, and the associated increase in excitability of the motoneuron pool, observed following stroke are likely due to a combination of changes in ionotropic and neuromodulatory drive (McPherson *et al.*, 2018c).

The results shown here contradict previous findings which did not show significant differences in ΔF estimates of PICs from the biceps brachii following stroke (Mottram *et al.*, 2009). However, the previous study performed the isometric torque ramps at a matched absolute torque

level. The data shown here was conducted to a matched effort level (as a percentage of maximum voluntary torque). Due to weakness in the paretic limb of stroke subjects, stroke participants in the previous study were conducting ramps at a higher contraction speed and to a higher peak torque relative to their maximum voluntary torque. Motor unit simulations have shown that ΔF decreases with higher contraction speeds if the model includes spike-threshold accommodation or spike-frequency adaptation (Revill & Fuglevand, 2011). Further, different parameters were used to determine the eligible motor unit pairs for the ΔF analysis in the current study, with the current study not requiring a minimum rate-rate slope and including a minimum derecruitment time difference in the current study. The parameters used here were chosen based on a systematic review of ΔF selection criteria previously conducted by the authors (Hassan *et al.*, 2020). Additionally, the current study utilized HD-sEMG decomposition which increased the motor unit yield from each contraction, and the model included data from both the biceps and triceps. Together these differences lead to a much larger data set in this study, which may explain the differences in statistical significance between these studies.

6.5.3 Impairments of rate modulation are observed in both the paretic biceps and triceps post-stroke

Our analysis of rate modulation with respect to torque showed reduced rate modulation in motor units from the paretic biceps and triceps in comparison to both the non-paretic limb of stroke participants and the dominant limb of healthy control participants. When calculating rate modulation with respect to nEMG, however, only the paretic triceps showed significant reductions. This may be due to the inherent noisiness and possible crosstalk of the EMG signals, and possibly due to the lack of EMG recordings during maximum contractions contributing to difficulty in

normalizing the EMG data. Previous investigations have shown impaired rate modulation following stroke using a paired motor unit analysis (Mottram *et al.*, 2014). This suggests that the impairments in rate modulation with respect to torque seen in the biceps are not an aberration caused by the other muscles acting at the elbow joint.

While previous work has shown deficits in rate modulation in the paretic biceps following stroke, this study is the first to quantify rate modulation in the triceps following stroke, and identify the motor unit firing rate impairments. We posit that the impairments in rate modulation are due to an alteration in ionotropic neural drive, following stroke-induced interruption of the high-resolution corticospinal pathway. The interruption in corticospinal drive and increased reliance on corticobulbospinal resources may lead to an inability to fully activate the motor unit pool. This shift in descending drive has been implicated in the reduced peak firing rates seen in motor units from the paretic limb in this study, as well as others (Gemperline *et al.*, 1995; Frontera *et al.*, 1997; Mottram *et al.*, 2014).

While the reduced firing rates and rate modulation seen in the paretic biceps have been attributed to the increased reliance on the corticoreticulospinal pathway, less is understood about bulbospinal drive to upper limb extensors following stroke. The upper limb extensor muscles may be facilitated through contralateral reticulospinal inputs, as has been seen in the monkey (Davidson & Buford, 2006; Davidson *et al.*, 2007), or possibly through the ipsilateral vestibulospinal tract, which facilitates extensor muscles and inhibits flexors (Wilson & Yoshida, 1968). However, much of this research was conducted in the cat hind limb, where extensors play a major role in anti-gravity support. The vestibulospinal tract has also been hypothesized to play a role in the observed hypertonicity and spasticity following stroke (Miller *et al.*, 2014a; Li & Francisco, 2015).

Additionally, the extensive interconnection between the vestibulospinal and reticulospinal tract (Carleton & Carpenter, 1983) may suggest both pathways may be involved in descending drive to the upper limb extensors following a stroke. However, more research is necessary to understand the involvement of vestibulospinal projections on post-stroke motor deficits.

Though increased utilization of bulbospinal pathways is likely related to the reduced rate modulation seen here, the direct mechanisms through which these pathways result in firing rate impairments are not fully understood. There is evidence for a reduction in excitatory input to the motor units, as corticospinal excitatory drive is interrupted and corticobulbospinal motor commands rely primarily on polysynaptic pathways, and evoke smaller EPSPs than those generated through corticospinal drive (Riddle *et al.*, 2009; Baker, 2011). If the observed rate modulation impairments were due to an overall reduction in excitatory input to the motor pool, the continued recruitment of later units, while earlier recruited units saturate, would be unlikely. Alterations in the amount or pattern of descending inhibition may also lead to the observed impairments in rate modulation. Simulation work has shown that balanced inhibition (where inhibition increases in parallel with excitation during a contraction) can produce flat rate modulation (Powers *et al.*, 2012). While presynaptic inhibition has been shown to be reduced following stroke (Aymard *et al.*, 2000; Lamy *et al.*, 2009), the changes in inhibition during active movement have not thoroughly investigated.

It is possible that an increase in PICs may also contribute to the rate modulation deficits observed in the paretic limb, as motor units with a strong PICs exhibit a non-linear firing pattern that includes a phase of rate saturation, following the post-recruitment acceleration phase (Binder & Powers, 2001; Heckman & Enoka, 2012; Johnson *et al.*, 2017). However, our ΔF results suggest

that PICs are increased in both the paretic and non-paretic biceps and triceps of the stroke participants, yet significant impairments of rate modulation were only observed in the paretic limb. This makes it unlikely that the increased neuromodulatory drive, and resulting PICs, are the cause of the observed impairments in rate modulation.

6.5.4 Limitations

A few limitations for this study most be noted. The sample size was relatively small, however, the consistency of the results is reflected in the large effect sizes. Additionally, the motor unit measures we utilized in this work can only provide an indirect measure of the neural changes following stroke, making it difficult to differentiate the mechanisms that underlie these changes.

6.6 Conclusion

This study confirms the previous findings of reduced motor unit firing rates and rate modulation in the paretic biceps brachii following stroke and presents the novel finding of reductions in firing rates and rate modulation in the triceps brachii post-stroke. Additionally, we present evidence of increased persistent inward currents in both upper limb flexors and extensors in both the paretic and non-paretic limbs of stroke survivors. Together these findings suggest a systemic increase in the level of monoaminergic drive following hemiparetic stroke, with the intact ionotropic corticospinal projections to the non-paretic limb playing a major role in the unilateral distribution of observed motor deficits. However, the results of this study highlight several questions that still remain regarding motor control following stroke. Further research into the changes that arise in the control of the non-paretic limb is necessary and there is a lack of thorough investigation into the changes in the upper limb extensors following stroke. Novel techniques

which allow for the recordings from multiple muscles simultaneously, may make the investigation of multiple muscles and multiple limbs substantially easier, reducing the need to focus solely on the more affected limb and muscles. This would enable a more complete characterization of motor control of the upper limb post-stroke.

7. Impaired post-stroke motor unit firing rate modulation is more pronounced during flexion synergy-driven contractions of the biceps brachii

7.1 Abstract

Following a hemiparetic stroke, individuals exhibit altered motor unit firing patterns during voluntary muscle contractions, including impairments in firing rate modulation and recruitment. These individuals also exhibit abnormal muscle coactivation through multi-joint synergies. Our goal was to determine if motor unit firing activity during flexion synergy-driven contractions of the paretic biceps brachii is different from that of voluntary contractions. To accomplish this, we calculated measures of motor unit firing rate, rate modulation, and recruitment patterns during isometric elbow flexion ramp contractions during synergy-driven and voluntary contractions of the paretic limb. Motor units during synergy-driven contractions displayed a significant reduction in rate modulation of 0.21 ± 0.04 pps/%MVT (χ^2 *(1) = 28.4, P < 0.0001*) when compared to motor units from voluntary contractions. Additionally, there was evidence of increased recruitment of motor units, including an increase in the average torque at which motor units were recruited, a reduction in average firing duration of motor units, and an increase in the amplitude of the biceps EMG during contractions at the same force level. These results demonstrate that motor unit firing activity is more affected during synergy-driven contractions than voluntary contractions. The neural mechanisms involved in generating the flexion synergy, namely recruitment of the reticulospinal system, may also contribute to the observed deficits in motor unit firing patterns.

7.2 Introduction

Individuals with chronic hemiparesis following a stroke display altered motor unit firing patterns in their paretic upper limb. Previous motor unit analyses in the stroke population have shown a reduction in motor unit firing rates for a given force level (Gemperline *et al.*, 1995) and compressed motor unit recruitment (Gemperline *et al.*, 1995; Hu *et al.*, 2015). Further, individuals with chronic post-stroke hemiparesis display both impaired modulation of motor unit firing rate (Gemperline *et al.*, 1995; Mottram *et al.*, 2009; Mottram *et al.*, 2014) and increased EMG amplitude associated with increased motor unit recruitment (Tang & Rymer, 1981) in the elbow flexors of the paretic limb during voluntary contractions.

The abnormal firing patterns observed post stroke are likely due to a change in descending neural drive following stroke-induced damage to the high-resolution corticofugal pathways (Gemperline *et al.*, 1995; Fang *et al.*, 2009; Mottram *et al.*, 2014; Hu *et al.*, 2015; Chen *et al.*, 2018). In addition to the direct loss of corticospinal drive, there is growing evidence that some motor deficits are associated with utilization of alternate descending neural pathways. For example, increased reliance on cortico-reticulospinal pathways is thought to play a major role in the loss of independent joint control observed post-stroke (Dewald *et al.*, 1995; McPherson *et al.*, 2018a; McPherson *et al.*, 2018b; McPherson & Dewald, 2019). Individuals with chronic hemiparetic stroke demonstrate an increase in non-linear corticomuscular connectivity associated with the multisynaptic nature of corticobulbospinal motor pathways (Yang *et al.*, 2020), and imaging of the brainstem and spinal cord has shown decreases in the integrity of the corticospinal tract combined with increases in the integrity of the recticulospinal tract that scale with with motor impairment following stroke (Karbasforoushan *et al.*, 2019). In the upper limb, the loss of independent joint control commonly presents via the multi-joint flexion synergy, where shoulder

abduction (SABD) is involuntarily coupled with elbow flexion (EF), supination, and wrist and finger flexion (Twitchell, 1951; Brunnstrom, 1970; Dewald *et al.*, 1995; Sukal *et al.*, 2007; Lan *et al.*, 2017; McPherson & Dewald, 2019). However, motor unit firing patterns during synergy-induced contractions have not been rigorously investigated.

Increased utilization of cortico-reticulospinal pathways may also directly contribute to the reduced motor unit firing rates and rate modulation seen following stroke. The ionotropic component of the cortico-reticulspinal system (i.e., the pathways carrying specific motor commands) may limit motoneuron firing rate as it relies primarily on slower, polysynaptic pathways (Riddle *et al.*, 2009; Baker, 2011), generates motoneuron EPSPs of substantially lower amplitude than the corticospinal pathways (Riddle *et al.*, 2009; Baker, 2011), and can lead to concurrent inhibition along with excitataion (Koizumi *et al.*, 1959). In addition, the metabotropic component of the reticulospinal system (i.e., raphespinal and ceuroleospinal pathways that dramatically alter alpha motoneuron excitability) is known to induce non-linear motor unit firing patterns in response to linear excitatory input through the induction of persistent inward currents (PICs) (Bennett *et al.*, 1998; Lee *et al.*, 2003). PIC related nonlinear motor unit firing patterns include periods of rate saturation, during which motor unit firing is not responsive to increases in descending input (Johnson *et al.*, 2017).

Because flexion synergy-induced contractions in the upper limb are thought to be primarily driven through these corticoreticulospinal pathways, an in-depth analysis of motor unit activity during these contractions will provide an opportunity to further probe how motor unit firing patterns are altered in response to both ionotropic and metabotropic associated corticoreticulospinal drive.

In this study, we ~~i~~nvestigate the relationship between changes in descending neural drive following stroke and altered motor unit firing patterns. To accomplish this, first, we compared voluntary contractions in the paretic and non-paretic limbs to expand upon previous studies, with the capability to record from larger populations of motor units through the utilization HDsEMG. We then quantified and compared motor unit firing rates, recruitment patterns, and rate modulation during both voluntary and synergy-driven contractions in the paretic limb. We expect to see a reduction in rate modulation in the paretic limb, as has been previously reported, and we hypothesize that we will see further reductions in firing rate modulation during synergy driven contractions, due to the postulated increased corticoreticulospinal drive during these contractions.

7.3 Methods

7.3.1 Participants

11 stroke survivors (1 female, 10 male) ranging in age from 48 to 73 (mean ± SD age: 61.91 ± 6.14) completed the study. Participants selected for this study displayed a broad range of upper limb impairment levels, as quantified using the Fugl-Meyer (FM) assessment (Fugl-Meyer *et al.*, 1975), with FM score range from 12/66 to 52/66 (mean ± SD FM score: 29.90 ± 15.67). For inclusion in this study stroke participants were required to have: (1) Paresis confined to one side, (2) At least one year post-stroke, (3) Absence of muscle tone abnormalities and motor or sensory impairment in the non-paretic limb, (4) Absence of severe wasting or contracture of the paretic upper limb, (5) Absence of severe cognitive or affective dysfunction, (6) Absence of severe concurrent medical problems (e.g. cardiorespiratory impairment), (7) Absence of brainstem and cerebellar lesions as determined from clinical or radiological reports. All participants provided written informed consent prior to participation in this experiment which was approved by the Institutional Review Board of Northwestern University.

7.3.2 Experimental Apparatus

The experimental apparatus is the same as that used in our previous work, which can be reviewed for further details (Hassan *et al.*, 2019), and is shown in Figure 7.1 below. Participants were seated in a Biodex experimental chair (Biodex Medical Systems, Shirley, NY) and secured with shoulder and waist straps to minimize trunk movement. The participant was connected to a six degree-of-freedom load cell (JR3, Inc., Woodland, CA), using a fiberglass cast at the forearm. A Jacobian based algorithm was used to convert forces and torques at the load cell and the arm

segment lengths and joint angles into elbow and shoulder torque. The arm was positioned at a shoulder abduction angle of 75º, a shoulder flexion angle of 40º, and an elbow flexion angle of 90º. Forces and torques measured at the forearm-load cell interface were recorded at 1024 Hz and converted into joint torques using custom MATLAB software (The MathWorks).

Multi-channel electrode grids were placed on the surface of the biceps brachii. EMG recordings were collected in single differential mode from the 64 electrode grids with 8mm inter-electrode distance (GR08MM1305, OT Bioelettronica, Inc., Turin, IT), using a Quattrocento signal amplifier (OT Bioelettronica, Inc., Turin, IT; input range: 33mVpp). All EMG signals were amplified (x150), band-pass filtered (10-500Hz), and sampled at 2048 Hz. A 1 second TTL pulse

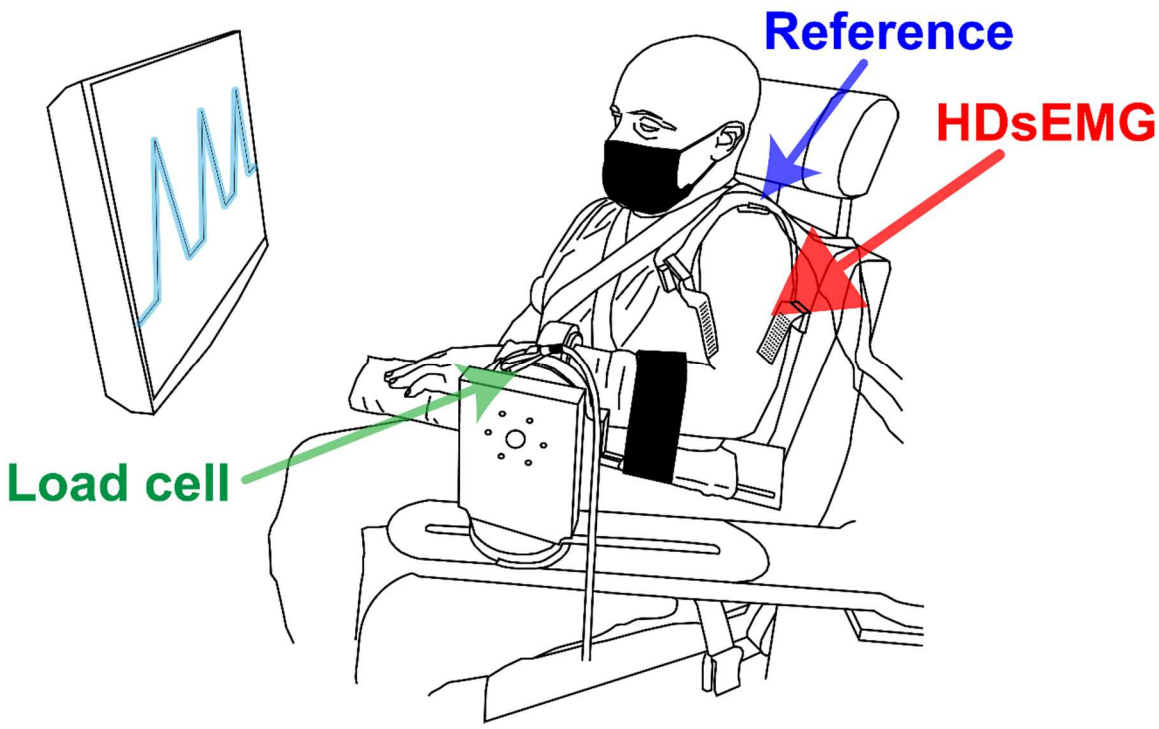

Figure 7.1: Illustration of the experimental setup.
Participants are seated in a biodex chair with their forearm secured to a 6 degree-of-freedom load cell. High-density EMG electrode grids are placed on the lateral head of the triceps brachii, and along the muscle belly of the biceps brachii. Real-time visual feedback of task performance was provided via a computer monitor in front of the participant.

was included as an additional channel on both the EMG and torque recordings, which allowed for off-line synchronization of the recordings.

7.3.3 Protocol

7.3.3.1 Maximum Voluntary Torque. In order to allow normalization across subjects and limbs, maximum voluntary torques (MVTs) were collected from both the paretic and non-paretic upper limbs of all participants. MVTs were collected for shoulder abduction (SABD), shoulder adduction (SADD), elbow flexion (EF), and elbow extension (EE). Participants received real-time visual feedback of their torque generation along with vocal encouragement from the experimenter. To ensure that an accurate MVT was attained, trials were repeated until the participant completed three trials in which the peak torque was within 10% of the maximum trial observed. Additionally, if the final trial showed the highest peak torque, subsequent trials were collected.

7.3.3.2 Submaximal Isometric Torque Ramps. For the experimental trials, participants generated submaximal triangular isometric EF torque ramps. Participants gradually increased their EF torque to ~20% MVT over 10 seconds and then gradually decreased their torque back to 0% MVT over the subsequent 10 seconds. Participants received visual feedback during the task including the desired time-torque profile and a trace of their torque generation which was updated in real-time. Submaximal ramp trials consisted of three EF ramps in succession. Trials included five seconds of baseline at the beginning and end of each trial and ten seconds of rest between ramps, where no torque generation was required. Participants were given several minutes of rest between trials and several practice trials with verbal coaching to become comfortable with the task. Each participant

completed five to six experimental trials that were used for subsequent analysis. Prior to motor unit analyses, all torque traces were visually inspected, and ramps that did not exhibit smoothly torque traces that matched the desired time-torque profile were removed. The submaximal EF torque ramps were collected in both the paretic and non-paretic limbs and were used for the between-limb comparisons.

7.3.3.3 Synergy-driven Isometric Contractions. Synergy-driven contractions of the biceps brachii in the paretic limb were elicited by having participants generate SABD torque ramps. The SABD torque level, which generated ~20% MVT in the direction of EF was determined for each participant over the course of several practice trials. Participants gradually increased SABD torque over 10 seconds to their identified target level, and then gradually decreased their SABD torque over the following 10 seconds. Participants were provided with the desired time-torque profile and real-time torque feedback in the direction of SABD only. Participants completed five to eight SABD trials. Due to difficulties in obtaining synergy-driven contractions of exactly 20% MVT, we sought to match the exact torque level generated during the synergy-driven EF during the voluntary contractions. Participants then conducted five to eight EF trials matching the EF torque level elicited during the SABD trials and were provided with desired time-torque profile and real-time torque feedback in the direction of EF for these matching trials. Each trial contained only 1 torque ramp, with five seconds of baseline at the beginning and end of each trial, where no torque generation was required.

7.3.4 Data Analysis

7.3.4.1 Motor unit decomposition. Each EMG channel was visually inspected and channels showing substantial artifacts, noise, or saturation of the A/D board were removed (typically zero to five channels were removed per trial). The remaining surface differential EMG channels were decomposed into motor unit spike trains using a convolutive blind source separation algorithm (Negro *et al.*, 2016) and its successive sparse deflation improvements (Martinez-Valdes *et al.*, 2017). Additionally, the rectified sum of the remaining EMG channels was used for estimates of EMG amplitude. The silhouette threshold for decomposition was set to 0.85. Despite these stringent requirements for decomposition accuracy, the blind source separation algorithm may extract some non-physiological motor unit discharge times and required visual inspection of the decomposed motor unit pulse train to identify and correct errors, as has been used extensively for the accurate estimation of motor unit discharge patterns (Boccia *et al.*, 2019; Hassan *et al.*, 2019; Afsharipour *et al.*, 2020; Del Vecchio *et al.*, 2020; Martinez-Valdes *et al.*, 2020). The errors encountered in our recordings were similar to those outlined by Afsharipour and colleagues (Afsharipour *et al.*, 2020) and were mainly cases of missed firing pulses producing firing rates that were half of the mean rate or incorrectly identifying multiple pulses near one firing time, leading to firing rates substantially above the mean rate. These errors were iteratively corrected and the motor unit pulse train was re-estimated at each iteration (Afsharipour *et al.*, 2020). Further, particular attention was paid to the initial and final portion of the motor unit spike train in order to estimate precisely the recruitment and derecruitment times and discharge rates. The instantaneous motor unit firing rates were calculated as the inverse of the interspike intervals of the motor unit spike trains. The instantaneous motor unit firing rates were smoothed using a 2 s Hanning window.

7.3.4.2 Motor unit matching. In order to enable a more robust comparison of motor unit activity between the synergy-driven and voluntary contractions, we utilized a motor unit tracking algorithm to match motor units across the two contraction types. The method is based on the similarity between motor unit action potential shapes identified in different contractions. In this study, we used the normalized cross-correlation of the 2D representation of the motor unit action potentials, similar to previous studies (Martinez-Valdes *et al.*, 2017; Vecchio & Farina, 2019). The method is based on the assumption that motor unit action potentials recorded by multiple electrodes over the surface of the muscle are likely to have a unique representation (Farina *et al.*, 2008). The action potentials of the individual motor units were estimated by spike-triggered averaging using the decomposed discharge times. In this procedure, all matches between two trials were visually inspected, and the identified motor units were classified as the same when they had a cross-correlation coefficient larger or equal to 0.80. Each matched motor unit was indexed to enable comparisons of the same unit during different contractions.

7.3.4.3 Quantification of Rate Modulation. Motor unit firing rate modulation is here defined as the response of the motor unit firing rate to increasing descending input during the post acceleration phase. A bilinear fit was used to estimate the slope of motor unit firing during the acceleration and the rate saturation phases. The transition from acceleration to rate saturation was determined through the iterative process to determine the best division between the first linear range and the second linear range of the ascending limb of the torque ramp. The bilinear fit with the least error, when compared to the actual firing rate, was utilized. In this paper, we used EF torque as a proxy for the descending excitatory input to the biceps brachii motoneurons. We quantified the rate modulation as the slope of the linear fit of the motor unit firing rate with respect to torque from

the end of the acceleration phase to the peak of the torque ramp. Motor units that were recruited after the peak in torque were excluded. Additionally, to ensure the motor units had completed the acceleration phase and had a substantial rate saturation phase, only those recruited at least three seconds before peak torque were included in the rate modulation analyses. Figure 7.2 shows the calculation of this rate modulation fit with respect to torque for a single motor unit from one stroke participant. To facilitate comparisons with previous analysis of motor unit rate modulation, we estimated the incidence of impaired motor firing rate modulation, by determining the proportion of motor units with firing rate slope relative to torque of less than 0 pps/%MVT.

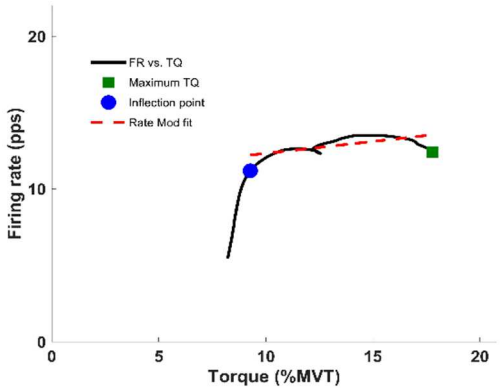

Figure 7.2: Rate modulation calculation.
Black line shows the motor unit firing rate plotted with respect to torque. The blue dot shows the inflection point found by the bilinear fit, separating the acceleration phase from the rate saturation phase. The red dotted line is the linear fit of the rate saturation phase, the slope of which is used as our measure of rate modulation.

As there are multiple muscles that produce torque at the elbow, we also quantified motor unit firing rate modulation with respect to the rectified sum of all EMG channels recorded from the biceps brachii. All channels which did not show significant noise or artifacts were rectified, and summed for each contraction and this summed rectified EMG was used as a proxy for descending excitatory input. However, as EMG recordings weren't consistently done during maximum voluntary torque trials, EMG values were normalized to the largest EMG values obtained during the submaximal torque ramps. Rate modulation was calculated with respect to normalized EMG (nEMG) in the same manner as it was for torque.

7.3.5 Statistical Analysis

Group values are presented as mean ± SD, unless otherwise noted. Mean values are first calculated for each participant, before averaging across all participants. Effect size (ES) was estimated using Cohen's *d* (Cohen, 1992) calculated from the differences of subject means across limb and contraction type. Group values and effect size calculations were conducted using GraphPad Prism software (version 9.0.0 for macOS, GraphPad Software, San Diego, California USA). The accuracy of torque traces was estimated by calculating the root mean squared error (RMSE) between the desired time-torque profile and the participant's torque trace and the RMSE between the desired torque slope and the slope of the participant's torque trace. The RMSE values are normalized by the range of the desired time-torque profile.

Differences across limb and type of contraction were investigated using a linear mixed effects model with limb (paretic, non-paretic for voluntary contractions) or type of contraction (voluntary, synergy-driven for paretic contractions) as a fixed effect and participant as a random effect. For comparisons of the matched units during voluntary vs. synergy-driven contractions, type of contraction was a fixed effect, and participant and motor unit index were random effects. We investigated the effect of limb (paretic vs. non-paretic) on the following dependent variables during voluntary contractions: peak motor unit firing rate, motor unit firing rate range, duration of motor unit firing, rate modulation slope with respect to torque and nEMG, and the proportion of units exhibiting negative rate modulation. We investigated the effect of contraction type (synergy-driven vs. voluntary) on the following dependent variables during EF contractions of the paretic limb: peak torque, slope of torque ramp, RMSE of the torque trace and the slope of the torque trace, peak motor unit firing rate, motor unit firing rate range, duration of motor unit firing, rate

modulation slope with respect to torque and nEMG, the proportion of units exhibiting negative rate modulation, torque at motor unit recruitment, motor unit recruitment time relative to peak torque, and EMG amplitude. For the comparisons of motor unit firing rate, duration, and rate modulation, the data in the linear mixed effects model were not averaged within participants and all motor units were considered as separate data points, while the differences between participants were estimated as a random effect. For the comparisons of torque traces and EMG amplitude, each trial was considered a separate data point. However, the proportion of motor units exhibiting negative rate modulation was determined across all trials for each study participant, and participant means were used for the linear mixed effect models for these comparisons. Visual inspection of the model residuals was conducted through Q-Q plots and residual plots across the range of fitted values to ensure the data met the assumptions of normality and homoscedasticity, respectively. Effects estimated from the linear mixed effects model are presented as model estimate ± SE. *P*-values were obtained using likelihood ratio tests of the full model including the effect of interest against a null model excluding the effect of interest. Linear mixed effects analyses were conducted using *lme4* (Bates & Maechler, 2015) in R (R Core Team 2020, R Foundation for Statistical Computing, Vienna, AUT). Statistical significance was set at $P < 0.05$ for all analyses.

7.4 Results

Decomposition from the non-paretic biceps brachii of seven stroke participants during the submaximal isometric torque ramps yielded 435 reliable motor unit spike trains (after the assessment and cleaning procedures), with an average of 4.0 ± 2.9 motor unit spike trains per trial. 655 reliable motor unit spike trains were decomposed from the paretic biceps brachii of eight

stroke participants during the submaximal isometric torque ramps, with an average yield of 5.2 ± 3.5 motor units per trial. Following the assessment and cleaning procedure, the mean silhouette values of the decomposed motor units were 0.92 ± 0.04 from the non-paretic biceps brachii, and 0.93 ± 0.04 from the paretic biceps brachii. All participants completed a minimum of 9 torque ramps in both the paretic and non-paretic submaximal torque ramp tasks. Figure 7.3 shows submaximal torque ramps and decomposed motor units from both the non-paretic (A) and paretic (B) biceps brachii of one moderately impaired stroke participant.

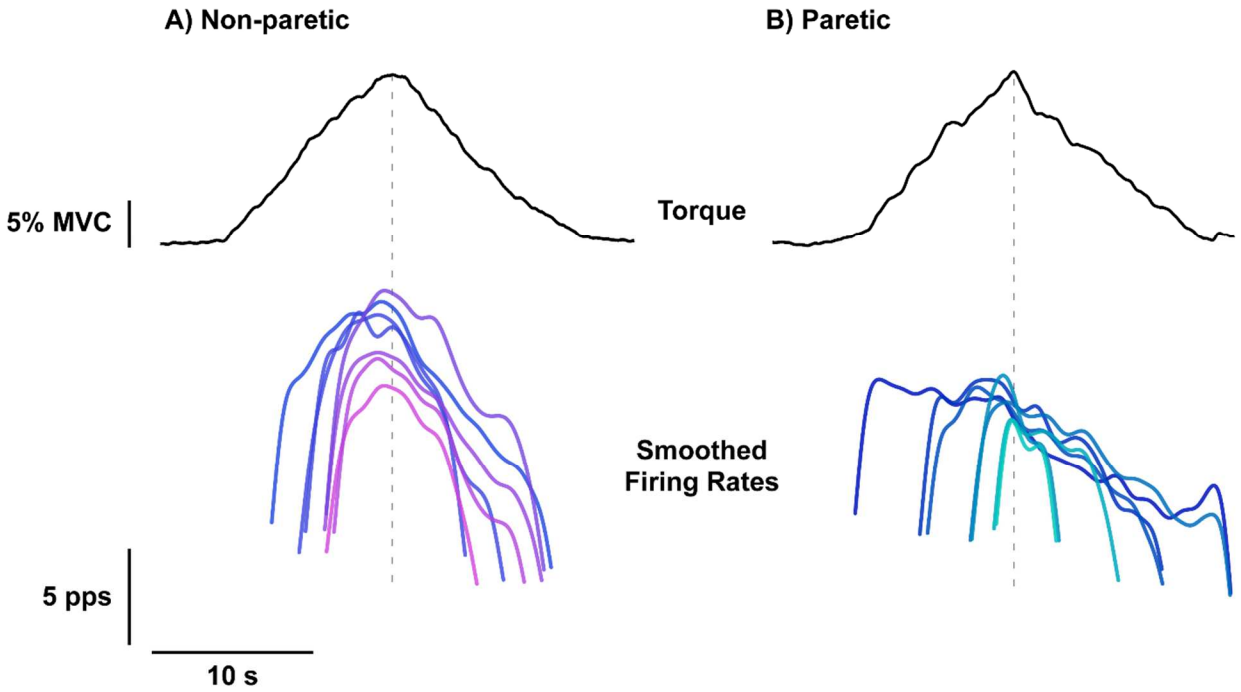

Figure 7.3: EF torque and decomposed biceps motor units from paretic and non-paretic limb
EF torque traces from the non-paretic (A) and paretic (B) limbs of one moderately impaired stroke subject are shown as black solid lines. The smoothed firing rates (FR) of decomposed motor units are shown in shades of purple for the non-paretic limb, and shades of blue for the paretic limb.

Additionally, decomposition yielded 394 motor unit spike trains from eight-stroke participants during synergy-driven contractions with an average yield of 6.4 ± 4.1 spike trains per trial. From the same eight participants, 383 motor unit spike trains were discriminated from the biceps brachii

during the matching voluntary trials, with an average yield of 5.2 ± 3.4 spike trains per trial. The silhouette values for the cleaned motor unit spike trains were 0.93 ± 0.03 during synergy-driven contractions and 0.93 ± 0.04 from the voluntary contractions. Each participant completed a minimum of 5 synergy-driven contractions and a minimum of 5 voluntary contractions at a torque level matched to the synergy-driven contractions.

7.4.1 Motor unit firing rate and duration in the paretic and non-paretic biceps brachii

Figure 7.4A shows the peak firing rates of biceps brachii during 20% MVT EF ramps. Data points represent the mean value from all motor units collected from each subject over repeated voluntary contractions. Group mean peak MU firing rates were higher in the non-paretic limb (14.9 ± 2.1 pps) than in the paretic limb (12.3 ± 2.5 pps; $ES = 1.39$). Linear mixed effects models revealed that limb had a significant effect on peak firing rate ($\chi^2\ (1) = 275.3,\ P < 0.0001$), with a reduction of 2.7 ± 0.2 pps in motor units from the paretic limb compared to the non-paretic limb. Additionally, Figure 7.4B shows reduced motor unit firing rate ranges in the paretic limb (7.0 ± 1.5 pps) compared to the non-paretic limb (8.8 ± 1.3 pps; $ES = 1.48$). A significant reduction in motor unit firing rate range (1.7 ± 0.1; $\chi^2\ (1) = 199.1,\ P < 0.0001$) was found between motor units from the non-paretic and paretic limb. The average duration of motor unit firing is shown in Figure 7.4C. An increase in the duration of motor unit activity in the participants' paretic versus non-paretic limbs (10.5 ± 2.7 s vs 13.9 ± 3.4 s; $ES = 0.80$) was seen in the group means. The limb had a significant effect on motor unit duration ($\chi^2\ (1) = 117.9,\ P < 0.0001$) in our model, with motor unit firing duration increasing by 4.1 ± 0.4 s in paretic limb contractions. This increased motor unit duration was present on both the ascending and descending limbs of the torque ramp. During the ascending torque ramp, the group means for motor unit active duration were 6.3 ± 1.2 s in the

paretic limb and 5.0 ± 1.3 s in the non-paretic limb (*ES = 0.77*). The limb had a significant effect on motor unit duration on the ascending limb of the torque ramp (χ^2 *(1) = 60.4, P < 0.0001*), with an increase in motor unit duration of 1.5 ± 0.2 s in the paretic limb. On the descending torque ramp, the group means for motor unit active duration were 7.5 ± 2.6 s in the paretic limb and 5.5 ± 2.0 s in the non-paretic limb (*ES = 0.59*). Limb also had a significant effect on motor unit duration during the descending limb torque ramp (χ^2 *(1) = 100.2, P < 0.0001*), with an increased motor unit duration of 2.6 ± 0.3 s in the paretic limb.

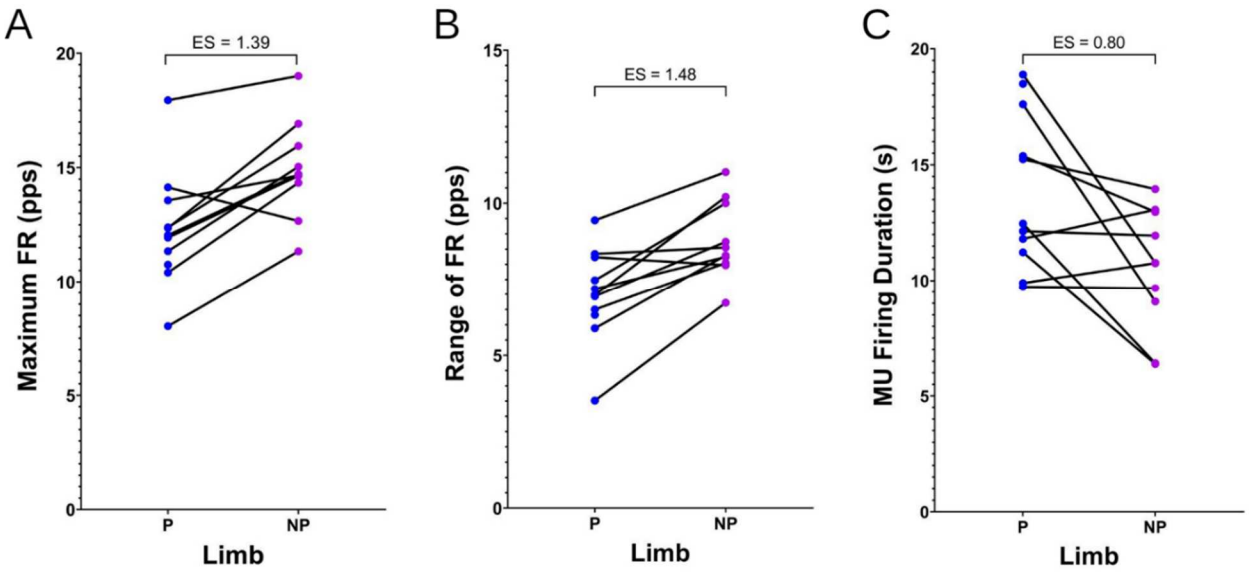

Figure 7.4: Motor unit firing rate and duration in paretic and non-paretic limbs
(A) Subject means for peak motor unit firing rate during 20% MVT EF task in both the non-paretic (NP) and paretic limbs (P) . (B) Subject means for the range of motor unit firing rates in both limbs. (C) Subject means for the duration of motor unit firing for both limbs. The linear models including all units from all participants had P value of <0.0001 for all 3 comparisons shown above

7.4.2 Motor unit firing rate modulation in the paretic and non-paretic biceps brachii

Previous research has shown impairments in motor unit firing rate modulation in the paretic biceps brachii of individuals with stroke using a paired motor unit analysis (Mottram *et al.*, 2014) and with respect to absolute torque (Gemperline *et al.*, 1995). Figure 7.5A shows motor unit firing rate modulation slope in the biceps brachii with respect to torque, during ramp contractions to a

matched effort level of 20% MVT. Consistent with previous results, lower rate modulation was seen in the paretic biceps (0.05 ± 0.03 pps/%MVT) than in the non-paretic biceps (0.18 ± 0.12 pps/%MVT, *ES = 1.21*); the reduction in rate modulation slope was observed in 9 of 10 participants who completed both the paretic and non-paretic torque ramps. The limb was shown to have a significant effect on rate modulation slope (χ^2 *(1) = 32.7, P < 0.0001*), with a reduction of 0.14 ± 0.02 pps/%MVT in motor units from the paretic limb relative to the non-paretic limb.

Further, in Figure 7.5B, we present the proportion of motor units that exhibit impaired rate modulation as a measure of the incidence of impaired firing rate modulation. Units are here labeled as displaying impaired rate modulation if the slope of the firing rate relative to torque is less than 0 pps/%MVT, i.e., motor units with decreasing post-acceleration firing rates during the ascending limb of the torque ramp. In accordance with the findings of Mottram et al. (2014), we observed a significantly higher proportion of units exhibiting impaired firing rate modulation in the paretic limb (0.44 ± 0.08) than in the non-paretic limb (0.25 ± 0.16; *ES = 1.14*). The proportion of motor units exhibiting impaired rate modulation was larger in the paretic limb of the same 9 participants as the reduction in mean motor unit rate modulation. A significant effect of limb was found on the proportion of units displaying negative rate modulation (χ^2 *(1) = 10.3, P = 0.0013*), with the paretic limb showing a 0.19 ± 0.05 increase in proportion of units exhibiting impaired modulation compared to the non-paretic limb.

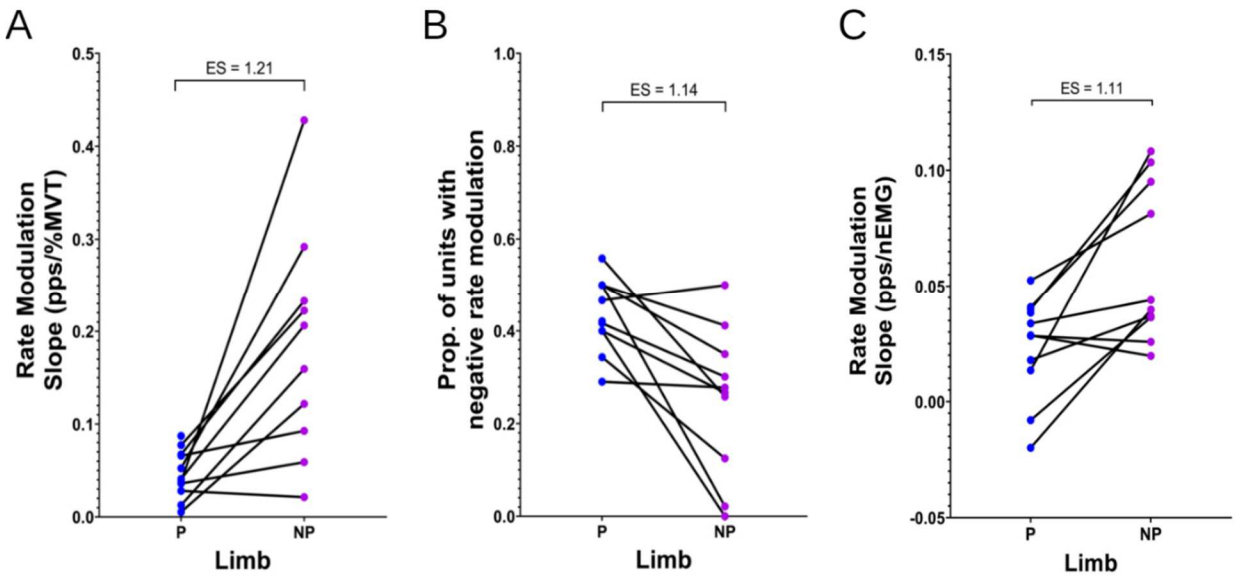

Figure 7.5: Rate modulation for paretic and non-paretic limbs
(A) Subject means for motor unit firing rate modulation relative to % maximum torque for both limbs (P < 0.0001). (B) Proportion of motor units displaying negative motor unit firing rate modulation (P = 0.0013). (C) Subject means for motor unit firing rate modulation relative to biceps nEMG for both limbs (P = 0.12). P values are obtained from the linear model using all units from all participants.

In order to eliminate the effects of other muscles acting about the elbow joint, we also calculated rate modulation with respect to nEMG of the biceps, shown in Figure 7.5C. With respect to EMG, lower rate modulation was still found in the paretic biceps (0.024 ± 0.022 pps/nEMG) than in the non-paretic biceps (0.059 ± 0.034 pps/nEMG; *ES = 1.11*). However, our mixed effects model did not show a significant effect of limb on rate modulation with respect to EMG (χ^2 *(1) = 2.42, P = 0.12*).

7.4.3 Isometric torque ramps during synergy-driven vs voluntary contractions in the paretic limb

Figure 7.6 shows the EF torque traces and decomposed biceps brachii motor units from voluntary (A) and synergy-driven (B) contractions in the paretic limb of one stroke participant

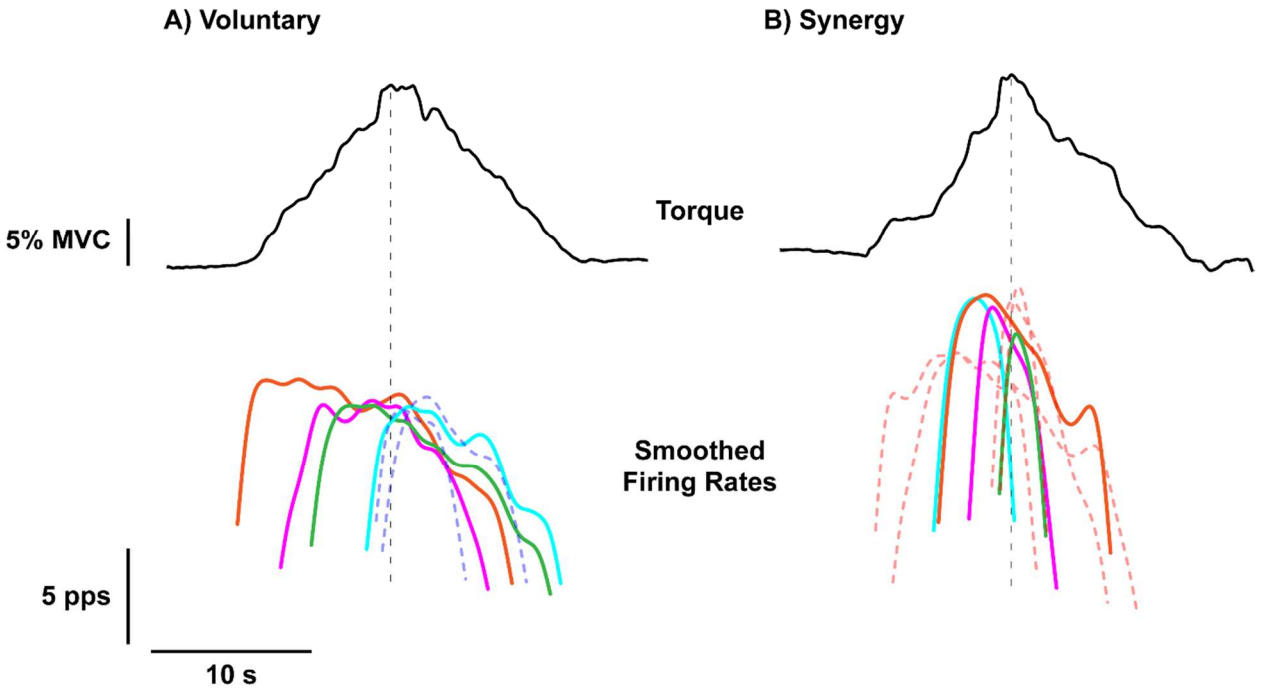

Figure 7.6: EF torque and decomposed biceps motor units during synergy-driven and voluntary contractions
EF torque traces from the paretic limb of one severely impaired stroke subject during voluntary (A) and synergy-driven (B) contractions are shown in black solid lines. The smoothed firing rate profiles are shown below. The matched units are shown in solid color lines, with the traces of the same color indicating a matched unit pair. Unmatched units are shown as dotted lines.

with severe motor deficits according to the Fugl-Meyer Motor Assessment score (20/66). The ascending limbs of the torque ramps are comparable between the synergy-driven and voluntary contractions, however, this subject displays a reduced ability to relax on the descending limb of the torque ramp. Stroke subjects displayed a variety of EF torque behavior on the descending portion of the synergy-driven torque ramps, with some subjects displaying poor relaxation as shown in Figure 7.6 and others going into elbow extension. Due to this variability, the following investigations into behavior during synergy-driven contractions is restricted to the ascending limb of the torque ramp. Participants generated 20.9 ± 4.7 %MVT EF torque (range 11.6 - 28.3 %MVT) during the synergy-driven contractions; the average SABD target used to elicit the synergy-driven EF was 30.8 ± 11.4 % MVT (range 17.9 - 45.7 %MVT). A simple linear regression revealed no significant relationship between participants FMA scores and the ratio of synergy-induced EF

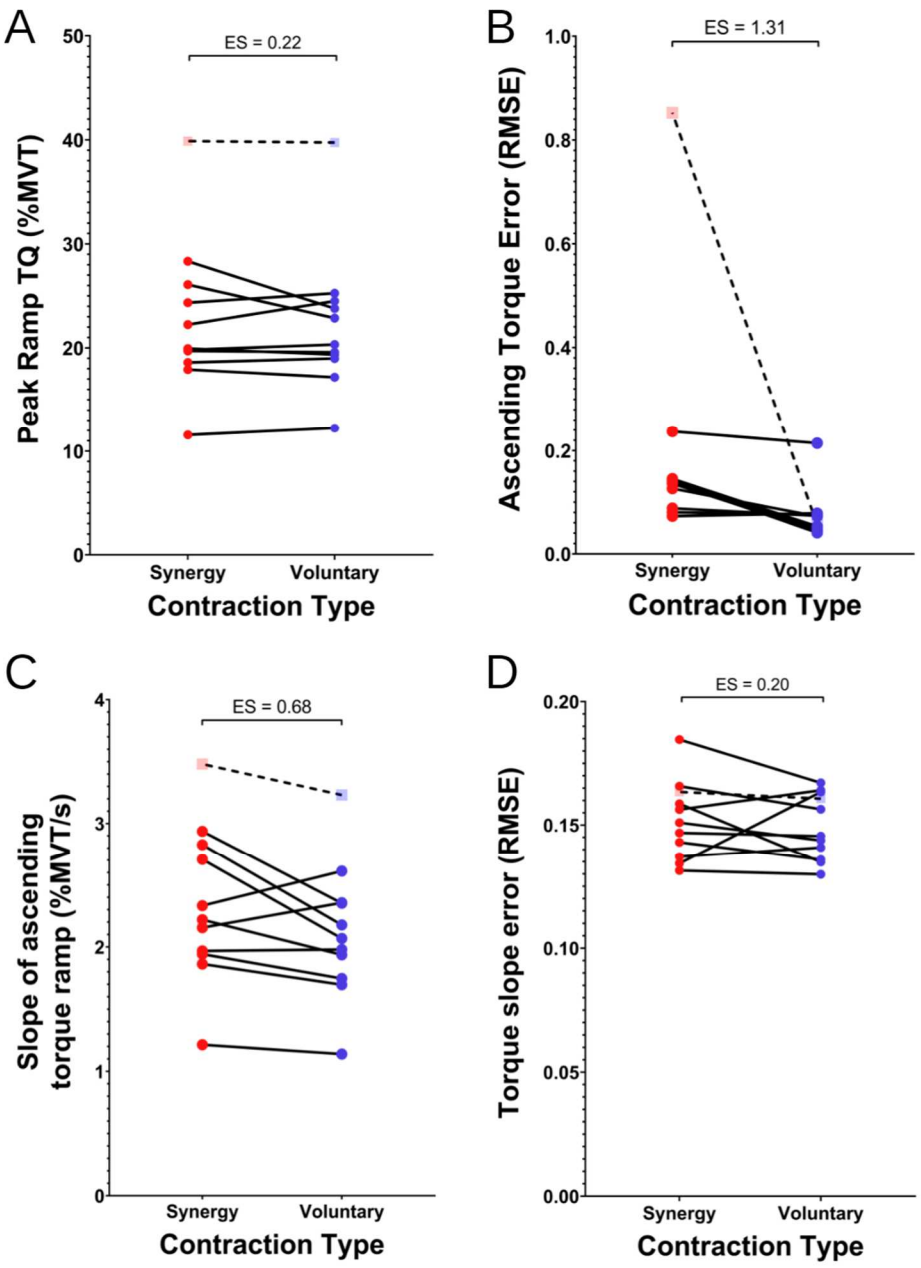

Figure 7.7: Torque statistics from synergy-driven and voluntary contractions
(A) Subject mean peak torques for the submaximal isometric torque ramps during synergy-driven and voluntary contractions (P = 0.4674). (B) The normalized RMSE during the ascending torque ramp, compared to the ideal time-torque profile (P = 0.0011). (C) Subject mean torque slopes during the ascending limb of the torque ramp (P = 0.0556). (D) The normalized RMSE of the slope of the ascending limb of the torque ramp, compared to the ideal slope-time profile (P = 0.5390). P values are obtained from the linear model using all units from all participants.

torque to SABD torque ($R^2 = 0.067$; $p = 0.5361$). As the synergy-driven EF contractions were spontaneously elicited during a SABD task, participants did not receive real-time visual feedback on their EF torque during these tasks. In order to compare the motor unit activity during the synergy-driven and voluntary contractions, we sought to ensure that the time-torque profile during these contractions was similar. Figure 7.7A shows the peak of the voluntary and synergy torque ramps for each subject. The torque levels of the voluntary

contractions were matched to the peak of the synergy contractions (group mean: 20.4 ± 3.9 %MVT for the voluntary contractions, 20.9 ± 4.7 %MVT for synergy-driven contractions, *ES = 0.22*), and no significant effect of contraction type was found on the peak ramp torque (χ^2 *(1) = 0.53, P = 0.4674*). Figure 7.7B shows the subject mean RMSE between the desired time-torque profile and the participants torque traces during the ascending limb of the torque ramp. The desired time-torque profile was a linear torque ramp, from 0% MVT to each participant's mean peak torque during the synergy contractions, over 10 seconds. One participant displayed very large deviations between his synergy-induced contractions and the desired time-torque profile (normalized RMSE 0.85). This participant did not generate steadily increasing EF torque in his synergy contractions, instead exhibiting a rapid increase in EF torque in the first few seconds which then leveled off to a constant EF torque for the rest of ascending portion of the SABD torque ramp. Due to the large discrepancies in the time-torque profile of this subject's synergy driven EF contractions, they were removed from all following analyses and are shown across all panels in Figure 7.7 as a lighter shaded square. After removing that participant, there was still a higher RMSE during the synergy driven contractions (0.13 ± 0.05), compared with the voluntary contractions (0.08 ± 0.05; *ES = 1.31*). Contraction type was found to significantly affect the RMSE of the torque trace (χ^2 *(1) = 10.6, P = 0.0011*), with synergy-driven contractions associated with an increase in RMSE of 0.06 ± 0.01 compared to voluntary contractions.

Additionally, no significant effect of contraction type was found on the slope of the torque ramps (χ^2 *(1) = 3.66, P = 0.0556*). The group mean slope of the torque ramps was 2.3 ± 0.62 %MVT/s in the synergy-driven contractions and 2.1 ± 0.54 %MVT/s during voluntary contractions (*ES = 0.68*), as shown in Figure 7.7C. The subject mean error in the ascending torque slope is shown in Figure 7.7D. The desired slope – time profile was a constant slope of each participant's

mean peak torque during the synergy contractions divided by 10 seconds. The normalized RMSE was similar for both the slope of the synergy-driven (0.15 ± 0.02) and voluntary contractions (0.15 ± 0.01; *ES = 0.20*), and there was no significant effect of contraction type on the normalized RMSE

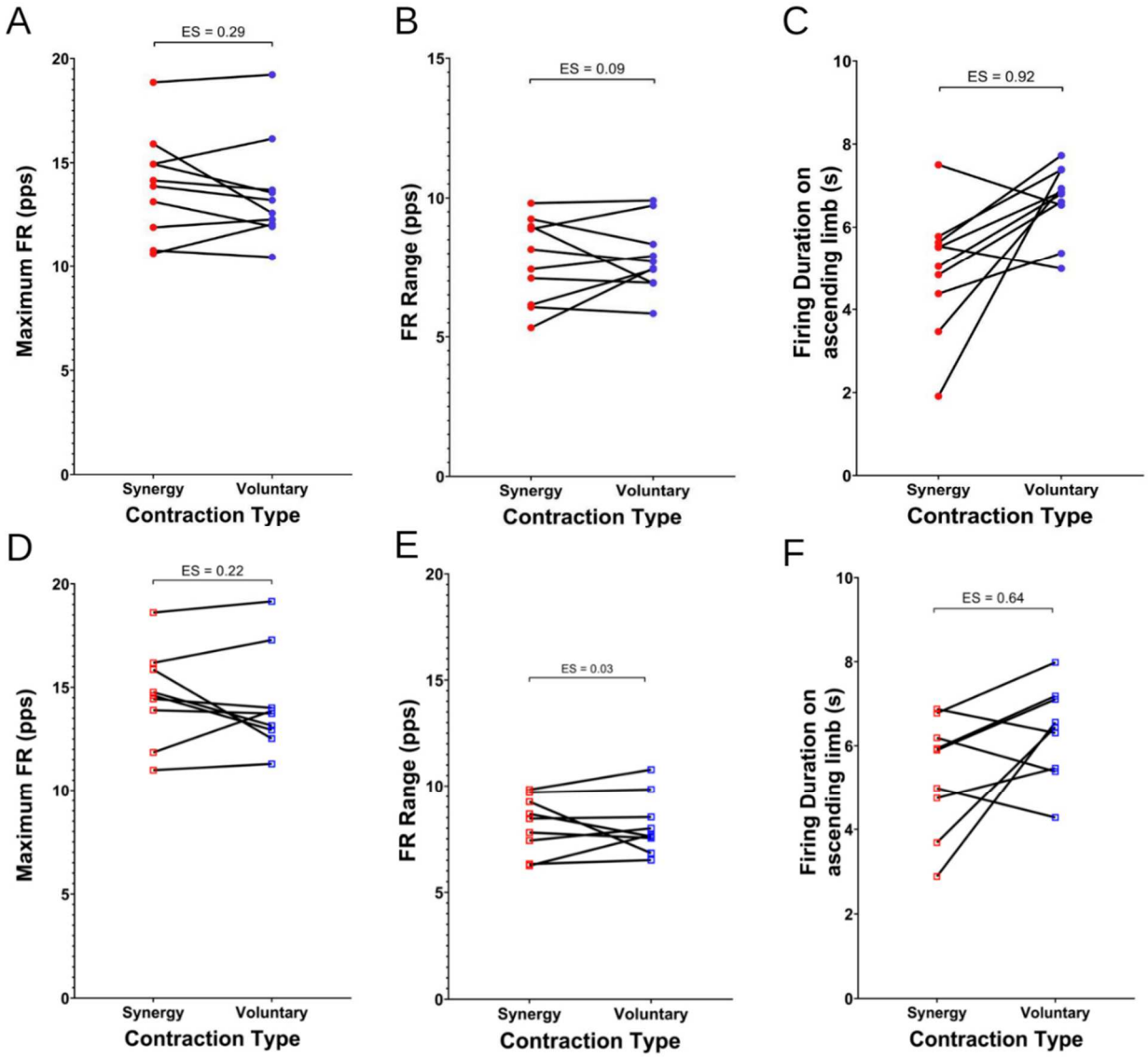

Figure 7.8: Motor unit firing rate and duration during synergy-driven and voluntary contractions
(A) Subject means for peak motor unit firing rate during synergy-driven and voluntary contractions in the biceps (P = 0.0026). (B) Subject means for the range of motor unit firing rates during synergy-driven and voluntary contractions (P = 0.1753). (C) Subject means for the duration of motor unit firing activity during the ascending limb of synergy-driven and voluntary contractions (P < 0.0001). The values for the motor units which were matched during the synergy-driven and voluntary contractions for peak motor unit firing rate (P < 0.0001), firing rate range (P < 0.0001), and firing duration (P < 0.0001) are shown in panels D, E, and F, respectively. P values are obtained from the linear model using all units from all participants.

of the torque ramp slopes (χ^2 *(1) = 0.38, P = 0.5390*).

7.4.4 Motor unit firing rate and duration during synergy-driven and voluntary contractions

Figure 7.8A shows the subject mean peak firing rates of the paretic biceps brachii during submaximal synergy-driven and voluntary EF ramp contractions at matched torque levels. We found slightly higher peak firing rates in synergy-driven (13.9 ± 2.5 pps) compared to voluntary contractions (13.5 ± 2.5 pps; *ES = 0.29*); contraction type had a significant effect on peak firing rate (χ^2 *(1) = 9.10, P = 0.0026*), with an estimated increase of 0.50 ± 0.17 pps in synergy-driven contractions. However, we found no significant effect of contraction type on the firing rate range of motor units (χ^2 *(1) = 1.84, P = 0.1753*) and group mean firing rate range was similar between synergy-driven (7.7 ± 1.5 pps) and voluntary contractions (7.8 ± 1.3 pps; *ES = 0.09*), as shown in Figure 7.8B. Motor units were active for a shorter duration during synergy-driven contractions (11.5 ± 2.2 s) than during voluntary contractions (13.7 ± 2.8 s; *ES = 0.96*) in the same limb, and contraction type was shown to significantly affect motor unit firing duration (χ^2 *(1) = 33.1, P < 0.0001*), with synergy-driven contractions seeing a 2.9 ± 0.5 s reduction in firing duration with respect to voluntary contractions. Additionally, the significant effect of contraction type on motor unit firing duration was maintained when restricting the analysis to the ascending limb of the torque ramp (χ^2 *(1) = 48.2, P < 0.0001*); synergy driven contractions were associated with a 1.8 ± 0.3 s reduction in motor unit firing activity prior to peak torque, in comparison to voluntary contractions (Group mean of 5.0 ± 1.5 s during synergy contractions and 6.7 ± 0.87 s during voluntary contractions; *ES = 0.92*). Subject means for motor unit duration during the ascending limb of synergy-driven and voluntary contractions are shown in Figure 7.8C.

Similar results were observed in our comparisons of matched motor units during the voluntary and synergy driven contractions. In our linear mixed effects model comparing only the motor units identified and matched across both contraction types, we found synergy-driven contractions were associated with a slight but significant (χ^2 *(1) = 26.4, P < 0.0001*) increase in peak firing rate of 0.61 ± 0.12 pps. These matched motor units also displayed a significant (χ^2 *(1) = 7.67, P = 0.0056*) increase in firing rate range during the synergy-driven contractions of 0.28 ± 0.10 pps. Synergy-driven contractions were associated with a significant (χ^2 *(1) = 22.2, P < 0.0001*) reduction of total motor unit firing duration of 1.4 ± 0.3 s and a significant (χ^2 *(1) = 27.7, P < 0.0001*) reduction of motor unit firing duration on the ascending limb of the torque ramp by 0.85 ± 0.16 s, compared to voluntary contractions.

7.4.5 Motor unit firing rate modulation during synergy-driven and voluntary contractions

Figure 7.9A shows the subject means for motor unit firing rate modulation slope during both synergy-driven and voluntary EF contractions of the biceps brachii of the paretic limb. Group mean rate modulation slope was reduced during the synergy-driven contractions (-0.10 ± 0.06 pps/%MVT) compared to voluntary contractions (0.04 ± 0.04 pps/%MVT; *ES = 1.67*). This

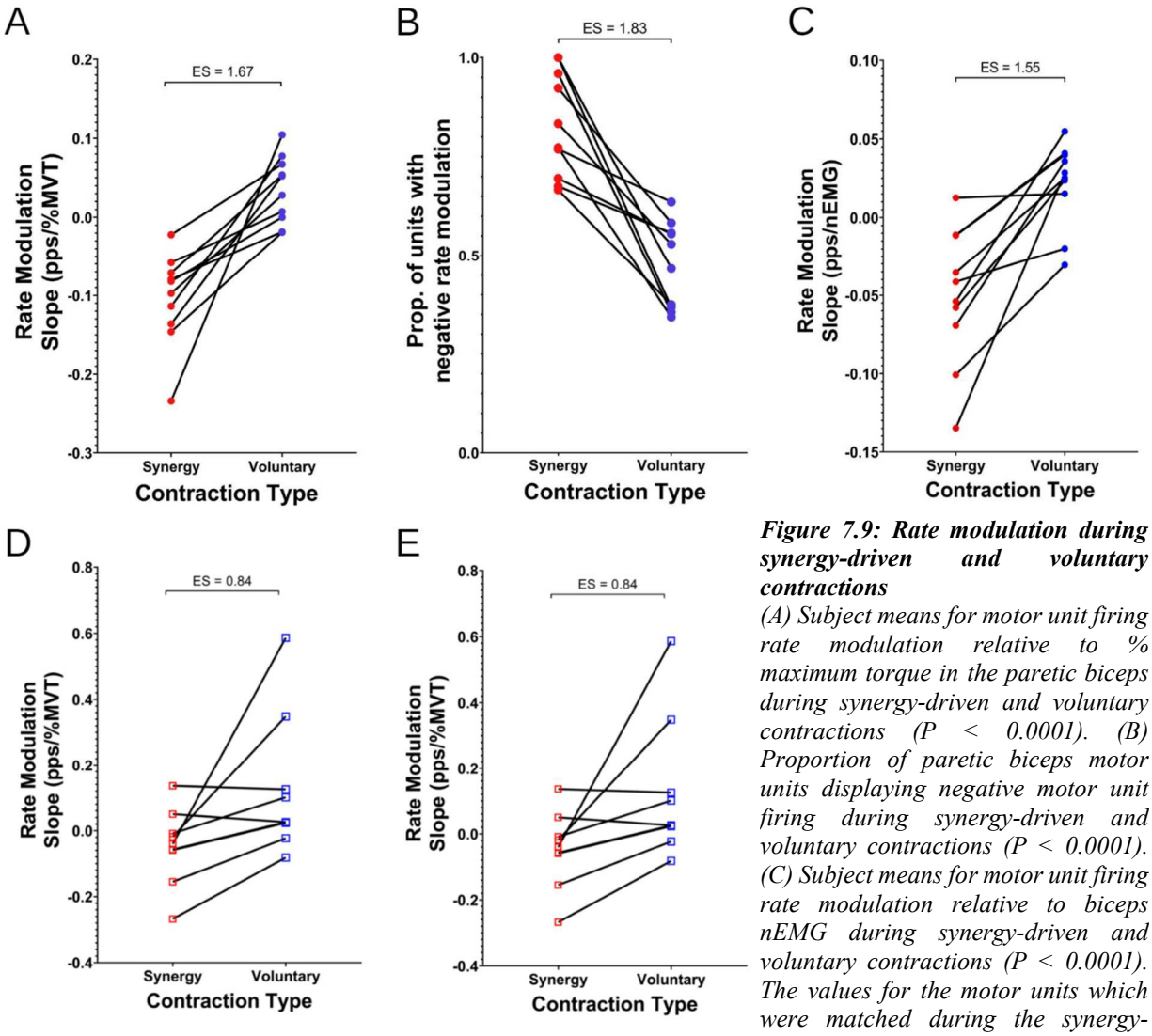

Figure 7.9: Rate modulation during synergy-driven and voluntary contractions

(A) Subject means for motor unit firing rate modulation relative to % maximum torque in the paretic biceps during synergy-driven and voluntary contractions (P < 0.0001). (B) Proportion of paretic biceps motor units displaying negative motor unit firing during synergy-driven and voluntary contractions (P < 0.0001). (C) Subject means for motor unit firing rate modulation relative to biceps nEMG during synergy-driven and voluntary contractions (P < 0.0001). The values for the motor units which were matched during the synergy-driven and voluntary contractions for rate modulation with respect to torque (P < 0.0001) and nEMG (P < 0.0001) are shown in panels D and E, respectively.

reduced rate modulation slope during synergy-driven contractions was seen consistently across all 10 participants; further, all participants displayed negative mean firing rate modulation during the synergy-driven contractions, while only 2 of the 10 participants displayed negative rate modulation during voluntary contractions. The effect of contraction type on motor unit rate modulation was significant (χ^2 *(1) = 42.5, P < 0.0001*), with synergy-driven contractions associated with a reduction of 0.19 ± 0.03 pps/%MVT compared to voluntary contractions.

The proportion of motor units displaying impaired rate modulation during synergy-driven and voluntary contractions is shown in Figure 7.9B. An increased proportion of motor units displayed negative firing rate modulation during synergy-driven contractions (0.83 ± 0.13) than in voluntary contractions (0.48 ± 0.11; *ES = 1.83*), and contraction type had a significant effect on this proportion (χ^2 *(1) = 24.1, P < 0.0001*), with an increase of 0.35 ± 0.05 in synergy-driven contractions. The increase in motor units displaying negative firing rate modulation was observed in all participants.

Additionally, rate modulation was also calculated with respect to nEMG of the paretic biceps during the synergy-driven and voluntary contractions, shown in Figure 7.9C. Rate modulation was lower during synergy-driven contractions (-0.050 ± 0.044 pps/nEMG) than during voluntary contractions (0.021 ± 0.027 pps/nEMG; *ES = 1.55*), with respect to nEMG. Contraction type had a significant effect on rate modulation with respect to EMG (χ^2 *(1) = 50.2, P < 0.0001*), with synergy-driven contractions associated with a reduction of 0.091 ± 0.012 pps/nEMG in comparison to voluntary contractions of the same limb.

In our models comparing only the motor units that were matched across both contraction types, a significant reduction in rate modulation with respect to both torque (χ^2 *(1) = 22.6, P < 0.0001*) and nEMG (χ^2 *(1) = 81.4, P < 0.0001*) during synergy-driven contractions was observed.

For the matched units, synergy-driven contractions showed a reduction of 0.17 ± 0.04 pps/%MVT in rate modulation with respect to torque and a reduction of 0.16 ± 0.017 pps/nEMG in rate modulation with respect to nEMG, in comparison to voluntary contractions.

7.4.6 Recruitment patterns during synergy-driven and voluntary contractions

As impaired rate modulation is prevalent during synergy-driven contractions, altered patterns of motor unit recruitment may be necessary to generate the observed torques. Figure 7.10A shows the subject mean torque at recruitment during both synergy-driven and voluntary contractions (note: the peak torque level varies across participant, but is matched between synergy-driven and voluntary contractions within each participant). The group mean motor unit recruitment threshold was higher during synergy-driven (10.4 ± 3.9 %MVT) than during voluntary contractions (7.7 ± 2.4 %MVT, $ES = 0.71$); contraction type significantly affected torque at recruitment ($\chi^2\ (1) = 29.5,\ P < 0.0001$), increasing it by 2.4 ± 0.4 %MVT during synergy-driven contractions. Seven of the ten participants displayed a higher mean torque at motor unit recruitment during synergy-driven contractions. Figure 7.10B shows the subject means for the time between motor unit recruitment and peak ramp torque. Group means displayed motor unit recruitment was closer to peak torque during synergy-driven contractions (6.1 ± 1.3 s) than during voluntary contractions (7.1 ± 0.8 s; $ES = 0.56$). Our model revealed a significant effect of contraction type on recruitment time relative to peak torque ($\chi^2\ (1) = 12.3,\ P = 0.0005$), with motor units recruited 0.88 ± 0.25 s closer to peak torque during synergy-driven contractions than during voluntary contractions. Eight of the ten participants showed mean motor unit recruitment time closer to peak torque during the synergy-driven contractions.

Figure 7.10C shows the subject means peak EMG amplitude during synergy-driven and voluntary contractions. Participants displayed an increase in peak EMG amplitude during the synergy-driven contractions (1.5 ± 1.1 mV), when compared to voluntary EF contractions (0.91 ± 0.46 mV, *ES* = 0.60) of the same torque level. Contraction type had a significant effect on peak

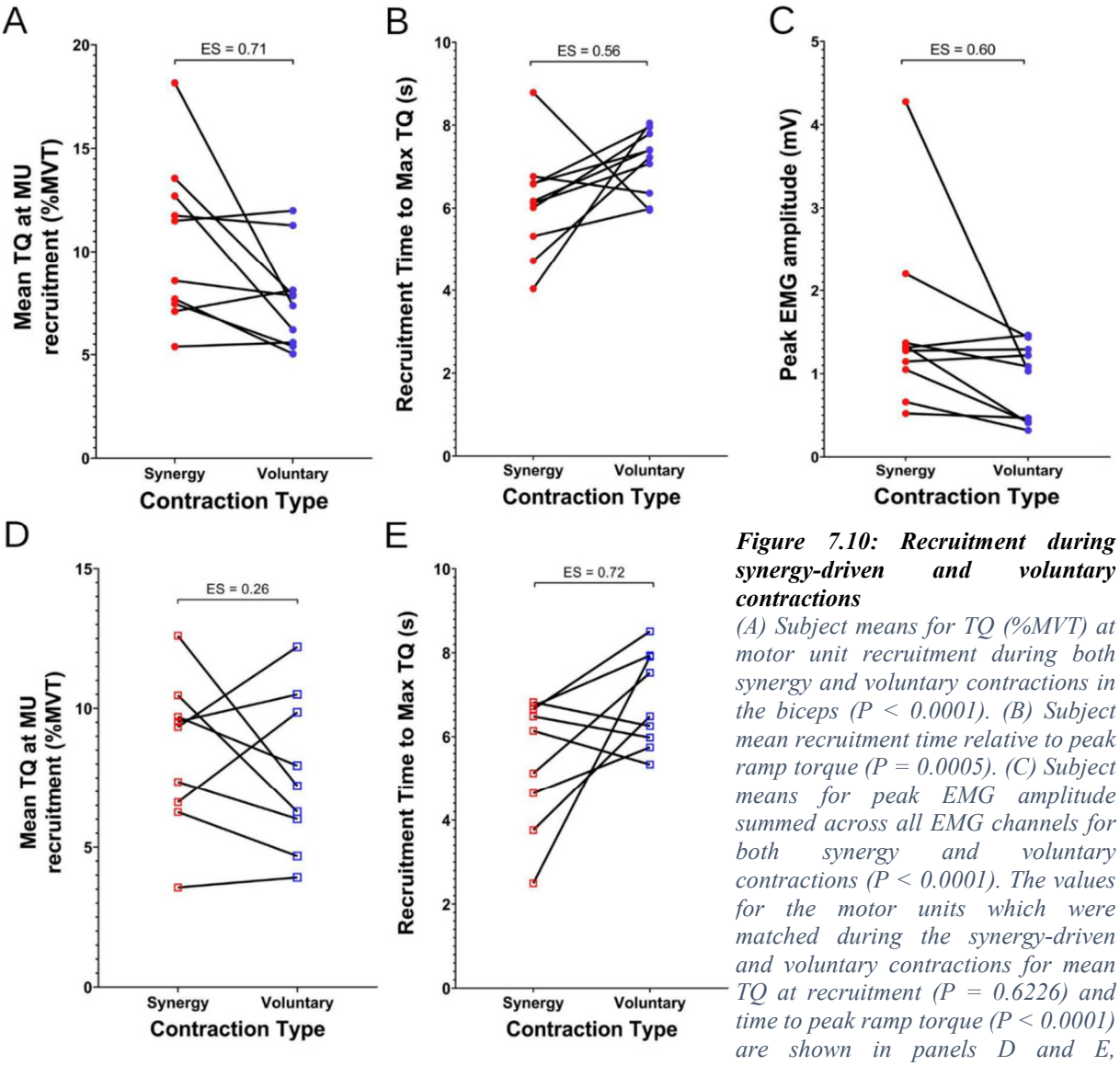

Figure 7.10: Recruitment during synergy-driven and voluntary contractions

(A) Subject means for TQ (%MVT) at motor unit recruitment during both synergy and voluntary contractions in the biceps ($P < 0.0001$). (B) Subject mean recruitment time relative to peak ramp torque ($P = 0.0005$). (C) Subject means for peak EMG amplitude summed across all EMG channels for both synergy and voluntary contractions ($P < 0.0001$). The values for the motor units which were matched during the synergy-driven and voluntary contractions for mean TQ at recruitment ($P = 0.6226$) and time to peak ramp torque ($P < 0.0001$) are shown in panels D and E, respectively. P values are obtained from the linear model using all units from all participants.

EMG amplitude (χ^2 *(1) = 39.6, P < 0.0001*) with synergy-driven contractions associated with an increase of 0.67 ± 0.10 mV.

When comparing the matched units from the voluntary and synergy-driven contractions, there was no significant effect of contraction type on mean torque at recruitment (χ^2 *(1) = 0.24, P = 0.6226*). However, the model of the matched units still revelaed a significant effect of contraction type on the time between motor unit recruitment and peak ramp torque (χ^2 *(1) = 35.7, P < 0.0001*). Motor units were recuited 1.2 ± 2.0 s closer to peak torque during synergy-driven contractions than during voluntary contractions.

7.5 Discussion

In this study, we first compared the motor unit firing patterns during voluntary contractions in the non-paretic and paretic biceps brachii, and then compared motor unit firing patterns in the paretic biceps brachii during synergy-driven and voluntary elbow flexion contractions. In alignment with previous work, we have found a reduction in peak motor unit firing rates, as well as reduced firing rate modulation in the paretic biceps. In comparing synergy-driven and voluntary contractions in the paretic biceps, we found rate modulation was further reduced during synergy-driven contractions, and motor units were recruited later and were active for a shorter duration during synergy contractions.

7.5.1 Confirmation of previously reported changes in motor unit firing behaviors post-stroke

We observed reduced motor unit peak firing rates and firing rate range in the paretic limb compared to the non-paretic limb (Figure 7.4A-B). Because the effort levels between limbs were

matched (i.e., we used normalized torque rather than absolute torque level), there were lower absolute torques generated by the paretic limb, which could play a role in the observed reduction in maximum firing rate and firing rate range. However, reduced peak motor unit firing rates have been shown previously in the paretic biceps brachii (Rosenfalck & Andreassen, 1980; Young & Mayer, 1982), even when matching torque level (Gemperline *et al.*, 1995).

The reduced peak FR and FR range are likely due to a disruption in descending synaptic drive. Decreased firing rates of individual motor units had been linked to a loss of corticospinal drive following stroke (Rosenfalck & Andreassen, 1980; Tang & Rymer, 1981). Additionally, stroke survivors show a decrease in voluntary activation of the biceps brachii (Garmirian *et al.*, 2019), indicating an inability to fully drive the muscle, as well as reduced integrity of the corticospinal tract (Karbasforoushan *et al.*, 2019). Following stroke, there is evidence for increased reliance on multisynaptic corticoreticulospinal pathways, including an increase in non-linear connectivity associated with the multisynaptic nature of corticobulbospinal motor pathways (Yang *et al.*, 2020), and an increase in reticulospinal tract integrity (Karbasforoushan *et al.*, 2019).

We also observed an increase in overall motor unit firing duration in the paretic limb (Figure 7.4C), with increases in firing duration on both the ascending and descending limbs of the torque ramps. The increased duration on the ascending limb of the torque ramps suggests earlier recruitment of higher threshold motor units. Previous work has shown compressed motor unit recruitment in the paretic limb of stroke subjects (Gemperline *et al.*, 1995).

The increased duration on the descending limb is greater than that on the ascending limb. This suggests an increase in recruitment-derecruitment hysteresis, possibly due to an increase in persistent inward currents (PICs). Previous work has shown evidence of increased

neuromodulatory drive to the paretic limb following stroke (McPherson *et al.*, 2008; McPherson *et al.*, 2018c) leading to increased induction of PICs.

Our results showed a decrease in motor unit firing rate modulation in the paretic limb of stroke participants. Previous work by Mottram et al. (Mottram *et al.*, 2014) has shown reduced rate modulation in the paretic biceps using a paired motor unit analysis. This study produced similar findings by using a calculation based on torque and single motor unit firing patterns. We observed a reduction in rate modulation slope, and an increased proportion of motor units displaying impaired rate modulation (Figure 7.3), similar to the increase proportion of trials displaying impaired modulation in Mottram's work. While the observed decrease in firing rate with respect to nEMG was not found to be significant, previous findings of impaired rate modulation were calculated using a paired motor unit analysis suggesting the reductions in rate modulation seen are not due to the activity of other muscles at the elbow. We believe the lack of significance seen here is due to the inherent noise of EMG or possible cross-talk leading to a large amount of within-subject variability. Previous investigations have hypothesized that reduced corticospinal input to motor units, increased PICs, and / or changes in patterns of inhibition may cause the observed reduced rate modulation seen in individuals post-stroke.

The torque based single motor unit calculation used in this study allows for a quantification of the extent firing rate modulation within each unit, and provides more granularity than a binary measure of impaired firing, or duration of impaired firing, which is reliant on the active duration of the motor unit. Additionally, this method for calculating rate modulation may be useful for situations where motor unit yield may not be optimal, and obtaining motor unit pairs with the desired recruitment spacing may be difficult.

7.5.2 Comparison of elbow flexion torque traces during synergy-driven and voluntary contractions

Participants in this study were capable of generating consistent elbow flexion torque traces during shoulder abduction ramps in the paretic limb. However, as the participants displayed a wide range of impairment levels, the amount of SABD necessary to elicit the EF torque varied between participants. Further, while these ramps were consistent during the ascending limb, participants showed a variety of behavior on the descending portion of the ramps. This variation is likely due to the fact that the subjects were not told to actively modulate this spontaneously generated torque, and did not receive any feedback about elbow torques that were generated.

While synergy-driven elbow flexion torques were generated at a consistent level on the ascending limb of the torque ramps, the torque traces during these contractions showed a higher level of error than during the voluntary contractions. This is also likely due to the lack of visual feedback provided for the elbow flexion torques that were spontaneously generated during shoulder abduction. While this increase in torque error was significant, the torque traces during the synergy ramps still showed torque increases at similar slopes as the voluntary contractions, and similar smoothness, as evidenced by the similar level of error seen in the slope of the torque ramps in both voluntary and synergy-driven contractions. These quantitative analyses of the ramp error in combination with qualitative inspection of the torque traces provide us with confidence that the differences in motor unit firing patterns seen here between voluntary and synergy-driven contractions are not due to differences in the elbow flexion torque-traces.

7.5.3 Differences in motor unit firing rate between voluntary and synergy-driven contractions

As shown in Figure 7.8A, we observed a slight increase in peak motor unit firing rate during synergy-driven contractions in comparison to the voluntary contractions. The increase in peak firing rate was found to be significant, although the magnitude was relatively low at 0.61 pps. Additionally, we found no difference in the range of firing rates displayed during synergy-driven and voluntary contractions when comparing all investigated units, and only a small (0.28 pps), though significant, difference was found in the firing rate range of the matched units across contraction type. One possible explanation for the slight increase in firing rate, is an increased corticobulbar drive to higher threshold units. As discussed in greater depth in discussion section 4.5, synergy-driven contractions display an increased reliance on higher threshold units. Synergy-driven contractions are thought to primarily receive reticulospinal input. However, a preferential drive to higher threshold units has not been established for the reticulospinal system.

7.5.4 Additional impairments in rate modulation during synergy-driven vs. voluntary contractions

A consistent and significant decrease in motor unit firing rate modulation and a larger proportion of units displaying negative rate modulation were found in synergy-driven contractions in comparison to voluntary contractions of the paretic biceps, as shown in Figure 7. These changes are likely due to an increased reliance on corticobulbospinal inputs during flexion synergy contractions, which are outlined in greater detail below.

7.5.4.1 Reduction in corticospinal input during synergy-driven contractions

Synergy-driven elbow flexion is thought to be elicited due to the diffuse connections of the reticulospinal pathway, being utilized during SABD following stroke. Due to this, the descending input to the biceps during the synergy-driven contraction is thought to be primarily reticulospinal, with little corticospinal input. However, during voluntary contractions individuals with stroke may utilize remaining corticospinal resources in concert with the compensatory drive from the corticoreticulospinal pathways. The reduced input from any remaining corticospinal connections and could play a role in the further reduction in rate modulation seen in synergy-driven contractions in comparison to voluntary contractions. Loss of corticospinal projections is postulated to cause an inability to fully activate motor units, as evidenced by the increased voluntary activation failure seen in stroke (Garmirian *et al.*, 2019). As synergy driven contractions likely utilize less of the remaining corticospinal resources, the ability to fully activate units may be further compromised during these contractions, when compared to voluntary contractions following stroke. These activation deficits may be related to the impaired rate modulation observed in this study. Increased use of corticoreticulospinal pathways during synergy-driven contractions may lead to the reduced rate modulation seen here, as the reticulospinal tract is primarily polysynaptic and generates smaller motoneuron EPSPs than corticospinal drive (Riddle *et al.*, 2009; Baker, 2011). The reticulospinal pathways may also contribute to the impaired rate modulation through alterations in neuromodulatory and / or inhibitory drive, as outlined in the following sections.

7.5.4.2 Increased neuromodulatory drive to the biceps during synergy-driven contractions

Neuromodulatory drive to the spinal cord has been shown to be state dependent, and may be adjusted to meet the demands of different motor tasks (Heckman *et al.*, 2008a). Monoaminergic

drive and resulting PICs have been strongly tied to postural tasks (Lee & Heckman, 1998b, a), and as such it may be higher during SABD tasks than during volitional EF tasks. Further, the descending projections of the monoaminergic system are highly diffuse, and increasing the excitability of one motor pool may increase the excitability of many pools acting at multiple joints (Skagerberg & Bjorklund, 1985; Heckman *et al.*, 2008b). Following lesions interrupting connections from the primary motor cortex (M1), however, the contralesional premotor (PM) and supplementary motor (SM) projections to the pontomedullary reticular formation (PMRF) are upregulated (Darling *et al.*, 2018; Fregosi *et al.*, 2018). In stroke, where there is a M1 or an internal capsule infarct, damage occurs not only to the crossed corticospinal tract but also to the crossed corticoreticular tract, due to their anatomical proximity. As a result, the balanced modulation of the PMRF by the M1 is lost and consequently the unbalanced excitation from PM and SM takes the upper hand. This may lead to an increase in monoaminergic drive to the biceps motor pools, leading to increased PIC activation during synergy induced contractions, compared to during voluntary contractions. Motor neurons with a strong PIC display a period of rapid acceleration, followed by a phase of rate saturation, where the unit is less sensitive to increases in descending excitatory input (Heckman & Binder, 1993; Lee & Heckman, 2000; Lee *et al.*, 2003; Johnson *et al.*, 2017). An increase in neuromodulatory drive during the synergy contractions could lead to the further saturation of motor unit firing rates observed.

7.5.4.3 Increased inhibitory input mediated through reticulospinal drive to Renshaw cells

Previous work has shown increased Renshaw cell excitability in individuals with spastic hemiplegia (Katz & Pierrot-Deseilligny, 1982). Further, descending drive from the reticulospinal tract has been shown to have an excitatory influence on Renshaw cells, and may play a primary

role in setting the level of excitability of Renshaw cells (Pompeiano, 1988; Mazzocchio & Rossi, 1997). Stimulation of the reticular formation shows that the reticulospinal drive can have excitatory effects on both interneuron and motoneurons (Koizumi *et al.*, 1959), leading to concurrent inhibition and excitation of the motoneuron. As the synergy-driven contractions are likely to involve more reticulospinal drive than voluntary contractions, there may be an increase in drive to Renshaw cells during these contractions, leading to the increased impairments in rate modulation seen. Additionally, recurrent inhibition mediated through Renshaw cells has been shown to occur across joints in the upper limb of primate models (Edgley *et al.*, 2020), which may explain the further saturation seen during these synergy-driven contractions.

7.5.4.4 Possible causes for consistently negative rate modulation

PIC deactivation during the synergy-driven contractions may be to blame for the consistent negative rate modulation values observed. PIC deactivation may be through PIC decay during these contractions. Previous work has shown that the PIC decays within a few seconds in FR and FF units (Lee & Heckman, 1998a). However, there is currently no evidence that synergy drive would preferentially activate these higher threshold units. Another possible cause of PIC deactivation is through an increase in inhibition. PICs have been shown to be very sensitive to inhibition (Hultborn *et al.*, 2003; Kuo *et al.*, 2003). As discussed in section 4.4.3, concurrent drive from the cortico-reticulospinal path to Renshaw cells may lead to an increased inhibition. The drop in firing rate consistently seen may be due to Renshaw mediated inhibition terminating the PIC while the unit is firing, while, the inhibition may not strong enough to derecruit the motor unit.

Changing patterns of inhibition may also lead to the negative rate modulation seen in synergy-driven contractions. Previous simulation work has shown proportional inhibition

(inhibition which increases in intensity along with excitation) can lead to negative firing rate modulation (Powers *et al.*, 2012). Proportional inhibition may occur due to concurrent drive to inhibitory Renshaw cells, while driving the motoneurons ionotropically via the reticulospinal tract. The increased descending input to propriospinal neurons following stroke (Pierrot-Deseilligny & Burke, 2005), likely from corticoreticulospinal projections, may also contribute to proportional inhibition. Propriospinal drive may utilize a combination of excitatory and inhibitory input to modulate the gain of the motoneuron pool (Chance *et al.*, 2002; Berg *et al.*, 2007). Further, propriospinal neurons project on to motoneurons of multiple muscles and span across joints (Alstermark *et al.*, 1990), which may explain the decrease in rate modulation seen in the synergy-driven contractions.

7.5.5 Alterations in motor unit recruitment patterns during synergy-driven contractions

The increased torque at recruitment and shortened time between recruitment and peak torque shown in Figure 7.10, and the shorter firing duration on the ascending limb shown in Figure 7.8C, suggest an increased recruitment of higher threshold units occurs during the synergy-driven contractions, when compared to voluntary contractions, in the paretic biceps. Comparisons of the matched units did not show a shift in torque at recruitment, suggesting different units are being recruited during the synergy-driven contractions, which have a later recruitment threshold. Further, the increased peak EMG amplitude shown in Figure 7.10C suggests an inefficiency in activating the muscle, which has previously been associated with an increase in motor unit recruitment (Tang & Rymer, 1981). This shift in recruitment pattern is likely a response to the impaired rate modulation seen in the synergy-driven contractions. As these units show severe impairments in

rate coding, the only mechanism by which to increase muscle force is the recruitment of additional units.

7.5.6 Limitations

We must note that this study has certain limitations. First, these analyses were not conducted in individuals without neurological injury, instead the non-paretic limb was used as a control. However, the non-paretic arm is not entirely unaffected post-stroke, and further investigations into how these measures vary between the non-paretic limb of stroke participants and the limbs of healthy control individuals are necessary. Additionally, we were unable to obtain consistent synergy torques on the descending limb of the torque ramps, preventing the calculation of motor unit hysteresis that reflects neuromodulatory drive. As we posit that changes in neuromodulatory drive may play a major role in the observed results, the inability to estimate relative neuromodulatory drive through motor unit hysteresis is a deficit of this work. Lastly, the possible mechanisms outlined above are all based on indirect evidence, and further investigation is necessary to confidently state the cause of the observed changes in motor unit firing patterns.

7.6 Conclusions

Our results confirm previous studies' findings of impaired motor unit modulation in the paretic upper limb, and show further impairments in rate modulation during synergy-driven contractions. These findings suggest that there are significant changes in neural drive during synergy-driven contractions. The consistently negative rate modulation seen during involuntary elbow flexion implies altered inhibitory drive may be playing a large role during these

contractions. Further investigation into changes in inhibition patterns in stroke, and of motor control during synergy-driven contractions is still needed to fully characterize the changes in neural drive following unilateral brain injury induced corticofugal pathway losses.

8. Conclusions and future directions

8.1 Conclusions

The work presented in this dissertation utilized novel motor unit recording methods to investigate motor units firing patterns involved in movement in both healthy individuals and those with brain injury induced motor impairments. To contextualize the results obtained with these novel motor unit decomposition methods and for the ease of comparison to previous work conducted with differing parameters, a thorough characterization of the properties of motor units obtained using HD-sEMG decomposition and a sensitivity analysis to determine the best parameter set for ΔF estimation was necessary. The studies presented in chapters 5-7 build upon that groundwork to investigate how motor unit firing patterns are altered with age and following unilateral brain injury, as well as how alterations in firing patterns may relate to the observed motor deficits in those populations.

Results from healthy young participants demonstrate the ability of HD-sEMG decomposition to discriminate a large number of motor unit spike trains from both elbow and ankle flexors and extensors. The population of decomposed motor units included a wide range of recruitment thresholds and surface action potential amplitudes. However, at higher contraction levels and higher contraction speeds motor unit decomposition yield was reduced and there was a reduction in the proportion of lower threshold motor units that were decomposed, producing a uniform distribution motor unit recruitment thresholds. This suggests that surface decomposition may be biased towards units with a larger surface signal magnitudes, including larger motor units and motor units which are located closer to the skin. Based on these results the other studies

presented in this dissertation avoided high intensity or speed contractions to ensure large decomposition yields.

As persistent inward currents (PICs) cannot be directly measured from human motoneurons, experimenters have relied on a paired motor unit analysis to estimate PIC amplitude. However, the selection criteria for motor unit pairs to be used in the ΔF analysis is inconsistent across studies. Utilizing the large populations of motor units, which can now be obtained, a robust sensitivity analysis of the selection parameters for the ΔF analysis was conducted. ΔF values were found to be relatively insensitive to minimum thresholds for rate-rate correlation between motor unit pairs, the filter used to smooth the instantaneous motor unit firing rates, and the removal of possibly saturated control units. However, the recruitment and derecruitment time difference of the motor unit pair had a strong effect on ΔF and should be properly controlled for in these analyses. The results of this sensitivity analysis were instrumental in the investigations of altered monoaminergic drive in aging and following stroke outlined in chapters 5 and 6 of this dissertation.

In the investigation of changes in motor unit firing patterns with aging, motor unit firing rates and firing rate ranges were both reduced in the older adults, in both the biceps and triceps. These findings are consistent with previous work conducted in the upper limb (Dalton *et al.*, 2010). Additionally, substantial and significant reductions in ΔF were found in both the elbow flexors and extensors of the older adults, as compared to younger adults. Further, within the older adults there was a predicted reduction of ΔF by ~1 pps per decade of age. Together these results suggest a reduction in motoneuron excitability with age, possibly due to reductions in neuromodulatory drive and/or changes in the magnitude or pattern of inhibitory drive. This investigation of motor unit firing patterns in the healthy aged population also provided valuable perspective for the investigations into motor unit activity following stroke, which often affects aged individuals.

In the paretic biceps of stroke participants, motor unit firing rates and rate modulation were reduced in comparison to motor units from the non-paretic biceps and the biceps of healthy controls in a similar age group. These results are consistent with previous motor unit investigations into stroke participants (Gemperline *et al.*, 1995; Mottram *et al.*, 2014). However, our study provides the first evidence of reductions in both firing rate and rate modulation in the paretic triceps following stroke. The firing rate impairments likely stem from a reduction in direct corticospinal drive following stroke-induced damage to descending pathways, along with an increased utilization of corticobulbospinal resources. In addition, the current data provides novel evidence of broad increases in monoaminergic drive post-stroke. ΔF estimates of PIC amplitude were increased in the paretic and non-paretic biceps and triceps of stroke participants, as compared to healthy controls.

Taken together, the results from chapters 5 and 6 suggest that the level of neuromodulatory input to motoneurons may be set at a systemic level, with ΔF increases/decreases being seen consistently across muscle and limb. This aligns with previous work that suggests that descending monoaminergic projections influence multiple motoneuron pools simultaneously (Skagerberg & Bjorklund, 1985; Prochazka, 1989), making them a poor conduit for task-dependent motor control. The diffuse pattern of monoaminergic input may be shaped by more precise local inhibition, in order to modulate motor unit firing patterns for different tasks (Heckman *et al.*, 2008a; Heckman *et al.*, 2008b).

In further exploration of motor unit firing patterns in stroke survivors, presented in chapter 8, motor unit firing rate modulation was consistently reduced during synergy-driven contractions of the paretic biceps, when compared to voluntary activation to the same contraction intensity. These findings suggest different motor pathways are activated during synergy-driven contractions,

and the reductions in rate modulation may be due to an increase in the involvement of corticobulbar resources and/or changes in the inhibitory drive to motor units during these contractions. Synergy-driven contractions also displayed evidence of altered motor unit recruitment patterns, with a higher average motor unit recruitment threshold, and increased EMG amplitude. This may provide additional evidence of inefficient activation of the muscle during synergy contractions. This work, is the first, to our knowledge, to thoroughly characterize motor unit activity during flexion-synergy induced contractions in the upper limb post-stroke, and further illuminates the mechanisms at play during these spontaneously coupled contractions.

8.2 Future directions

While the work presented in this dissertation provides substantial insight into how changes in motor unit firing patterns relate to motor control, it also unveils new questions and opens new avenues to investigate. As technology for the recording of motor units and imaging of neural structures advances, the near future may allow for more direct investigation that was not feasible during these studies.

The limitations of time enforced by the relatively short research tenure of a PhD student leaves many stones unturned. One casualty of these time constraints are the sample sizes in the studies included in this dissertation. Our understanding of age-related changes is limited to 2 relatively condensed age groups. A broader investigation of age related motor deficits is necessary, with participants spanning a much larger age range, preferably sampled densely and evenly from all ages. Additionally, it would be invaluable to conduct a longitudinal study to understand how aging changes the motor unit activity of the same participant at several different time points.

Broadening the range of stroke participants from those included in the studies presented here may also provide valuable insight. Stroke survivors exhibit a range of motor deficits and impairment level can vary greatly between individuals. Understanding how these motor unit firing metrics vary across the range of impairment levels could provide further insight into the neural mechanisms at play. Further, as damage to corticospinal projections is implicated here as a main driver of the impaired motor unit firing patterns, it would be advantageous to correlate the measures used in this dissertation with measures of integrity of the descending pathways, possibly utilizing diffusion-MRI based methods.

In addition to expanding the current research to a broader range of participants, much can be gained from investigating changes in multiple muscle groups, with different functional roles, across limbs. In response to the results presented in this dissertation, we posit that the level of neuromodulatory drive may be set systemically. However, further investigation into different muscle groups and across limbs is still necessary to fully understand the resolution of the monoaminergic descending inputs.

Historically, much of the investigation into motor control following stroke has focused on the affected side, and often on the more affected muscles. Yet, as has been demonstrated in both this dissertation and elsewhere, the non-paretic limb of stroke survivors is not truly unaffected. Further investigation into changes in neural control of the non-paretic limb, along with the under investigated muscles (upper limb extensors and lower limb flexors) is necessary to understand the balance between the multiple compensatory changes in neural control that occur following a stroke. Failure to fully characterize the system can lead to ineffective, or even deleterious, interventions and therapies.

Additionally, the current capability to quantify both the amplitude and patterns of inhibitory motor commands in human motoneurons is severely lacking. The rate modulation quantification utilized in chapters 4 and 5 may help to elucidate the pattern of inhibition (Johnson *et al.*, 2017), substantial further investigation is needed to validate the effects of inhibition on this metric. While computer simulations have demonstrated the effect of differing inhibition patterns on motor unit rate modulation (Powers *et al.*, 2012), additional investigations should conducted in reduced animal preparations where the level of inhibition can be modulated by the experimenters would provide necessary understanding of the effect of varying inhibition on motor unit firing patterns.

The work presented here has served to observe motor control patterns during typical movement conditions. However, understanding how motor unit activity can be modulated in response to pharmaceutical probes or physical training could provide immeasurable insight towards developing effective therapies to combat motor deficits.

Previous work has found that many changes in motor unit behavior associated with age may be mitigated through strength training. Masters athletes have shown greater estimates of MU numbers (Power *et al.*, 2010), and strength training has been shown to reduce AHP duration which normally increases with age (Christie & Kamen, 2010). Further, Latella and colleagues (Latella, 2021) have called for the investigation of strength trainings effects on motor unit firing patterns, in particular PICs. The possibility of ameliorating the losses in motoneuron excitability in older adults shown in chapter 5, through strength training or other interventions is clearly deserving of further investigation.

Further understanding of the role of neuromodulatory drive in stroke could be achieved through the use of pharmaceutical interventions. Previous work from our lab has shown that

pharmaceutical modulation of descending monoaminergic drive can reduce the expression of the flexion synergy following stroke (McPherson *et al.*, 2018b). Probing the system to both increase and decrease the level of neuromodulation to the motoneurons and evaluating the how stroke-induced motor deficits are affected, could provide insight for the use of pharmaceutical interventions aimed at reducing impairment while also illuminating the compensatory role that monoamines may play in generating movement post-stroke. Coupling pharmaceutical interventions with motoneuron recordings may also enable the development of an additional biomarker to understand the level of monoaminergic drive present.

9. References

Adrian ED & Bronk DW. (1929). The discharge of impulses in motor nerve fibres: Part II. The frequency of discharge in reflex and voluntary contractions. *J Physiol* **67,** i3-151.

Afsharipour B, Manzur N, Duchcherer J, Fenrich KF, Thompson CK, Negro F, Quinlan KA, Bennett DJ & Gorassini MA. (2020). Estimation of self-sustained activity produced by persistent inward currents using firing rate profiles of multiple motor units in humans. *J Neurophysiol* **124,** 63-85.

Alstermark B, Kummel H, Pinter MJ & Tantisira B. (1990). Integration in descending motor pathways controlling the forelimb in the cat. 17. Axonal projection and termination of C3-C4 propriospinal neurones in the C6-Th1 segments. *Exp Brain Res* **81,** 447-461.

Alstermark B, Lundberg A & Sasaki S. (1984). Integration in descending motor pathways controlling the forelimb in the cat. 12. Interneurones which may mediate descending feed-forward inhibition and feed-back inhibition from the forelimb to C3-C4 propriospinal neurones. *Exp Brain Res* **56,** 308-322.

Aston-Jones G, Rajkowski J & Cohen J. (2000). Locus coeruleus and regulation of behavioral flexibility and attention. *Prog Brain Res* **126,** 165-182.

Aymard C, Katz R, Lafitte C, Lo E, Penicaud A, Pradat-Diehl P & Raoul S. (2000). Presynaptic inhibition and homosynaptic depression: a comparison between lower and upper limbs in normal human subjects and patients with hemiplegia. *Brain* **123 (Pt 8),** 1688-1702.

Baker SN. (2011). The primate reticulospinal tract, hand function and functional recovery. *J Physiol* **589,** 5603-5612.

Baker SN, Zaaimi B, Fisher KM, Edgley SA & Soteropoulos DS. (2015). Pathways mediating functional recovery. *Prog Brain Res* **218,** 389-412.

Barry BK, Pascoe MA, Jesunathadas M & Enoka RM. (2007). Rate coding is compressed but variability is unaltered for motor units in a hand muscle of old adults. *J Neurophysiol* **97,** 3206-3218.

Barton K. (2018). Multi-model inference. R package version 1.42. 1.

Bates D & Maechler M. (2015). M, Bolker B, Walker S (2014) lme4: linear mixed-effects models using Eigen and S4. R package version 1.1-7.

Beer RF, Given JD & Dewald JP. (1999). Task-dependent weakness at the elbow in patients with hemiparesis. *Arch Phys Med Rehabil* **80,** 766-772.

Bellemare F, Woods JJ, Johansson R & Bigland-Ritchie B. (1983). Motor-unit discharge rates in maximal voluntary contractions of three human muscles. *J Neurophysiol* **50,** 1380-1392.

Bennett DJ, Hultborn H, Fedirchuk B & Gorassini M. (1998). Synaptic activation of plateaus in hindlimb motoneurons of decerebrate cats. *J Neurophysiol* **80,** 2023-2037.

Bennett DJ, Li Y, Harvey PJ & Gorassini M. (2001a). Evidence for plateau potentials in tail motoneurons of awake chronic spinal rats with spasticity. *J Neurophysiol* **86,** 1972-1982.

Bennett DJ, Li Y & Siu M. (2001b). Plateau potentials in sacrocaudal motoneurons of chronic spinal rats, recorded in vitro. *J Neurophysiol* **86,** 1955-1971.

Berg RW, Alaburda A & Hounsgaard J. (2007). Balanced inhibition and excitation drive spike activity in spinal half-centers. *Science* **315,** 390-393.

Binder MD & Powers RK. (2001). Relationship between simulated common synaptic input and discharge synchrony in cat spinal motoneurons. *J Neurophysiol* **86,** 2266-2275.

Binder MD, Powers RK & Heckman CJ. (2020). Nonlinear Input-Output Functions of Motoneurons. *Physiology (Bethesda)* **35,** 31-39.

Binder MD, Robinson FR & Powers RK. (1998). Distribution of effective synaptic currents in cat triceps surae motoneurons. VI. Contralateral pyramidal tract. *J Neurophysiol* **80,** 241-248.

Blouin JS, Siegmund GP, Carpenter MG & Inglis JT. (2007). Neural control of superficial and deep neck muscles in humans. *J Neurophysiol* **98,** 920-928.

Boccia G, Martinez-Valdes E, Negro F, Rainoldi A & Falla D. (2019). Motor unit discharge rate and the estimated synaptic input to the vasti muscles is higher in open compared with closed kinetic chain exercise. *Journal of Applied Physiology* **127,** 950-958.

Brouns R & De Deyn PP. (2009). The complexity of neurobiological processes in acute ischemic stroke. *Clin Neurol Neurosurg* **111,** 483-495.

Brunnstrom S. (1970). *Movement therapy in hemiplegia: a neurophysiological approach*. Medical Dept., New York,.

Bryndum B & Marquardsen J. (1964). The Tendon Reflexes in Old Age. *Gerontol Clin (Basel)* **6,** 257-265.

Butchart P, Farquhar R, Part NJ & Roberts RC. (1993). The effect of age and voluntary contraction on presynaptic inhibition of soleus muscle Ia afferent terminals in man. *Exp Physiol* **78,** 235-242.

Cameron WE, Jodkowski JS, Fang H & Guthrie RD. (1991). Electrophysiological properties of developing phrenic motoneurons in the cat. *J Neurophysiol* **65,** 671-679.

Canning CG, Ada L, Adams R & O'Dwyer NJ. (2004). Loss of strength contributes more to physical disability after stroke than loss of dexterity. *Clin Rehabil* **18,** 300-308.

Carel RS, Korczyn AD & Hochberg Y. (1979). Age and sex dependency of the Achilles tendon reflex. *Am J Med Sci* **278,** 57-63.

Carleton SC & Carpenter MB. (1983). Afferent and efferent connections of the medial, inferior and lateral vestibular nuclei in the cat and monkey. *Brain Res* **278,** 29-51.

Chance FS, Abbott LF & Reyes AD. (2002). Gain modulation from background synaptic input. *Neuron* **35,** 773-782.

Chase MH, Morales FR, Boxer PA & Fung SJ. (1985). Aging of motoneurons and synaptic processes in the cat. *Exp Neurol* **90,** 471-478.

Chen M & Zhou P. (2015). A novel framework based on FastICA for high density surface EMG decomposition. *IEEE Transactions on Neural Systems and Rehabilitation Engineering* **24,** 117-127.

Chen X, Xie P, Zhang Y, Chen Y, Cheng S & Zhang L. (2018). Abnormal functional corticomuscular coupling after stroke. *Neuroimage Clin* **19,** 147-159.

Christie A & Kamen G. (2010). Short-term training adaptations in maximal motor unit firing rates and afterhyperpolarization duration. *Muscle Nerve* **41,** 651-660.

Clark BC, Taylor JL, Hong SL, Law TD & Russ DW. (2015). Weaker Seniors Exhibit Motor Cortex Hypoexcitability and Impairments in Voluntary Activation. *J Gerontol A Biol Sci Med Sci* **70,** 1112-1119.

Cogliati M, Cudicio A, Martinez-Valdes E, Tarperi C, Schena F, Orizio C & Negro F. (2020). Half marathon induces changes in central control and peripheral properties of individual motor units in master athletes. *J Electromyogr Kinesiol* **55,** 102472.

Cohen J. (1992). Statistical power analysis. *Current directions in psychological science* **1,** 98-101.

Colebatch JG & Gandevia SC. (1989). The distribution of muscular weakness in upper motor neuron lesions affecting the arm. *Brain* **112 (Pt 3),** 749-763.

Connelly DM, Rice CL, Roos MR & Vandervoort AA. (1999). Motor unit firing rates and contractile properties in tibialis anterior of young and old men. *J Appl Physiol (1985)* **87,** 843-852.

Conway BA, Halliday DM, Farmer SF, Shahani U, Maas P, Weir AI & Rosenberg JR. (1995). Synchronization between motor cortex and spinal motoneuronal pool during the performance of a maintained motor task in man. *J Physiol* **489 (Pt 3),** 917-924.

Dalton BH, Jakobi JM, Allman BL & Rice CL. (2010). Differential age-related changes in motor unit properties between elbow flexors and extensors. *Acta Physiol (Oxf)* **200,** 45-55.

Damien J, Colloca L, Bellei-Rodriguez CE & Marchand S. (2018). Pain Modulation: From Conditioned Pain Modulation to Placebo and Nocebo Effects in Experimental and Clinical Pain. *Int Rev Neurobiol* **139,** 255-296.

Darling WG, Ge J, Stilwell-Morecraft KS, Rotella DL, Pizzimenti MA & Morecraft RJ. (2018). Hand Motor Recovery Following Extensive Frontoparietal Cortical Injury Is Accompanied by Upregulated Corticoreticular Projections in Monkey. *J Neurosci* **38,** 6323-6339.

Davidson AG & Buford JA. (2006). Bilateral actions of the reticulospinal tract on arm and shoulder muscles in the monkey: stimulus triggered averaging. *Exp Brain Res* **173,** 25-39.

Davidson AG, Schieber MH & Buford JA. (2007). Bilateral spike-triggered average effects in arm and shoulder muscles from the monkey pontomedullary reticular formation. *J Neurosci* **27,** 8053-8058.

De Luca CJ & Contessa P. (2012). Hierarchical control of motor units in voluntary contractions. *J Neurophysiol* **107,** 178-195.

De Luca CJ & Erim Z. (1994). Common drive of motor units in regulation of muscle force. *Trends Neurosci* **17,** 299-305.

De Luca CJ, Foley PJ & Erim Z. (1996). Motor unit control properties in constant-force isometric contractions. *J Neurophysiol* **76,** 1503-1516.

Del Vecchio A, Holobar A, Falla D, Felici F, Enoka RM & Farina D. (2020). Tutorial: Analysis of motor unit discharge characteristics from high-density surface EMG signals. *J Electromyogr Kinesiol* **53,** 102426.

Del Vecchio A, Negro F, Felici F & Farina D. (2018). Distribution of muscle fibre conduction velocity for representative samples of motor units in the full recruitment range of the tibialis anterior muscle. *Acta Physiol (Oxf)* **222**.

deVries HA, Wiswell RA, Romero GT & Heckathorne E. (1985). Changes with age in monosynaptic reflexes elicited by mechanical and electrical stimulation. *Am J Phys Med* **64,** 71-81.

Dewald JP & Beer RF. (2001). Abnormal joint torque patterns in the paretic upper limb of subjects with hemiparesis. *Muscle Nerve* **24,** 273-283.

Dewald JP, Pope PS, Given JD, Buchanan TS & Rymer WZ. (1995). Abnormal muscle coactivation patterns during isometric torque generation at the elbow and shoulder in hemiparetic subjects. *Brain* **118 (Pt 2),** 495-510.

Doherty TJ, Vandervoort AA, Taylor AW & Brown WF. (1993). Effects of motor unit losses on strength in older men and women. *J Appl Physiol (1985)* **74,** 868-874.

Duchateau J & Enoka RM. (2011). Human motor unit recordings: origins and insight into the integrated motor system. *Brain Res* **1409,** 42-61.

Dunia R, Buckwalter G, Defazio T, Villar FD, McNeill TH & Walsh JP. (1996). Decreased duration of Ca(2+)-mediated plateau potentials in striatal neurons from aged rats. *J Neurophysiol* **76,** 2353-2363.

Earles D, Vardaxis V & Koceja D. (2001). Regulation of motor output between young and elderly subjects. *Clin Neurophysiol* **112,** 1273-1279.

Edgley SA, Williams ER & Baker SN. (2020). Spatial and Temporal Arrangement of Recurrent Inhibition in the Primate Upper Limb. *J Neurosci*.

Ellis MD, Drogos J, Carmona C, Keller T & Dewald JP. (2012). Neck rotation modulates flexion synergy torques, indicating an ipsilateral reticulospinal source for impairment in stroke. *J Neurophysiol* **108,** 3096-3104.

Ellis MD, Sukal-Moulton T & Dewald JP. (2009). Progressive shoulder abduction loading is a crucial element of arm rehabilitation in chronic stroke. *Neurorehabil Neural Repair* **23,** 862-869.

Enoka RM & Fuglevand AJ. (2001). Motor unit physiology: some unresolved issues. *Muscle Nerve* **24,** 4-17.

Erim Z, Beg MF, Burke DT & de Luca CJ. (1999). Effects of aging on motor-unit control properties. *J Neurophysiol* **82,** 2081-2091.

Fang Y, Daly JJ, Sun J, Hvorat K, Fredrickson E, Pundik S, Sahgal V & Yue GH. (2009). Functional corticomuscular connection during reaching is weakened following stroke. *Clin Neurophysiol* **120,** 994-1002.

Farina D & Negro F. (2015). Common synaptic input to motor neurons, motor unit synchronization, and force control. *Exerc Sport Sci Rev* **43,** 23-33.

Farina D, Negro F, Gazzoni M & Enoka RM. (2008). Detecting the unique representation of motor-unit action potentials in the surface electromyogram. *J Neurophysiol* **100,** 1223-1233.

Farmer SF, Halliday DM, Conway BA, Stephens JA & Rosenberg JR. (1997). A review of recent applications of cross-correlation methodologies to human motor unit recording. *J Neurosci Methods* **74,** 175-187.

Favre I, Zeffiro TA, Detante O, Krainik A, Hommel M & Jaillard A. (2014). Upper limb recovery after stroke is associated with ipsilesional primary motor cortical activity: a meta-analysis. *Stroke* **45,** 1077-1083.

Feiereisen P, Duchateau J & Hainaut K. (1997). Motor unit recruitment order during voluntary and electrically induced contractions in the tibialis anterior. *Exp Brain Res* **114,** 117-123.

Fisher KM, Zaaimi B & Baker SN. (2012). Reticular formation responses to magnetic brain stimulation of primary motor cortex. *J Physiol* **590,** 4045-4060.

Fling BW, Knight CA & Kamen G. (2009). Relationships between motor unit size and recruitment threshold in older adults: implications for size principle. *Exp Brain Res* **197,** 125-133.

Fregosi M, Contestabile A, Badoud S, Borgognon S, Cottet J, Brunet JF, Bloch J, Schwab ME & Rouiller EM. (2018). Changes of motor corticobulbar projections following different lesion types affecting the central nervous system in adult macaque monkeys. *Eur J Neurosci* **48,** 2050-2070.

Frontera WR, Grimby L & Larsson L. (1997). Firing rate of the lower motoneuron and contractile properties of its muscle fibers after upper motoneuron lesion in man. *Muscle Nerve* **20,** 938-947.

Fugl-Meyer AR, Jaasko L, Leyman I, Olsson S & Steglind S. (1975). The post-stroke hemiplegic patient. 1. a method for evaluation of physical performance. *Scand J Rehabil Med* **7,** 13-31.

Garmirian LR, Dewald JP & Acosta AM. (2019). Reduction in voluntary activation of elbow and wrist muscles in individuals with chronic hemiparetic stroke. *bioRxiv***,** 689364.

Geertsen SS, Willerslev-Olsen M, Lorentzen J & Nielsen JB. (2017). Development and aging of human spinal cord circuitries. *J Neurophysiol* **118,** 1133-1140.

Gemperline JJ, Allen S, Walk D & Rymer WZ. (1995). Characteristics of motor unit discharge in subjects with hemiparesis. *Muscle Nerve* **18,** 1101-1114.

Giboin LS, Tokuno C, Kramer A, Henry M & Gruber M. (2020). Motor learning induces time-dependent plasticity that is observable at the spinal cord level. *J Physiol* **598,** 1943-1963.

Glaser V & Holobar A. (2019). Motor Unit Identification From High-Density Surface Electromyograms in Repeated Dynamic Muscle Contractions. *IEEE Trans Neural Syst Rehabil Eng* **27,** 66-75.

Gorassini M, Yang JF, Siu M & Bennett DJ. (2002). Intrinsic activation of human motoneurons: possible contribution to motor unit excitation. *J Neurophysiol* **87,** 1850-1858.

Gorassini MA, Bennett DJ & Yang JF. (1998). Self-sustained firing of human motor units. *Neurosci Lett* **247,** 13-16.

Gorassini MA, Knash ME, Harvey PJ, Bennett DJ & Yang JF. (2004). Role of motoneurons in the generation of muscle spasms after spinal cord injury. *Brain* **127,** 2247-2258.

Gordon T, Hegedus J & Tam SL. (2004). Adaptive and maladaptive motor axonal sprouting in aging and motoneuron disease. *Neurol Res* **26,** 174-185.

Grashorn W, Sprenger C, Forkmann K, Wrobel N & Bingel U. (2013). Age-dependent decline of endogenous pain control: exploring the effect of expectation and depression. *PLoS One* **8,** e75629.

Grosse P & Brown P. (2003). Acoustic startle evokes bilaterally synchronous oscillatory EMG activity in the healthy human. *J Neurophysiol* **90,** 1654-1661.

Harvey PJ, Li X, Li Y & Bennett DJ. (2006). Endogenous monoamine receptor activation is essential for enabling persistent sodium currents and repetitive firing in rat spinal motoneurons. *J Neurophysiol* **96,** 1171-1186.

Hassan A, Thompson CK, Negro F, Cummings M, Powers RK, Heckman CJ, Dewald JPA & McPherson LM. (2020). Impact of parameter selection on estimates of motoneuron excitability using paired motor unit analysis. *J Neural Eng* **17,** 016063.

Hassan AS, Thompson CK, Negro F, Cummings MQ, Powers RK, Heckman CJ, Dewald J & McPherson LM. (2019). Impact of parameter selection on estimates of motoneuron excitability using paired motor unit analysis. *Journal of Neural Engineering*.

Heckman CJ & Binder MD. (1988). Analysis of effective synaptic currents generated by homonymous Ia afferent fibers in motoneurons of the cat. *J Neurophysiol* **60,** 1946-1966.

Heckman CJ & Binder MD. (1993). Computer simulations of motoneuron firing rate modulation. *J Neurophysiol* **69,** 1005-1008.

Heckman CJ & Enoka RM. (2012). Motor unit. *Comprehensive Physiology* **2,** 2629-2682.

Heckman CJ, Hyngstrom AS & Johnson MD. (2008a). Active properties of motoneurone dendrites: diffuse descending neuromodulation, focused local inhibition. *J Physiol* **586,** 1225-1231.

Heckman CJ, Johnson M, Mottram C & Schuster J. (2008b). Persistent inward currents in spinal motoneurons and their influence on human motoneuron firing patterns. *Neuroscientist* **14,** 264-275.

Henneman E, Somjen G & Carpenter DO. (1965). Functional Significance of Cell Size in Spinal Motoneurons. *J Neurophysiol* **28,** 560-580.

Hepple RT & Rice CL. (2016). Innervation and neuromuscular control in ageing skeletal muscle. *J Physiol* **594,** 1965-1978.

Holobar A, Farina D, Gazzoni M, Merletti R & Zazula D. (2009). Estimating motor unit discharge patterns from high-density surface electromyogram. *Clin Neurophysiol* **120,** 551-562.

Holobar A, Minetto MA, Botter A, Negro F & Farina D. (2010). Experimental analysis of accuracy in the identification of motor unit spike trains from high-density surface EMG. *IEEE Transactions on Neural Systems and Rehabilitation Engineering* **18,** 221-229.

Holobar A, Minetto MA & Farina D. (2014). Accurate identification of motor unit discharge patterns from high-density surface EMG and validation with a novel signal-based performance metric. *J Neural Eng* **11,** 016008.

Holobar A & Zazula D. (2007). Multichannel blind source separation using convolution kernel compensation. *IEEE Transactions on Signal Processing* **55,** 4487-4496.

Hortobagyi T, del Olmo MF & Rothwell JC. (2006). Age reduces cortical reciprocal inhibition in humans. *Exp Brain Res* **171,** 322-329.

Hounsgaard J, Hultborn H, Jespersen B & Kiehn O. (1984). Intrinsic membrane properties causing a bistable behaviour of alpha-motoneurones. *Exp Brain Res* **55,** 391-394.

Hounsgaard J & Kiehn O. (1989). Serotonin-induced bistability of turtle motoneurones caused by a nifedipine-sensitive calcium plateau potential. *J Physiol* **414,** 265-282.

Hu X, Suresh AK, Rymer WZ & Suresh NL. (2015). Assessing altered motor unit recruitment patterns in paretic muscles of stroke survivors using surface electromyography. *J Neural Eng* **12,** 066001.

Hultborn H, Denton ME, Wienecke J & Nielsen JB. (2003). Variable amplification of synaptic input to cat spinal motoneurones by dendritic persistent inward current. *J Physiol* **552,** 945-952.

Hyngstrom AS, Johnson MD & Heckman CJ. (2008). Summation of excitatory and inhibitory synaptic inputs by motoneurons with highly active dendrites. *J Neurophysiol* **99,** 1643-1652.

Jacobs BL, Martin-Cora FJ & Fornal CA. (2002). Activity of medullary serotonergic neurons in freely moving animals. *Brain Res Brain Res Rev* **40,** 45-52.

Johnson H, Ulfhake B, Dagerlind A, Bennett GW, Fone KC & Hokfelt T. (1993). The serotoninergic bulbospinal system and brainstem-spinal cord content of serotonin-, TRH-, and substance P-like immunoreactivity in the aged rat with special reference to the spinal cord motor nucleus. *Synapse* **15,** 63-89.

Johnson MD, Hyngstrom AS, Manuel M & Heckman CJ. (2012). Push-pull control of motor output. *J Neurosci* **32,** 4592-4599.

Johnson MD, Thompson CK, Tysseling VM, Powers RK & Heckman CJ. (2017). The potential for understanding the synaptic organization of human motor commands via the firing patterns of motoneurons. *J Neurophysiol* **118,** 520-531.

Johnson PC. (2014). Extension of Nakagawa & Schielzeth's R2GLMM to random slopes models. *Methods in ecology and evolution* **5,** 944-946.

Kalmar JM, Button DC, Gardiner K, Cahill F & Gardiner PF. (2009). Caloric restriction does not offset age-associated changes in the biophysical properties of motoneurons. *J Neurophysiol* **101,** 548-557.

Kamen G & Knight CA. (2004). Training-related adaptations in motor unit discharge rate in young and older adults. *J Gerontol A Biol Sci Med Sci* **59,** 1334-1338.

Kamen G, Sison SV, Du CC & Patten C. (1995). Motor unit discharge behavior in older adults during maximal-effort contractions. *J Appl Physiol (1985)* **79,** 1908-1913.

Kamen G, Sullivan R, Rubinstein S & Christie A. (2006). Evidence of self-sustained motoneuron firing in young and older adults. *J Electromyogr Kinesiol* **16,** 25-31.

Kanda K & Hashizume K. (1989). Changes in properties of the medial gastrocnemius motor units in aging rats. *J Neurophysiol* **61,** 737-746.

Karbasforoushan H, Cohen-Adad J & Dewald JPA. (2019). Brainstem and spinal cord MRI identifies altered sensorimotor pathways post-stroke. *Nat Commun* **10,** 3524.

Katz R & Pierrot-Deseilligny E. (1982). Recurrent inhibition of alpha-motoneurons in patients with upper motor neuron lesions. *Brain* **105,** 103-124.

Kido A, Tanaka N & Stein RB. (2004). Spinal excitation and inhibition decrease as humans age. *Can J Physiol Pharmacol* **82,** 238-248.

Kiehn O & Eken T. (1997). Prolonged firing in motor units: evidence of plateau potentials in human motoneurons? *J Neurophysiol* **78,** 3061-3068.

Kim EH, Wilson JM, Thompson CK & Heckman CJ. (2020). Differences in estimated persistent inward currents between ankle flexors and extensors in humans. *J Neurophysiol* **124,** 525-535.

Kirk EA, Gilmore KJ & Rice CL. (2018). Neuromuscular changes of the aged human hamstrings. *J Neurophysiol* **120,** 480-488.

Kirk EA, Gilmore KJ, Stashuk DW, Doherty TJ & Rice CL. (2019). Human motor unit characteristics of the superior trapezius muscle with age-related comparisons. *J Neurophysiol* **122,** 823-832.

Klass M, Baudry S & Duchateau J. (2005). Aging does not affect voluntary activation of the ankle dorsiflexors during isometric, concentric, and eccentric contractions. *J Appl Physiol (1985)* **99,** 31-38.

Klass M, Baudry S & Duchateau J. (2008). Age-related decline in rate of torque development is accompanied by lower maximal motor unit discharge frequency during fast contractions. *J Appl Physiol (1985)* **104,** 739-746.

Ko ML, King MA, Gordon TL & Crisp T. (1997). The effects of aging on spinal neurochemistry in the rat. *Brain Res Bull* **42,** 95-98.

Koizumi K, Ushiyama J & Brooks CM. (1959). A study of reticular formation action on spinal interneurons and motoneurons. *Jpn J Physiol* **9,** 282-303.

Kukulka CG & Clamann HP. (1981). Comparison of the recruitment and discharge properties of motor units in human brachial biceps and adductor pollicis during isometric contractions. *Brain Res* **219,** 45-55.

Kuo JJ, Lee RH, Johnson MD, Heckman HM & Heckman CJ. (2003). Active dendritic integration of inhibitory synaptic inputs in vivo. *J Neurophysiol* **90,** 3617-3624.

Kuo JJ, Lee RH, Zhang L & Heckman CJ. (2006). Essential role of the persistent sodium current in spike initiation during slowly rising inputs in mouse spinal neurones. *J Physiol* **574,** 819-834.

Kuypers HG. (1964). The Descending Pathways to the Spinal Cord, Their Anatomy and Function. *Prog Brain Res* **11,** 178-202.

Kuznetsova A, Brockhoff PB & Christensen RH. (2017). lmerTest package: tests in linear mixed effects models. *Journal of statistical software* **82,** 1-26.

Lamy JC, Wargon I, Mazevet D, Ghanim Z, Pradat-Diehl P & Katz R. (2009). Impaired efficacy of spinal presynaptic mechanisms in spastic stroke patients. *Brain* **132,** 734-748.

Lan Y, Yao J & Dewald JPA. (2017). The Impact of Shoulder Abduction Loading on Volitional Hand Opening and Grasping in Chronic Hemiparetic Stroke. *Neurorehabil Neural Repair* **31,** 521-529.

Latella C. (2021). Pick me, Pick me! Rationale for investigating persistent inward currents (PICs) and associated exercise effects in the ageing neuromuscular system. *J Physiol* **599,** 1957-1959.

Lawrence DG & Kuypers HG. (1968). The functional organization of the motor system in the monkey. I. The effects of bilateral pyramidal lesions. *Brain* **91,** 1-14.

Lee RH & Heckman CJ. (1998a). Bistability in spinal motoneurons in vivo: systematic variations in persistent inward currents. *J Neurophysiol* **80,** 583-593.

Lee RH & Heckman CJ. (1998b). Bistability in spinal motoneurons in vivo: systematic variations in rhythmic firing patterns. *J Neurophysiol* **80,** 572-582.

Lee RH & Heckman CJ. (2000). Adjustable amplification of synaptic input in the dendrites of spinal motoneurons in vivo. *J Neurosci* **20,** 6734-6740.

Lee RH & Heckman CJ. (2001). Essential role of a fast persistent inward current in action potential initiation and control of rhythmic firing. *J Neurophysiol* **85,** 472-475.

Lee RH, Kuo JJ, Jiang MC & Heckman CJ. (2003). Influence of active dendritic currents on input-output processing in spinal motoneurons in vivo. *J Neurophysiol* **89,** 27-39.

Lemon RN. (2008). Descending pathways in motor control. *Annu Rev Neurosci* **31,** 195-218.

Lemon RN & Griffiths J. (2005). Comparing the function of the corticospinal system in different species: organizational differences for motor specialization? *Muscle Nerve* **32,** 261-279.

Li S & Francisco GE. (2015). New insights into the pathophysiology of post-stroke spasticity. *Front Hum Neurosci* **9,** 192.

Li Y, Gorassini MA & Bennett DJ. (2004). Role of persistent sodium and calcium currents in motoneuron firing and spasticity in chronic spinal rats. *J Neurophysiol* **91,** 767-783.

Liddell EGT & Sherrington CS. (1925). Recruitment and some other features of reflex inhibition. *Proceedings of the Royal Society of London Series B, Containing Papers of a Biological Character* **97,** 488-518.

Liu KY, Kievit RA, Tsvetanov KA, Betts MJ, Duzel E, Rowe JB, Cam CAN, Howard R & Hammerer D. (2020). Noradrenergic-dependent functions are associated with age-related locus coeruleus signal intensity differences. *Nat Commun* **11,** 1712.

Maraka S, Jiang Q, Jafari-Khouzani K, Li L, Malik S, Hamidian H, Zhang T, Lu M, Soltanian-Zadeh H, Chopp M & Mitsias PD. (2014). Degree of corticospinal tract damage correlates with motor function after stroke. *Ann Clin Transl Neurol* **1,** 891-899.

Martinez-Valdes E, Farina D, Negro F, Del Vecchio A & Falla D. (2018). Early Motor Unit Conduction Velocity Changes to High-Intensity Interval Training versus Continuous Training. *Med Sci Sports Exerc* **50,** 2339-2350.

Martinez-Valdes E, Negro F, Falla D, Dideriksen JL, Heckman CJ & Farina D. (2020). Inability to increase the neural drive to muscle is associated with task failure during submaximal contractions. *J Neurophysiol* **124,** 1110-1121.

Martinez-Valdes E, Negro F, Laine CM, Falla D, Mayer F & Farina D. (2017). Tracking motor units longitudinally across experimental sessions with high-density surface electromyography. *J Physiol* **595,** 1479-1496.

Matsuyama K, Takakusaki K, Nakajima K & Mori S. (1997). Multi-segmental innervation of single pontine reticulospinal axons in the cervico-thoracic region of the cat: anterograde PHA-L tracing study. *J Comp Neurol* **377,** 234-250.

Mazzocchio R & Rossi A. (1997). Involvement of spinal recurrent inhibition in spasticity. Further insight into the regulation of Renshaw cell activity. *Brain* **120 (Pt 6),** 991-1003.

McNeil CJ, Doherty TJ, Stashuk DW & Rice CL. (2005). Motor unit number estimates in the tibialis anterior muscle of young, old, and very old men. *Muscle Nerve* **31,** 461-467.

McNeil CJ & Rice CL. (2018). Neuromuscular adaptations to healthy aging. *Appl Physiol Nutr Metab* **43,** 1158-1165.

McPherson JG, Chen A, Ellis MD, Yao J, Heckman CJ & Dewald JPA. (2018a). Progressive recruitment of contralesional cortico-reticulospinal pathways drives motor impairment post stroke. *J Physiol* **596,** 1211-1225.

McPherson JG, Ellis MD, Harden RN, Carmona C, Drogos JM, Heckman CJ & Dewald JPA. (2018b). Neuromodulatory Inputs to Motoneurons Contribute to the Loss of Independent Joint Control in Chronic Moderate to Severe Hemiparetic Stroke. *Front Neurol* **9,** 470.

McPherson JG, Ellis MD, Heckman CJ & Dewald JP. (2008). Evidence for increased activation of persistent inward currents in individuals with chronic hemiparetic stroke. *J Neurophysiol* **100,** 3236-3243.

McPherson JG, McPherson LM, Thompson CK, Ellis MD, Heckman CJ & Dewald JPA. (2018c). Altered Neuromodulatory Drive May Contribute to Exaggerated Tonic Vibration Reflexes in Chronic Hemiparetic Stroke. *Front Hum Neurosci* **12,** 131.

McPherson LM & Dewald JPA. (2019). Differences between flexion and extension synergy-driven coupling at the elbow, wrist, and fingers of individuals with chronic hemiparetic stroke. *Clin Neurophysiol* **130,** 454-468.

Mendell LM & Henneman E. (1971). Terminals of single Ia fibers: location, density, and distribution within a pool of 300 homonymous motoneurons. *J Neurophysiol* **34,** 171-187.

Michaud M, Balardy L, Moulis G, Gaudin C, Peyrot C, Vellas B, Cesari M & Nourhashemi F. (2013). Proinflammatory cytokines, aging, and age-related diseases. *J Am Med Dir Assoc* **14,** 877-882.

Miller DM, Klein CS, Suresh NL & Rymer WZ. (2014a). Asymmetries in vestibular evoked myogenic potentials in chronic stroke survivors with spastic hypertonia: evidence for a vestibulospinal role. *Clin Neurophysiol* **125,** 2070-2078.

Miller LC & Dewald JP. (2012). Involuntary paretic wrist/finger flexion forces and EMG increase with shoulder abduction load in individuals with chronic stroke. *Clin Neurophysiol* **123,** 1216-1225.

Miller LC, Thompson CK, Negro F, Heckman CJ, Farina D & Dewald JP. (2014b). High-density surface EMG decomposition allows for recording of motor unit discharge from proximal and distal flexion synergy muscles simultaneously in individuals with stroke. *Conf Proc IEEE Eng Med Biol Soc* **2014,** 5340-5344.

Milne JS & Williamson J. (1972). The ankle jerk in older people. *Gerontol Clin (Basel)* **14,** 86-88.

Milner-Brown HS, Stein RB & Yemm R. (1972). Mechanisms for increased force during voluntary contractions. *J Physiol* **226,** 18P-19P.

Mitchell WK, Williams J, Atherton P, Larvin M, Lund J & Narici M. (2012). Sarcopenia, dynapenia, and the impact of advancing age on human skeletal muscle size and strength; a quantitative review. *Front Physiol* **3,** 260.

Morales FR, Boxer PA, Fung SJ & Chase MH. (1987). Basic electrophysiological properties of spinal cord motoneurons during old age in the cat. *J Neurophysiol* **58,** 180-194.

Morita H, Shindo M, Yanagawa S, Yoshida T, Momoi H & Yanagisawa N. (1995). Progressive decrease in heteronymous monosynaptic Ia facilitation with human ageing. *Exp Brain Res* **104,** 167-170.

Moritz CT, Lucas TH, Perlmutter SI & Fetz EE. (2007). Forelimb movements and muscle responses evoked by microstimulation of cervical spinal cord in sedated monkeys. *J Neurophysiol* **97,** 110-120.

Mottram CJ, Heckman CJ, Powers RK, Rymer WZ & Suresh NL. (2014). Disturbances of motor unit rate modulation are prevalent in muscles of spastic-paretic stroke survivors. *J Neurophysiol* **111,** 2017-2028.

Mottram CJ, Suresh NL, Heckman CJ, Gorassini MA & Rymer WZ. (2009). Origins of abnormal excitability in biceps brachii motoneurons of spastic-paretic stroke survivors. *J Neurophysiol* **102,** 2026-2038.

Murray KC, Nakae A, Stephens MJ, Rank M, D'Amico J, Harvey PJ, Li X, Harris RL, Ballou EW, Anelli R, Heckman CJ, Mashimo T, Vavrek R, Sanelli L, Gorassini MA, Bennett DJ & Fouad K. (2010). Recovery of motoneuron and locomotor function after spinal cord injury depends on constitutive activity in 5-HT2C receptors. *Nat Med* **16,** 694-700.

Murray KC, Stephens MJ, Ballou EW, Heckman CJ & Bennett DJ. (2011). Motoneuron excitability and muscle spasms are regulated by 5-HT2B and 5-HT2C receptor activity. *J Neurophysiol* **105,** 731-748.

Nakagawa S & Schielzeth H. (2013). A general and simple method for obtaining R2 from generalized linear mixed□effects models. *Methods in ecology and evolution* **4,** 133-142.

Nakagawa S & Schielzeth H. (2017). Extending R2 and intra-class correlation coefficient from generalized linear mixed-effects models: capturing and characterizing biological variation. *bioRxiv***,** 095851.

Nardelli P, Powers R, Cope TC & Rich MM. (2017). Increasing motor neuron excitability to treat weakness in sepsis. *Ann Neurol* **82,** 961-971.

Nathan P & Smith MC. (1982). The rubrospinal and central tegmental tracts in man. *Brain: a journal of neurology* **105,** 223-269.

Negro F, Muceli S, Castronovo AM, Holobar A & Farina D. (2016). Multi-channel intramuscular and surface EMG decomposition by convolutive blind source separation. *J Neural Eng* **13,** 026027.

Newton JP, Yemm R & McDonagh MJ. (1988). Study of age changes in the motor units of the first dorsal interosseous muscle in man. *Gerontology* **34,** 115-119.

Nielsen JB, Morita H, Wenzelburger R, Deuschl G, Gossard JP & Hultborn H. (2019). Recruitment gain of spinal motor neuron pools in cat and human. *Exp Brain Res* **237,** 2897-2909.

Nikoletopoulou V & Tavernarakis N. (2012). Calcium homeostasis in aging neurons. *Front Genet* **3,** 200.

O'Dwyer NJ, Ada L & Neilson PD. (1996). Spasticity and muscle contracture following stroke. *Brain* **119 (Pt 5),** 1737-1749.

Onodera S & Hicks TP. (2010). Carbocyanine dye usage in demarcating boundaries of the aged human red nucleus. *PLoS One* **5,** e14430.

Oya T, Riek S & Cresswell AG. (2009). Recruitment and rate coding organisation for soleus motor units across entire range of voluntary isometric plantar flexions. *J Physiol* **587,** 4737-4748.

Pagano G, Niccolini F, Fusar-Poli P & Politis M. (2017). Serotonin transporter in Parkinson's disease: A meta-analysis of positron emission tomography studies. *Ann Neurol* **81,** 171-180.

Pascoe MA, Holmes MR & Enoka RM. (2011). Discharge characteristics of biceps brachii motor units at recruitment when older adults sustained an isometric contraction. *J Neurophysiol* **105,** 571-581.

Pierrot-Deseilligny E & Burke D. (2005). *The circuitry of the human spinal cord: its role in motor control and movement disorders*. Cambridge university press.

Piotrkiewicz M, Kudina L, Mierzejewska J, Jakubiec M & Hausmanowa-Petrusewicz I. (2007). Age-related change in duration of afterhyperpolarization of human motoneurones. *J Physiol* **585,** 483-490.

Pompeiano O. (1988). The role of Renshaw cells in the dynamic control of posture during vestibulospinal reflexes. *Prog Brain Res* **76,** 83-95.

Power GA, Dalton BH, Behm DG, Vandervoort AA, Doherty TJ & Rice CL. (2010). Motor unit number estimates in masters runners: use it or lose it? *Med Sci Sports Exerc* **42,** 1644-1650.

Power GA, Dalton BH, Doherty TJ & Rice CL. (2016). If you don't use it you'll likely lose it. *Clin Physiol Funct Imaging* **36,** 497-498.

Powers RK, Elbasiouny SM, Rymer WZ & Heckman CJ. (2012). Contribution of intrinsic properties and synaptic inputs to motoneuron discharge patterns: a simulation study. *J Neurophysiol* **107,** 808-823.

Powers RK & Heckman CJ. (2015). Contribution of intrinsic motoneuron properties to discharge hysteresis and its estimation based on paired motor unit recordings: a simulation study. *J Neurophysiol* **114,** 184-198.

Powers RK, Nardelli P & Cope TC. (2008). Estimation of the contribution of intrinsic currents to motoneuron firing based on paired motoneuron discharge records in the decerebrate cat. *J Neurophysiol* **100,** 292-303.

Powers RK, Robinson FR, Konodi MA & Binder MD. (1993). Distribution of rubrospinal synaptic input to cat triceps surae motoneurons. *J Neurophysiol* **70,** 1460-1468.

Prochazka A. (1989). Sensorimotor gain control: a basic strategy of motor systems? *Prog Neurobiol* **33,** 281-307.

Prut Y & Perlmutter SI. (2003a). Firing properties of spinal interneurons during voluntary movement. I. State-dependent regularity of firing. *J Neurosci* **23,** 9600-9610.

Prut Y & Perlmutter SI. (2003b). Firing properties of spinal interneurons during voluntary movement. II. Interactions between spinal neurons. *J Neurosci* **23,** 9611-9619.

Revill AL & Fuglevand AJ. (2011). Effects of persistent inward currents, accommodation, and adaptation on motor unit behavior: a simulation study. *J Neurophysiol* **106,** 1467-1479.

Revill AL & Fuglevand AJ. (2017). Inhibition linearizes firing rate responses in human motor units: implications for the role of persistent inward currents. *J Physiol* **595,** 179-191.

Riddle CN, Edgley SA & Baker SN. (2009). Direct and indirect connections with upper limb motoneurons from the primate reticulospinal tract. *J Neurosci* **29,** 4993-4999.

Roos MR, Rice CL, Connelly DM & Vandervoort AA. (1999). Quadriceps muscle strength, contractile properties, and motor unit firing rates in young and old men. *Muscle Nerve* **22,** 1094-1103.

Rosenfalck A & Andreassen S. (1980). Impaired regulation of force and firing pattern of single motor units in patients with spasticity. *J Neurol Neurosurg Psychiatry* **43,** 907-916.

Scaglioni G, Narici MV, Maffiuletti NA, Pensini M & Martin A. (2003). Effect of ageing on the electrical and mechanical properties of human soleus motor units activated by the H reflex and M wave. *J Physiol* **548,** 649-661.

Schwindt PC & Crill WE. (1980). Properties of a persistent inward current in normal and TEA-injected motoneurons. *J Neurophysiol* **43,** 1700-1724.

Shibata E, Sasaki M, Tohyama K, Kanbara Y, Otsuka K, Ehara S & Sakai A. (2006). Age-related changes in locus ceruleus on neuromelanin magnetic resonance imaging at 3 Tesla. *Magn Reson Med Sci* **5,** 197-200.

Skagerberg G & Bjorklund A. (1985). Topographic principles in the spinal projections of serotonergic and non-serotonergic brainstem neurons in the rat. *Neuroscience* **15,** 445-480.

Somjen G, Carpenter DO & Henneman E. (1965). Responses of motoneurons of different sizes to graded stimulation of supraspinal centers of the brain. *J Neurophysiol* **28,** 958-965.

Sommerfeld DK, Gripenstedt U & Welmer AK. (2012). Spasticity after stroke: an overview of prevalence, test instruments, and treatments. *Am J Phys Med Rehabil* **91,** 814-820.

Steinbusch HWM, Dolatkhah MA & Hopkins DA. (2021). Anatomical and neurochemical organization of the serotonergic system in the mammalian brain and in particular the involvement of the dorsal raphe nucleus in relation to neurological diseases. *Prog Brain Res* **261,** 41-81.

Stephenson JL & Maluf KS. (2011). Dependence of the paired motor unit analysis on motor unit discharge characteristics in the human tibialis anterior muscle. *J Neurosci Methods* **198,** 84-92.

Stienen AH, Moulton TS, Miller LC & Dewald JP. (2011). Wrist and Finger Torque Sensor for the quantification of upper limb motor impairments following brain injury. *IEEE Int Conf Rehabil Robot* **2011,** 5975464.

Stinear CM, Barber PA, Smale PR, Coxon JP, Fleming MK & Byblow WD. (2007). Functional potential in chronic stroke patients depends on corticospinal tract integrity. *Brain* **130,** 170-180.

Sukal TM, Ellis MD & Dewald JP. (2007). Shoulder abduction-induced reductions in reaching work area following hemiparetic stroke: neuroscientific implications. *Exp Brain Res* **183,** 215-223.

Swash M & Fox KP. (1972). The effect of age on human skeletal muscle. Studies of the morphology and innervation of muscle spindles. *J Neurol Sci* **16,** 417-432.

Tang A & Rymer WZ. (1981). Abnormal force--EMG relations in paretic limbs of hemiparetic human subjects. *J Neurol Neurosurg Psychiatry* **44,** 690-698.

Tatton WG, Greenwood CE, Verrier MC, Holland DP, Kwan MM & Biddle FE. (1991). Different rates of age-related loss for four murine monoaminergic neuronal populations. *Neurobiol Aging* **12,** 543-556.

Thompson CK, Negro F, Johnson MD, Holmes MR, McPherson LM, Powers RK, Farina D & Heckman CJ. (2018). Robust and accurate decoding of motoneuron behaviour and prediction of the resulting force output. *J Physiol* **596,** 2643-2659.

Tomlinson BE & Irving D. (1977). The numbers of limb motor neurons in the human lumbosacral cord throughout life. *J Neurol Sci* **34,** 213-219.

Trajano GS, Taylor JL, Orssatto LBR, McNulty CR & Blazevich AJ. (2020). Passive muscle stretching reduces estimates of persistent inward current strength in soleus motor units. *J Exp Biol* **223**.

Twitchell TE. (1951). The restoration of motor function following hemiplegia in man. *Brain* **74,** 443-480.

Udina E, D'Amico J, Bergquist AJ & Gorassini MA. (2010). Amphetamine increases persistent inward currents in human motoneurons estimated from paired motor-unit activity. *J Neurophysiol* **103,** 1295-1303.

Vecchio AD & Farina D. (2019). Interfacing the neural output of the spinal cord: robust and reliable longitudinal identification of motor neurons in humans. *J Neural Eng* **17,** 016003.

Werring DJ, Toosy AT, Clark CA, Parker GJ, Barker GJ, Miller DH & Thompson AJ. (2000). Diffusion tensor imaging can detect and quantify corticospinal tract degeneration after stroke. *J Neurol Neurosurg Psychiatry* **69,** 269-272.

Wienecke J, Zhang M & Hultborn H. (2009). A prolongation of the postspike afterhyperpolarization following spike trains can partly explain the lower firing rates at derecruitment than those at recruitment. *J Neurophysiol* **102,** 3698-3710.

Wilson JM, Thompson CK, Miller LC & Heckman CJ. (2015). Intrinsic excitability of human motoneurons in biceps brachii versus triceps brachii. *J Neurophysiol* **113,** 3692-3699.

Wilson VJ & Yoshida M. (1968). Vestibulospinal and reticulospinal effects on hindlimb, forelimb, and neck alpha motoneurons of the cat. *Proc Natl Acad Sci U S A* **60,** 836-840.

Yang Y, Sinha N, Tian R, Gurari N, Drogos JM & Dewald JPA. (2020). Quantifying Altered Neural Connectivity of the Stretch Reflex in Chronic Hemiparetic Stroke. *IEEE Trans Neural Syst Rehabil Eng* **28,** 1436-1441.

Yavuz US, Negro F, Sebik O, Holobar A, Frommel C, Turker KS & Farina D. (2015). Estimating reflex responses in large populations of motor units by decomposition of the high-density surface electromyogram. *J Physiol* **593,** 4305-4318.

Young JL & Mayer RF. (1982). Physiological alterations of motor units in hemiplegia. *J Neurol Sci* **54,** 401-412.

Zackowski KM, Dromerick AW, Sahrmann SA, Thach WT & Bastian AJ. (2004). How do strength, sensation, spasticity and joint individuation relate to the reaching deficits of people with chronic hemiparesis? *Brain* **127,** 1035-1046.

Zijdewind I, Bakels R & Thomas CK. (2014). Motor unit firing rates during spasms in thenar muscles of spinal cord injured subjects. *Front Hum Neurosci* **8,** 922.